

Preparation and Calibration of Pressure-Sensitive and Temperature-Sensitive Paints for Fluorescence Lifetime Imaging Applications

DISSERTATION ZUR ERLANGUNG DES DOKTORGRADES DER
NATURWISSENSCHAFTEN

(Dr. rer. nat.)

DER NATURWISSENSCHAFTLICHEN FAKULTÄT IV
- CHEMIE UND PHARMAZIE -
DER UNIVERSITÄT REGENSBURG



vorgelegt von

Matthias I. J. Stich

aus Regensburg

Februar 2009

Diese Doktorarbeit entstand in der Zeit von Januar 2006 bis Februar 2009 am Institut für Analytische Chemie, Chemo- und Biosensorik der Universität Regensburg.

Die Arbeit wurde angeleitet von Prof. Dr. Otto S. Wolfbeis

Promotionsgesuch eingereicht am:	4. Februar 2009
Kolloquiumstermin:	12. März 2009
Prüfungsausschuß:	Vorsitzender: Prof. Dr. M. Scheer
	Erstgutachter: Prof. Dr. O. S. Wolfbeis
	Zweitgutachter: Prof. Dr. A. Göpferich
	Drittprüfer: Prof. Dr. H.-A. Wagenknecht

**This work was financed by the German Aerospace Center
(Deutsches Zentrum für Luft- und Raumfahrt, DLR)**



„Insanity: doing the same thing over and over again and expecting different results.“

(Albert Einstein)

“I love deadlines. I like the whooshing sound they make as they go by.”

(Douglas Adams)

“The great tragedy of science: the slaying of a beautiful hypothesis by an ugly fact.”

(Thomas Henry Huxley)

Acknowledgements

Most importantly, I have to thank **Prof. Dr. Otto S. Wolfbeis** for selecting and issuing this interesting thesis and the excellent working conditions at his chair.

Also, I appreciate very much all the help and support of my tutor **Dr. Michael Schäferling** throughout this work.

I gratefully acknowledge the support and consultancy provided by **Dr. Ulrich Henne**, **Dr. Yasuhiro Egami**, and **Dr. Christian Klein** from the Institute of Aerodynamics and Flow Technology of the German Aerospace Center (DLR), Göttingen, and **Dr. Vladimir Ondrus** from the Institute of Chemistry, University of Hohenheim.

I am also obliged to many other present and former colleagues for the excellent atmosphere and lots of help concerning so many things throughout this work, particularly **Martin Link**, **Lorenz Fischer**, **Dominik Grögel**, **Daniela Achatz**, **Robert Meier**, **Maximilian Oberleitner**, **Simone Moises**, **Dr. Sergey Borisov**, **Dr. Péter Kele**, **Dr. Stefan Nagl**, and **Dr. Petra Schrenkhammer** as well as to my former research student **Julia Manetsberger**.

No less, I am indebted to the secretary and the “heart and soul” of the institute **Edeltraud Schmid**, the technicians **Gisela Hierlmeier**, **Barbara Goricnik**, and **Angela Haberkern**. Thank you for all the help and advice and the really good time at the institute. I also appreciate the support and help of **Dr. Klaus-Peter Ruess**, **Dr. Rudi Hutterer**, the technicians **Angelika Stoiber**, **Gisela Emmert**, and **Joachim Rewitzer**.

Furthermore, I wish to thank my good friends **Anna “d’Chefin” Hezinger**, **Michael “Mitch” Kuhn**, **Alexander “Dr. Pavlov” Schätz**, **Klaus “Harrarar” Harrar**, **Tobias “Walter” Olbrich**, **Alexander “ein bißchen” Tereshchenko**, **Florian “Flo” Sahr**, and **Markus “der General” Hager** for all the beer, steaks, and fun we had, the advice and backup in hard times, and for making the university a better place.

Finally, special thanks to my parents, **Anna** and **Ignaz Stich**, for their emotional and financial support.

CHAPTER 1: Introduction

1.1. Historical Overview	1
1.2. Motivation	2
1.3. References	3

CHAPTER 2: Luminescence Imaging of Sensor Paints and Layers

2.1. Quenching of Luminescence	5
2.2. Pressure-Sensitive and Temperature-Sensitive Paints	8
2.3. Materials for Use in PSPs and TSPs	8
2.3.1. Indicators for Use in PSPs	9
2.3.2. Polymers for Use in PSPs	11
2.3.3. Electrochemical Coating	14
2.3.4. Indicators for Use in TSPs	14
2.3.5. Polymers for Use in TSPs	16
2.4. Spectroscopic Methods of Interrogation	17
2.4.1. Intensity Imaging	18
2.4.2. Fluorescence Lifetime Imaging (FLIM)	21
2.4.2.1. <i>Phase Delay Rationing (PDR)</i>	22
2.4.2.2. <i>Dual Lifetime Referencing (DLR)</i>	23
2.4.2.3. <i>Rapid Lifetime Determination (RLD)</i>	24
2.4.2.4. <i>Dual Lifetime Determination (DLD)</i>	25
2.4.2.5. <i>Alternative Schemes</i>	27
2.5. Requirements and Characteristics of the Imaging Setup	28
2.5.1. Camera Systems	28
2.5.1.1. <i>Interline Cameras</i>	29
2.5.1.2. <i>Frame Transfer Cameras</i>	29
2.5.1.3. <i>Full Frame Cameras</i>	29
2.5.1.4. <i>Intensified CCD Cameras</i>	30
2.5.1.5. <i>Areas of Application of the Various Cameras</i>	30
2.5.2. Light Sources	32
2.6. State of the Art	33
2.7. References	33

CHAPTER 3: Dual Pressure-Sensitive and Temperature-Sensitive Paint for Wind Tunnel Applications

3.1. Wind Tunnels and Model Analysis	38
3.2. The System PtTFPL and Ru(phen)₃(TMS)₂/PAN in FIB	41
3.2.1. Choice of Materials	41
3.2.1.1. PtTFPL	41
3.2.1.2. Ru(phen) ₃ (TMS) ₂ in Poly(acrylonitrile)	44
3.2.1.3. FIB Matrix Polymer	45
3.2.2. Intensity versus Time-Resolved Imaging	46
3.3. Application of the Paint	48
3.3.1. Composition and Coating Tests	48
3.3.2. Wind Tunnel Test	50
3.3.2.1. Aircraft Model and Experimental Setup	50
3.3.2.2. Results	53
3.3.2.2.1. Calibration	53
3.3.2.2.2. Image Design	54
3.3.2.2.3. Raw Images	55
3.3.2.2.4. Temperature-Sensitive Probe	57
3.3.2.2.5. Pressure-Sensitive Probe	58
3.3.2.2.6. Further Investigations	59
3.3.2.3. Discussion	62
3.4. Conclusion	63
3.5. Experimental	64
3.5.1. Materials and Methods	64
3.5.2. Preparation of Temperature-Sensitive Particles	65
3.5.3. Paint Composition and Coating	65
3.5.4. Experimental Setup and Parameters	66
3.6. References	67

CHAPTER 4: A Dual Luminescent Sensor Material for Simultaneous Imaging of Pressure and Temperature on Surfaces.

4.1. Introduction	71
4.2. Results and Discussion	72
4.2.1. Sensor Composition	72
4.2.2. Calibration of the Dual Sensor Material	75
4.2.3. Sensor Validation	80
4.3. Conclusion	83
4.4. Experimental	83
4.4.1. Materials and Methods	83
4.4.2. Preparation and Characterisation of Oxygen-Sensitive Particles	84
4.4.3. Preparation and Characterisation of Temperature-Sensitive Particles	84
4.4.4. Sensor Preparation	85
4.4.5. Acquisition of Spectra and Experimental Setup	85
4.5. References	86

CHAPTER 5: Read-Out of Multiple Optical Chemical Sensors by Means of Digital Color Cameras

5.1. Introduction	88
5.2. Results and Discussion	91
5.2.1. Carbon Dioxide Sensor	91
5.2.2. Temperature Sensor	92
5.3. Conclusion	93
5.4. Experimental	95
5.4.1. Materials	95
5.4.2. Preparation of the Dual Sensor	95
5.4.3. Calibration of the Dual Sensor	96
5.4.4. Data Evaluation	96
5.5. References	97

CHAPTER 6: Multicolored Fluorescent and Permeation-Selective Microbeads Enable Simultaneous Sensing of pH, Oxygen and Temperature	
6.1. Introduction	98
6.2. Sensor Composition	99
6.2.1. First Triple Sensor System	100
6.2.2. Second Triple Sensor System	101
6.3. Results and Discussion	102
6.4. Conclusion	105
6.5. Experimental	106
6.5.1. Materials	106
6.5.2. Preparation of Oxygen-Sensitive Beads	106
6.5.3. Preparation of pH-Sensitive Beads	107
6.5.4. Preparation of Temperature-Sensitive Beads	107
6.5.5. Preparation of Triple Sensor TS-1	107
6.5.6. Preparation of Triple Sensor TS-2	108
6.5.7. Acquisition of Spectra and Experimental Setup	108
6.5.8. Response Functions of Triple Sensor TS-1	108
6.5.9. Response Functions of Triple Sensor TS-2	109
6.6. References	110
 CHAPTER 7: Summary	 112
 CHAPTER 8: Abbreviations, Acronyms, and Symbols	 114
 CHAPTER 9: Curriculum Vitae	 118
 CHAPTER 10: Patents, Publications, and Presentations	 120

CHAPTER 1

Introduction

1.1. Historical Overview

The determination of oxygen is most important in almost every field of science, research, and technology. Pressure (or oxygen partial pressure, pO_2) as well as temperature are omnipresent factors, influencing almost every measurements of other parameters. The problem of determining the pressure of the ambient atmosphere was solved in the seventeenth century. However, it took quite a long time until it was possible to continuously measure the concentration of oxygen in liquids. This was achieved by Leland Clark in 1954 with his so-called Clark oxygen electrode.^[1] This was the first commercially available device for pO_2 determination, but it was not applicable to measurements of oxygen distribution or surface flow.

In the early 1930's, Kautsky and Hirsch described the decrease of the luminescence intensity of organic dyes adsorbed onto silica when exposed to oxygen.^[2] Fifty years later, Peterson and Fitzgerald utilized this effect for studies of flow over airfoil shapes.^[3] The idea of pressure-sensitive paints was born therewith (it has to be emphasized that pressure-sensitivity, in this context, always means sensitivity to barometric pressure and never to mechanical pressure). First research on the application of pressure-sensitive paints (PSPs) was performed in the former Soviet Union at the Central Institute of Aerohydrodynamics in Moscow (TsAGI). However, scientists in the rest of the world were oblivious of the research done in this field.^[4] In the late 1980's the PSP technique was independently introduced and established by scientists at the University of Washington in Seattle (M. Gouterman, J. Callis).^[5] Since then, numerous other aerodynamic research facilities all over the world have applied and advanced the technique. These include NASA (USA),^[6] JAXA (Japan),^[7] ONERA (France),^[8] and DLR (Germany).^[9]

Since every pressure-sensitive dye displays a more or less strong cross-sensitivity towards temperature, there is also a large interest in temperature-

sensitive paints (TSPs). This technique enables for gathering information about the two-dimensional temperature distribution for referencing and compensating the temperature effect of the PSP. The first substances applied for this purpose were inorganic compounds, the so-called thermographic phosphors. Temperature distribution imaging was therefore formerly termed thermographic phosphor thermography (TPT). They are now referred to as temperature-sensitive paints.^[10-14]

Aside from its use in aerodynamic research, pressure and oxygen imaging has become important in medical and pharmaceutical sciences. Oxygen and temperature are the two factors which, besides pH, are the most crucial parameters for point-of-care diagnostics. The dual pressure-sensitive and temperature-sensitive paint approach offers the possibility of performing non-invasive online measurements of these two parameters.^[15-27]

1.2 Motivation

At the Institute of Analytical Chemistry, Chemo- and Biosensors (IACCB) of the University of Regensburg, extensive research has been performed on fluorescence-based sensing and on lifetime imaging. Various sensor systems have been developed for the imaging of e.g. carbon dioxide partial pressure^[28], pH,^[18,29] metal ions,^[30] oxygen partial pressure^[31,32] etc. Based on the previous results, this work aims on the development of dual paints for wind tunnel applications. A “dual paint” is defined as a material (a coating) capable of simultaneously reporting two parameters, here specifically the oxygen partial pressure (pO_2) and temperature. The ambition was to develop new materials and to eliminate the common and well known disadvantages and problems of the PSP and TSP systems, like e. g. pressure dependence of the temperature probe or insufficient signal separation.

In this dissertation, new and improved pressure- and temperature-sensitive paint systems are introduced. Up to the present, the information about pressure distributions provided by PSPs is mainly acquired using the luminescence intensity of the probe as the analytical information. In cooperation with the Institute of Aerodynamics and Flow Technology of the German Aerospace Center (Institut für

Aerodynamik und Strömungsmechanik, Deutsches Zentrum für Luft- und Raumfahrt, DLR), we have assembled a novel optical setup for measuring and evaluating pressure-dependent luminescence lifetime of the indicator probe instead of its intensity, entailing advantages like higher accuracy, independence from the overall intensity and paint distribution, just to mention a few.

The pressure-sensitive paints were combined with temperature-sensitive probes to build dual sensor systems capable of determining both pO_2 and T . The dual sensors and the single components were characterized and the resulting dual sensors were calibrated. Furthermore, two new methods of interrogation for dual sensors are introduced and discussed. Based on these approaches, the principle of optical dual sensors and the corresponding signal separation was expanded and improved, resulting in the first optical triple sensors ever described.

1.3 References

- [1] L. C. Clark Jr., *Trans. Am. Soc. Artif. Intern. Organs.* **1956**, 2, 41
- [2] H. Kautsky, A. Hirsch, *Z. anorg. u. allg. Chem.* **1935**, 222, 126
- [3] J. I. Peterson, R. V. Fitzgerald, *Rev. Sci. Instrum.* **1980**, 51, 670
- [4] T. Liu, J. P. Sullivan, *Pressure and Temperature Sensitive Paints. Springer Series on Fluid Mechanics* (eds: R. J. Adrian, M. Gharib, W. Merzkirch, D. Rockwell, J. H. Whitelaw), Springer, Berlin, **2004**
- [5] J. Kavandi, J. Callis, M. Gouterman, G. Khalil, D. Wright, E. Green, D. Burns, B. McLachlan, *Rev. Sci. Instrum.* **1990**, 61, 3340
- [6] A. E. Baron, J. D. S. Danielson, M. Gouterman, J. R. Wan, B. McLachlan, *Rev. Sci. Instrum.* **1993**, 64, 3394
- [7] K. Nakakita, M. Kurita, K. Mitsuo, S. Watanabe, *Meas. Sci. Technol.* **2006**, 17, 359
- [8] M.-C. Merienne, Y. Le Sant, J. Ancelle, D. Soulevant, *Meas. Sci. Technol.* **2004**, 15, 2349
- [9] C. Klein, R. H. Engler, U. Henne, W. E. Sachs, *Exp. Fluids* **2005**, 39, 475
- [10] J. I. Eldridge, T. J. Benic, S. W. Allison, D. L. Beshears, *J. Therm. Spray. Tech.* **2004**, 13, 44
- [11] A. Omrane, G. Särner, M. Alden, *Appl. Phys. B* **2004**, 79, 431
- [12] J. P. Feist, A. L. Heyes, S. Seefeldt, *Meas. Sci. Technol.* **2003**, 14, N17
- [13] L. M. Coyle, M. Gouterman, *Sens. Actuators B* **1999**, 61, 92
- [14] S. W. Allison, G. T. Gillies, *Rev. Sci. Instrum.* **1997**, 68, 2615
- [15] D. B. Papkovsky, T. C. O'Riordan, G. G. Guilbault, *Anal. Chem.* **1999**, 71, 1568
- [16] C. Preininger, I. Klimant, O. S. Wolfbeis, *Anal. Chem.* **1994**, 66, 1841
- [17] K. Kellner, G. Liebsch, I. Klimant, O. S. Wolfbeis, T. Blunk, M. B. Schulz, A. Göpferich, *Biotechnol. Bioeng.* **2002**, 80, 73
- [18] S. Arain, G. T. John, C. Krause, J. Gerlach, O. S. Wolfbeis, *Sens. Actuators B* **2006**, 113, 639
- [19] S. Arain, S. Weiss, E. Heinzle, G. T. John, C. Krause, I. Klimant, *Biotech. Bioeng.* **2005**, 90, 271

- [20] J. Gerlach, B. Pohn, W. Karl, M. Schneideler, M. Uray, H. Bischof, H. Schwab, I. Klimant, *Sens. Actuators B* **2006**, 114, 984
- [21] V. I. Ogurtsov, D. B. Papkovsky, *Sens. Actuators B* **2006**, 113, 608
- [22] V. I. Ogurtsov, D. B. Papkovsky, *Sens. Actuators B* **2006**, 113, 917
- [23] J. Hynes, T. C. O’Riordan, J. Curtin, T. G. Cotter, D. B. Papkovsky, *J. Immunol. Methods* **2005**, 306, 193
- [24] F. C. O’Mahony, C. O’Donovan, J. Hynes, T. Moore, J. Davenport, D. B. Papkovsky, *Environ. Sci. Technol.* **2005**, 39, 5010
- [25] J. Alderman, J. Hynes, S. M. Floyd, J. Krüger, R. O’Connor, D. B. Papkovsky, *Biosens. Bioelect.* **2004**, 19, 1529
- [26] A. Apostolidis, I. Klimant, D. Andrzejewski, O. S. Wolfbeis 2004, *J. Comb. Chem.* **2004**, 6, 325
- [27] G. T. John, I. Klimant, C. Wittmann, E. Heinzle, *Biotech. Bioeng.* **2003**, 81, 829
- [28] S. M. Borisov, G. Neuraüter, C. Schroeder, I. Klimant, O. S. Wolfbeis, *Appl. Spec.* **2006**, 60, 1167
- [29] G. S. Vasylevska, S. M. Borisov, C. Krause, O. S. Wolfbeis, *Chem. Mater.* **2006**, 18, 4609
- [30] T. Mayr, C. Igel, G. Liebsch, I. Klimant, O. S. Wolfbeis, *Anal. Chem.* **2003**, 75, 4389
- [31] S. M. Borisov, O. S. Wolfbeis, *Anal. Chem.* **2006**, 78, 5094
- [32] I. Klimant, F. Ruckruh, G. Liebsch, A. Stangelmayer, O. S. Wolfbeis, *Mikrochim. Acta* **1999**, 131, 35

CHAPTER 2

Luminescence Imaging of Sensor Paints and Layers

The phenomenon of the quenching of luminescence by quenchers such as oxygen not only forms the basis for various methods and applications in (bio)analytical chemistry and in physics, but also is the fundamental process for barometric pressure paints (so-called pressure-sensitive paints; PSPs). The mechanisms and principles of luminescence itself are not presented and discussed in the following, as they are described in pertinent physical-chemistry textbooks.^[1-4]

2.1. Quenching of Luminescence

The intensity of fluorescence can be decreased by various processes and mechanisms. One of these processes, beside energy transfer and electron transfer, is called quenching. Common quenchers include molecular oxygen, halides, heavy metal ions, amines, and electron deficient molecules like nitroaromatics and acrylamide. Generally, two different mechanisms of quenching are observed, namely collisional dynamic and static quenching.^[1-4] The phenomenon of static quenching, where the quencher is forming a complex with the fluorophore, will not be discussed here since it plays no role in pressure-sensitive and temperature-sensitive paint technology. Collisional quenching occurs when the excited state of a fluorophore is deactivated via molecular collisions. The fluorophores are not chemically altered in this process. The excited state is depopulated in a non-radiative way. The quantum yield (QY , Φ) decreases with the rate of non-radiative decay. The luminescence lifetime (LT , τ) also decreases with decreasing quantum yield.^[4-7] Most organic luminophores emit from a singlet excited state with decay times up to 20 ns (with a few exceptions). Metal-ligand complexes (MLCs) in contrast, emit from a state of higher multiplicity and have much longer decay times. Therefore, they are easily quenched by oxygen (which itself has a triplet ground state) via triplet-triplet annihilation. Not all MLCs are quenched by oxygen to the same extent. For instance, ruthenium complexes are

more strongly affected than europium complexes. This is due to the possibility of the transition of the triplet state to the f-orbital of the europium metal center, resulting in a long-lived luminescence from that state. Thus, the triplet state is depopulated by this mechanism before being annihilated by triplet oxygen.

For collisional quenching, a relationship between the luminescence intensity, and thus lifetime, and oxygen partial pressure (or air pressure) was described by Stern and Volmer in 1919:^[8]

$$\frac{I_{ref}}{I} = 1 + K_{SV} \cdot [Q] = \frac{\tau_{ref}}{\tau} \quad eq. 2.1$$

where K_{SV} is the Stern-Volmer quenching constant, $[Q]$ the concentration of the quencher, I the intensity, and τ the lifetime, whilst I_{ref} and τ_{ref} , respectively, are the intensities and lifetimes under reference conditions, in the majority of the cases in absence of the quencher. *Equation 2.1* is the simplest form of the Stern-Volmer equation and well applicable to molecules in solution. K_{SV} contains the unquenched luminescence lifetime and a diffusion-controlled bimolecular rate constant. In solution, the diffusion of the dye molecule and the quenching species remains the same throughout the entire volume. Plotting the intensity or lifetime ratio versus the quencher concentration gives a linear dependency with the Stern-Volmer constant K_{SV} as slope.

The PSP and TSP technique makes use of solid phases. Thus, free diffusion of the dye and the quencher is compromised, and deviations can occur from the strictly linear dependence of the intensity or lifetime on the quencher concentration. Hence, a modified Stern-Volmer equation has to be applied that reflects the fact that fluorophores are located at different chemical and physical environment (e.g. inside polymer particles and matrices) and thus have different quencher accessibility:

$$\frac{I}{I_{ref}} = \frac{\tau}{\tau_{ref}} = \frac{f_1}{1 + K_{SV}^{(1)} \cdot [Q]} + \frac{f_2}{1 + K_{SV}^{(2)} \cdot [Q]} + \frac{f_3}{1 + K_{SV}^{(3)} \cdot [Q]} + \dots \quad eq. 2.2$$

with f_1 , f_2 , and f_3 as the emissive fractions of the fluorophore in the different environment, K_{SV} as the Stern-Volmer constants in the different environments, and $[Q]$ as the quencher concentration. It turns out that terminating *eq 2.2* after the second term is an acceptable simplification to describe quenching in heterogeneous systems. The simplified equation is referred to as the two-site-model.^[9-11]

Quenching by temperature (in contrast to oxygen quenching) is not based on the interaction of two species. Rather, it is directly affected by the energy levels of the orbitals involved, e.g. the d-d orbital and the metal-ligand charge transfer (MLCT) in metal-ligand complexes, and the energy gaps between these. For luminescence to occur, the d-d state has to lie above the MLCT state.^[12] The energy of the states involved can be altered by the addition of thermal energy. Furthermore, additional thermal energy increases the probability of electron transitions between the two states involved. This happens with a defined rate constant and depends on the characteristics of the molecule. The rate constant changes with temperature and can be described by

$$\frac{d \ln k}{dT} = \frac{E_a}{RT^2} \quad \text{eq. 2.3}$$

or the integrated form

$$\ln k = \left(A - \frac{E_a}{RT} \right) \quad \text{eq. 2.4}$$

The temperature sensitivity of a pressure-sensitive or temperature-sensitive paint can thus be described by

$$\frac{1}{\tau} = k_0 + k_1 \cdot \exp\left(-\frac{\Delta E}{R \cdot T}\right) \quad \text{eq. 2.5}$$

where τ is the lifetime, k_0 the temperature independent decay rate for the deactivation of the excited state (the sum of radiative and nonradiative decay constants from the emitting state to the ground state), k_1 the preexponential factor, ΔE the energy gap between the emitting level and an upper deactivating excited state, R the gas constant, and T the absolute temperature.^[13-16] If the energy gap between the electronic states involved is small, luminescence is quenched by temperature. An increase in temperature will then cause a large decrease of both luminescence intensity and lifetime.

2.2. Pressure-Sensitive Paints and Temperature-Sensitive Paints

The function of PSPs relies on the principle of collisional quenching of luminescence. The indicator dyes are incorporated into a polymeric matrix (also referred to as binder) or encapsulated inside polymer particles. The PSP then is cast on the surface or structure of interest. The photoluminescence intensity (and lifetime) depends on the oxygen partial pressure of the ambient air. The process is fully reversible. By imaging the surface, pressure distributions can be visualised with high spatial resolution.

All dyes employed in PSPs are more or less sensitive to temperature. Metal-ligand complexes (MLCs) are often used as pressure indicators due to their large Stokes' shifts. The temperature dependence of MLCs is particularly expressed. Since altering the pressure flow often entails a change in temperature, the calculation of the pressure at a certain point is only possible with the knowledge of the temperature at this point.

Intensity is the parameter most often acquired. This is convenient but implies several problems and sources of error. These include (a) small deviations in the PSP distribution, (b) inhomogeneities of the paint, (c) defects on the sample surface, and (d) imperfectly installed light sources. Time-gated luminescence lifetime imaging can help to avoid these disadvantages.^[17,18]

2.3. Materials for Use in PSPs and TSPs

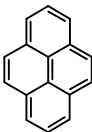
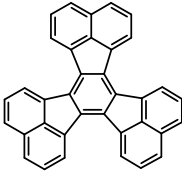
All materials applied in paint formulations have to meet a variety of stipulations. Indicators are expected to possess high quantum yields, large absorption coefficients (and thus brightness), high photostability, and they should be excitable with low-cost light sources. Polymers for use in PSPs are expected to be good solvents for the luminophores, to have good and fast permeability for oxygen, to be sprayable, and to have good adhesion to the support.

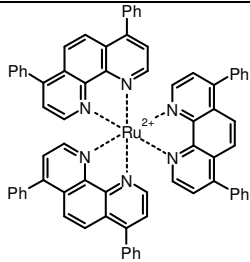
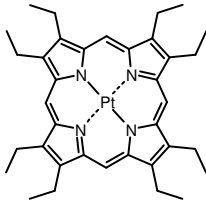
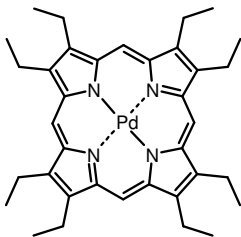
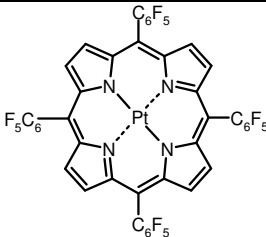
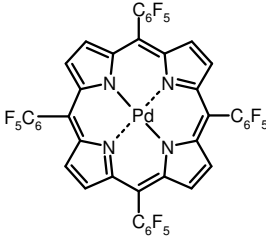
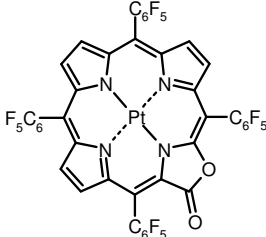
2.3.1. Indicators for Use in PSPs

Amongst the variety of luminescent molecules, only a few are suitable for use in pressure-sensitive paints. With respect to luminescence intensity, the dyes have to be as bright as possible. The brightness (B_s) of a luminophore is defined as the product of molar absorbance (ϵ) at the excitation wavelength and the quantum yield Φ . For example, the $\text{Ru}(\text{dpp})_3^{2+}$ complex has a molar absorbance (ϵ) of $\sim 30,000 \text{ L}/(\text{mol}\cdot\text{cm})$, and a quantum yield Φ of 0.36 and thus a brightness of 10,800 for deoxygenated conditions. Under ambient air pressure, the quantum yield drops to about 0.2, and the brightness therefore to $\sim 6,000$.^[19-23]

One of the widely used class of molecules is the family of the polycyclic aromatic hydrocarbons (PAHs) like pyrene. The luminescence decay of pyrene occurs in the nanosecond timescale, which makes it more difficult to determine lifetime changes due to quenching. Metal-ligand complexes typically display lifetimes between hundreds of nanoseconds up to several milliseconds, but only a few have quantum yields comparable to PAHs. In fact, there is no ideal luminescent molecule, suitable for all kinds of PSP measurements. Important probes for use in PSPs are listed in *table 2.1*.

Table 2.1. Names, acronyms, chemical structures, and spectral characteristics of typical indicators for use in pressure-sensitive paints (with *S*: Soret-band; *Q*: Q-band).

Compound [acronym]	Chemical Structure	$\lambda_{\text{abs}}(\text{max})$	$\lambda_{\text{em}}(\text{max})$	Ref.
Pyrene		335 nm	395 nm (monomer) 475 nm (excimer)	27,28,29
Decacyclene		385 nm	510 nm	24,30,31

Ruthenium(II)-tris(4,7-diphenyl-1,10-phenanthroline) [Ru(dpp)₃²⁺] (various counter ions)		337 nm 457 nm	610 nm	19,20,21, 22,23
Platinum(II)-2,3,7,8,12,13,17,18-octaethylporphyrin [PtOEP]		381 nm (S) 535 nm (Q)	646 nm	17,26,32
Palladium(II)-2,3,7,8,12,13,17,18-octaethylporphyrin [PdOEP]		393 nm (S) 512 nm (Q) 546 nm (Q)	663 nm	26,33
Platinum(II)-5,10,15,20-tetrakis(2,3,4,5,6-pentafluorophenyl)porphyrin [PtTFPP]		395 nm (S) 541 nm (Q)	648 nm	34,35
Palladium(II)-5,10,15,20-tetrakis(2,3,4,5,6-pentafluorophenyl)porphyrin [PdTFPP]		407 nm (S) 518 nm (Q) 552 nm (Q)	653 nm	11
Platinum(II)-5,10,15,20-tetrakis(2,3,4,5,6-pentafluorophenyl)porpholactone [PtTFPL]		392 nm (S) 572 nm (Q)	745 nm	18,36,37

The polycyclic aromatic hydrocarbons (PAHs) are efficiently quenched by oxygen and were the first applied in optical (fiber) sensors.^[24,25] They exhibit bright emission but many of them lack photostability and some need shortwave excitation.

Ruthenium-tris(4,7-diphenyl-1,10-phenanthroline) is not a very bright luminophore compared to the PAHs, but possesses an unusually long luminescence lifetime. The complexes are more stable against photodecomposition and are excitable with violet or blue light. In the past, this was a great advantage due to the high costs of light sources for the UV region.^[26]

The porphyrin platinum complexes show intense luminescence at room temperature, possess a high quantum yield $< 50\%$, and therefore are very bright: PtTFPP, for example, has a Φ of 0.1 and an ϵ of 323,000 (Soret band) and 23,200 (non-Soret band, so-called Q-band), respectively.^[38] Obviously, the brightness is much higher if excitation is performed at the wavelength of the Soret band. The palladium or platinum octaethyl porphyrins immobilised in polymer matrices undergo photobleaching.^[26,39] Fluorinated porphyrin derivatives like PtTFPL are more photostable.^[34,40]

2.3.2. Polymers for Use in PSPs

The polymer (often referred to as the “binder”) is the second important component of a PSP.^[41,42] It attaches the indicator on the solid support. However, not all kinds of polymers are suitable for the use in PSP formulations. The pressure-sensitive indicator dye has to be soluble in the binder (unless it is suspended). Furthermore, the binder has to be soluble in an appropriate solvent so that it can be sprayed or spread on the surface of interest. It is of particular importance that the polymer is inert. It should not contain any functional groups that can affect the luminescence behaviour of the pressure-sensitive dye. Even carboxy groups, for instance, can act as a quencher.

Moreover, the polymer has to comply with two important conditions. It should be mechanically stable and also display a high and constant permeability for oxygen. This permeability depends on various factors and is not directly a function of the polymer's chemical structure. Rather, it depends on the orientation and density of the macromolecules, and on the thickness of the coating. The most common parameter for quantifying the diffusion of oxygen through a polymer is the so-called permeability coefficient P .

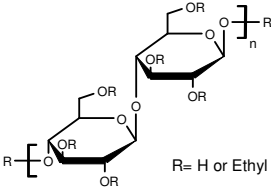
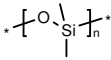
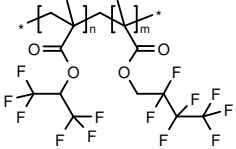
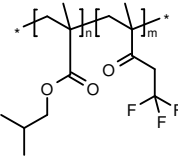
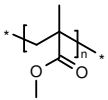
$$P = \frac{(\text{thickness of the polymer film}) \cdot (\text{quantity of oxygen})}{(\text{area}) \cdot (\text{time}) \cdot (\text{pressure drop across the film})} \quad \text{eq. 2.6}$$

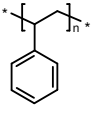
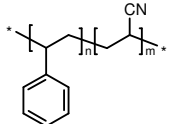
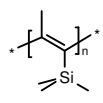
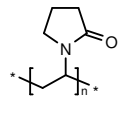
The temperature dependence of the permeability coefficient is given by:

$$P = P_0 \cdot \exp\left(-\frac{E_P}{RT}\right) \quad \text{eq. 2.7}$$

where P_0 is a pre-exponential factor, E_P the activation energy of permeation, R the gas constant, and T the absolute temperature in Kelvin.^[43] For the application in PSP, the permeability coefficient should be (more or less) constant over a wide temperature range or ideally be completely independent of temperature. An overview on polymers for the application in PSPs and their properties is given in table 2.2.

Table 2.2. Names, acronyms, chemical structures, and figures of merit of selected polymers for use in pressure-sensitive paints.

Polymer [acronym]	Chemical Structure	T [°C]	P [$10^{-13} \text{ cm}^2 \cdot \text{s}^{-1} \cdot \text{Pa}^{-1}$]	Ref.
Ethyl cellulose [EC]		25	11.0	44
Poly(dimethyl siloxane) [PDMS]		35	695	45
Poly(hexafluoroisopropyl methacrylate-co-heptafluoro- n-butyl methacrylate) [FIB]			n.d.	46 47
Poly(isobutyl methacrylate- co-trifluoroethyl methacrylate) [Poly(IBM-co-TFEM)]			n.d.	47 48
Poly(methyl methacrylate) [PMMA]		34	0.116	47 49

Polystyrene [PS]		25	1.9	47 49
Poly(styrene-co-acrylonitrile) [PSAN]		25	0.0032	47 50
Poly(trimethylsilyl propyne) [PolyTMSP]			n.d.	51
Poly(vinyl pyrrolidone) [PVP]				

Polymers for use in PSPs can be divided in three classes: silicones, organic glassy polymers, and fluoropolymers. Silicones like poly(trimethylsilyl propyne) excel in oxygen permeability, but often are not stable over a long period of time. In case of polyTMSP, the double bond is not stable towards irradiation. This makes the polymer lose its outstanding permeability over time.

Organic glassy polymers like polystyrene or poly(styrene-co-acrylonitrile) are much easier to handle. They do not possess the high permeability compared to the silicones but are mechanically stable and their properties are not altered when cast on solid supports in PSP applications. The field of practicability of some components is limited due to the rather low glass transition temperature and the rather low melting point of certain polymers. Polystyrene, for instance, has a glass transition temperature of $\sim 90^\circ\text{C}$ and a melting point of $\sim 240^\circ\text{C}$.^[52,53] Thus, polystyrene is not suitable for application in high-temperature oxygen sensing. Due to the simple chemistry behind the synthesis of the organic glassy polymers, it is possible to tailor binders with properties close to those desired.

The fluoropolymers feature high oxygen permeability and often are more stable than the silicones. Like highly fluorinated indicators, they are more resistant to photooxidation. The carbon-fluorine bond is stable to the highly reactive singlet oxygen that is being formed after photoexcitation of the probe.^[54] Because of their outstanding properties, the fluorinated polymers have become important in aeronautic applications. Poly(hexafluoroisopropyl methacrylate-co-heptafluoro-n-butyl methacrylate) ("FIB", from **f**luoro/**i**sopropyl/**b**utyl) is the American standard

binder in PSPs.^[46] However, FIB polymers require the use of hazardous solvents such as 4-chloro- α,α,α -trifluorotoluene in order to make it sprayable.

Polymers like poly(vinyl pyrrolidone) or some polyurethane-based polymers are soluble in water and/or ethanol, and are more easy to handle. The corresponding solvents are less toxic or less environmentally harmful. The permeability of these polymers for oxygen unfortunately strongly depends on the fraction of water in the polymer. Thus, the binders are cross-sensitive to humidity. Accordingly, these kinds of polymers are not suitable for high-temperature PSPs.^[55-58]

2.3.3. Electrochemical Coating

Any binder will decrease the accessibility of oxygen to the luminescent indicator. This compromises the response times of paints. The groups of Sakaue et al. and of Asai et al. have developed an approach in which no polymer binder is needed, reducing the response time to a minimum. Aluminum surfaces were treated with different acids and bases, and then were electrochemically anodised. This results in a porous metal surface. The size and depth of the pores are very uniform, with a pore diameter of ~20 nm and a layer thickness of ~10 μ m. Treated with its concentrated solution, the pressure indicator diffuses into the pores and will be adsorbed at the surface of the anodised aluminum (AA). In this kind of PSPs the response time to pressure shocks and pulses is only limited by the luminescence lifetime of the indicator applied and can be compared to those of electric pressure transducers.^[19,27,47,59-61] This approach is limited, unfortunately, to aluminum surfaces. Furthermore, the adsorption of indicators onto the porous aluminum surface turns out to be difficult in some cases (e.g. large surfaces).

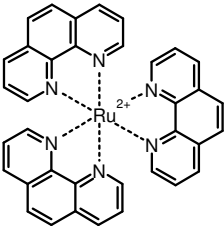
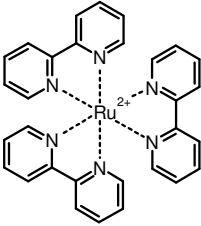
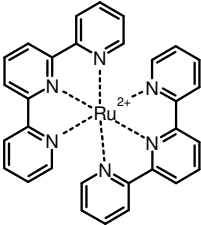
2.3.4. Indicators for Use in TSPs

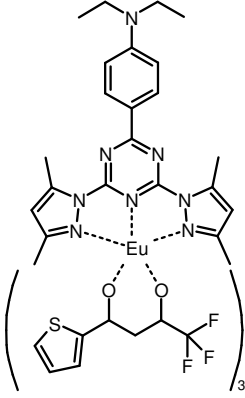
All known indicators for use in pressure-sensitive paints have a temperature-dependent luminescence to a certain extent. Additionally, the oxygen diffusion through the binder is more effective at higher temperatures. This affects both

intensity and lifetime. Nevertheless, in most cases mathematical algorithms can be used to correct the effects of temperature. Alternatively, a temperature-sensitive (but oxygen-insensitive) probe may be added to the pressure-sensitive paint.^[62]

There is also a need to determine exclusively temperature, for instance in cryogenic wind tunnel tests or for combustion studies in turbochargers and turbines. Consequently, certain indicators have to withstand temperatures up to 2000 °C. The first substances applied for that purpose were inorganic compounds, the so-called thermographic phosphors. More recently, metal-ligand complexes are being used as temperature probes but are hardly applicable at temperatures above 200 °C.^[58,63-66] Important indicators for application in TSPs are listed in *table 2.3*.

Table 2.3. Names, acronyms, chemical structures, and photoluminescent properties of typical indicators for use in temperature-sensitive paints

Compound [acronym]	Chemical Structure	$\lambda_{\text{abs}}(\text{max})$	$\lambda_{\text{em}}(\text{max})$	Ref.
$\text{La}_2\text{O}_2\text{S}:\text{Eu}^{3+}$	solid state	385 nm	514 nm	63 65
Ruthenium-tris(1,10-phenanthroline) [Ru(phen) ₃] ²⁺ (various counter ions)		448 nm	579 nm	67 68 69
Ruthenium-tris(2,2'-bipyridine) [Ru(bpy) ₃] ²⁺ (various counter ions)		320 nm 452 nm	588 nm	70
Ruthenium-bis(2,2':6',2''-terpyridine) [Ru(trpy) ₂] ²⁺ (various counter ions)		310 nm 475 nm	620 nm	71

Europium(III)- tris(thenoyltrifluoroacetylacetonato)- (2-(4-diethylaminophenyl)-4,6- bis(3,5-dimethylpyrazol-1-yl)-1,3,5- triazine) [Eu(tta) ₃ (dpbt)]		417 nm	614 nm	50 69 72
--	---	--------	--------	----------------

There is a large variety of indicators for thermographic phosphor thermography, for example $\text{La}_2\text{O}_2\text{S}:\text{Eu}^{3+}$, $\text{Y}_2\text{O}_3:\text{Eu}$, or $\text{YAG}:\text{Dy}$.^[64] These inorganic compounds are very robust in terms of thermal stability. Nevertheless, the development of temperature-sensitive metal-ligand complexes for certain temperature ranges is currently still a field of intensive research. This is because of (a) the lack of sensitivity in the range between 0 and 100 °C, and (b) the limited brightness of thermographic phosphors since they have low molar absorbances.

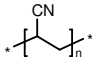
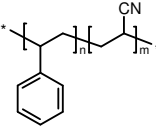
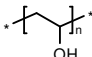
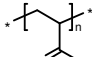
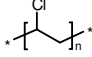
Temperature sensing may also be performed using infrared cameras. This method (IR-thermography) is a powerful tool for direct visualisation of temperature gradients but is applicable to only a limited extent since the spatial resolution of infrared cameras is rather poor and the sensitivity at low temperatures is inadequate. This can be improved, however, by cooling the CCD chip with liquid nitrogen or helium.^[73]

2.3.5 Polymers for Use in TSPs

Like in the case of PSPs, the polymers for use in TSPs have to be mechanically stable. On the other side, they need to be impermeable for oxygen or other gases.^[42] The chemical stability and photostability of the paint is a critical issue since the paint tends to crack because of the uneven thermal contraction and expansion of the binder and the thermographic phosphor, respectively.^[63-65] To eliminate any cross-sensitivity of temperature probes to oxygen, gas-blocking polymers have been used preferably. The chemical structures and properties of common binders for TSP applications are listed in *table 2.4*, respectively. The

polymers listed in *table 2.4* have very low P values and thus prevent diffusion of singlet oxygen which can be harmful to both the probe and the polymer.

Table 2.4. Names, acronyms, chemical structures, and figures of merit of selected polymers for use in temperature-sensitive paints.

Polymer [acronym]	Chemical Structure	P [$10^{-13} \text{ cm}^2 \cdot \text{s}^{-1} \cdot \text{Pa}^{-1}$]	Ref.
Poly(acrylonitrile) [PAN]		0.00015	43 69
Poly(styrene-co-acrylonitrile) [PSAN]		0.0032	43 69
Poly(vinyl alcohol) [PVA]		0.00665 ^{a)}	43
Poly(vinyl methyl ketone) [PVMK]		n. d.	69
Poly(vinyl chloride) [PVC]		0.034 ^{b)}	43

a) at 0% relative humidity

b) unplasticized

2.4. Spectroscopic Methods of Interrogation

There is a large variety of methods for calibrating and evaluating PSPs and TSPs. The most common optical parameters determined are the intensity and decay time of luminescence. They can be measured using different calibration schemes, each of them having advantages and limits. The parameters intensity and lifetime are compared in *table 2.5*, with respect to their pros and cons.

Table 2.5. Advantages and disadvantages of the pressure sensing and temperature sensing based on measurement of I and τ , respectively

Pros	Cons
Intensity: High intensity in case of strong light sources Simple Inexpensive Numerous indicators available	Prone to errors (caused by e. g. uneven coatings, changes in the experimental geometry, or deviations in dye concentration) Dependent on several factors Light field has to be very homogeneous Not self-referenced
Lifetime: Independent of the intensity of the excitation light Self-referenced Independent on the setup Defined lifetime for given indicator	More expensive experimental setup More complex data acquisition Limited number of indicators available

2.4.1. Intensity Imaging

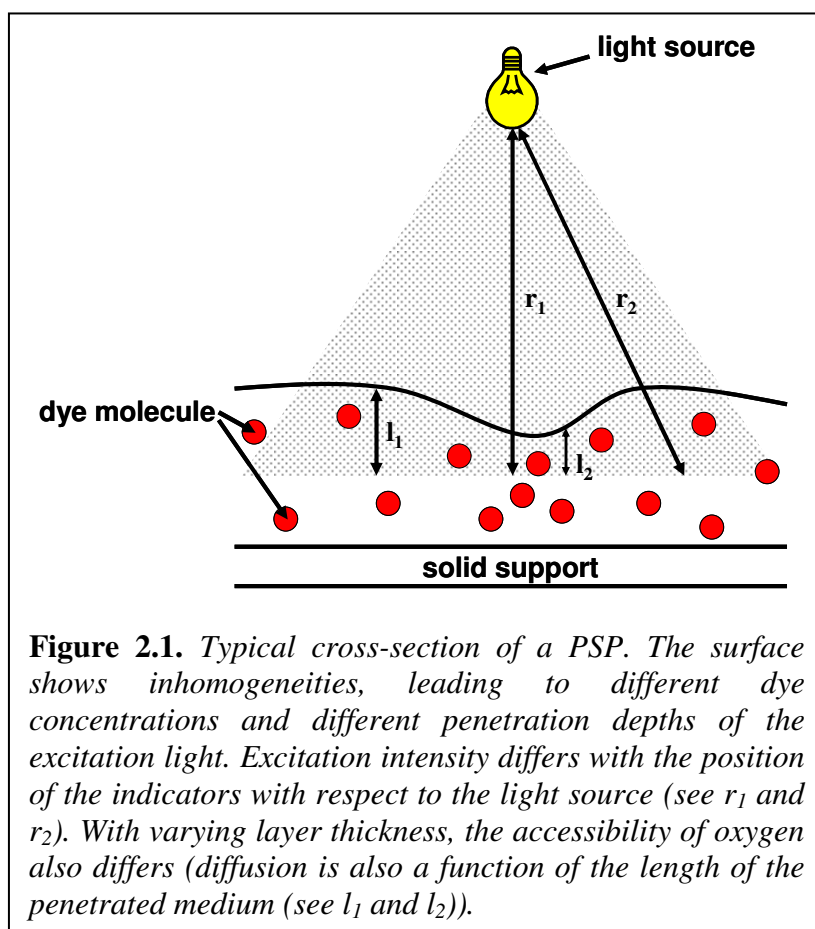
In the simplest case, luminescence is excited continuously and luminescence intensity is imaged. The light source and the CCD camera are controlled and triggered by a computer. The data are conveyed to the CPU and processed. This method is common not only in the case of PSPs and TSPs, but also in fluorescence microscopy, where the analyte (oxygen in the case of PSPs) causes a change in the luminescence intensity of the sensor which is related to its concentration.^[74,75] However, the luminescence intensity detected by the CCD camera not only is dependent on the probe concentration, which becomes apparent when regarding Parker's law:

$$I_L = I_0 \cdot \phi \cdot k \cdot \varepsilon \cdot l \cdot c \quad \text{eq. 2.8}$$

With I_L the intensity of the luminescence, I_0 the intensity of the excitation light, ϕ the quantum yield of the fluorophore, k a geometric constant of the setup, l the length (or thickness) of the penetrated medium, and c the concentration of the

fluorophore in the medium. As it can be seen from *equation 2.8*, the intensity response of a PSP is directly dependent on the intensity of the excitation light. On the one hand, this is an advantage because very high intensities can be achieved by making use of lasers. On the other hand, small deviations in the excitation light field will cause variations in the local intensity. Furthermore, the light intensity is a function of distance. The intensity decreases by $1/(\text{distance})^2$. This effect is very important when considering 3D models.

There is no perfect PSP at present. Deviations in the layer thickness and dye concentration c result in a non-homogeneous intensity response of the sensor (see *figure 2.1*). To avoid this problem, reference dyes are incorporated into the PSP



composition that are widely inert to temperature. Thus, the intensity response of the indicator can be related to the intensity of the reference dye, resulting in a ratio of intensities being only dependent on oxygen concentration.

Additionally, white pigments are often added in order to increase the intensity of luminescence. The emission of light from

PSPs and TSPs has no preferred direction. White additives like titanium dioxide can increase the luminescence seen by the camera.

When studying non-flat surfaces and models with a 3D structure, additional problems may arise. The excitation light may be reflected at a surface and can excite the PSP or TSP of another area, leading to falsified images. This effect can be prevented to some extent by using base coats. These are pigments either applied as additional layer with an extra polymer, or incorporated in the paint.

Base coats can be designed to absorb in the UV-region, thus eliminating the reflection of UV excitation light.

One example for such an intensity based PSP formulation is the system applied at the German Aerospace Center (Deutsches Zentrum für Luft- und Raumfahrt, DLR). It is composed of a pyrene derivative acting as a pressure-sensitive probe, and a europium complex as a reference dye whose emission is not affected by pressure. Both components are excited at 337 nm. The excimer emission of the pyrene is monitored to acquire the pressure information, while the emission of the reference dye is only dependent on the amount of the complex excited.^[28] The ratio R between S_{PSP} and S_{ref} is independent of light source fluctuations. In addition, the adverse effect of uneven surfaces, reflections and scattering of excitation of the excitation beam can be eliminated for the most part. In wind tunnel applications, these measurements are called wind-off images, taken at a well known pressure and defined temperature. The pressure- and temperature dependence of the paint can be described by a modified Stern-Volmer relationship:^[8]

$$f_T(p, p_0) = \frac{I(p_0, T)}{I(p, T)} \quad \text{eq. 2.9}$$

for the pressure dependence of the intensity at a constant temperature, and

$$g_P(T, T_0) = \frac{I(p, T)}{I(p, T_0)} \quad \text{eq. 2.10}$$

for the temperature dependence of the intensity at constant pressure, with p_0 and T_0 as reference pressure and temperature, respectively. The pressure-sensitive paint is called ideal if the function $f_T(p, p_0)$ is independent of temperature and if $g_P(T, T_0)$ is independent of pressure. In wind tunnel applications, the intensity of the wind-off measurements is divided by the results of the intensity obtained at airflow. For the ideal paints, the ratio can be written as

$$\frac{I(p_0, T_0)}{I(p, T)} \approx \frac{f(p, p_0)}{g(T, T_0)} \quad \text{eq. 2.11}$$

If the temperature-dependency of the luminescence of the paint has been determined experimentally, *equation 2.11* can be rewritten as

$$g(T, T_0) \cdot \frac{I(p_0, T_0)}{I(p, T)} \approx f(p, p_0) \quad \text{eq. 2.12}$$

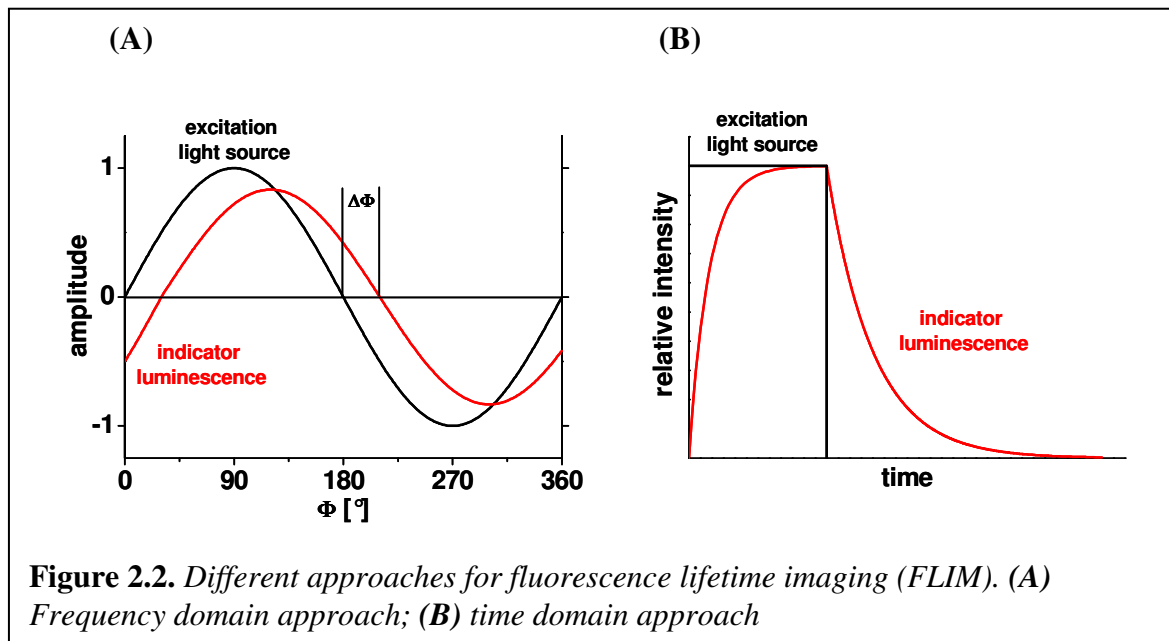
If temperature is known, e.g. from IR thermography, the ratio of signals obtained at wind-off and at wind-on can be multiplied by a single function $g(T, T_0)$ to obtain the

temperature-corrected pressure dependent function $f(p, p_0)$. In the non ideal case, the ratio of wind-off and wind-on measurements has to be multiplied by a function $g_P(T, T_0)$, which unfortunately is dependent on pressure. Thus, the temperature correction becomes more difficult, if not completely impossible.^[45,46]

2.4.2. Fluorescence Lifetime Imaging (FLIM)

The measurement of fluorescence lifetime is superior to the intensity-based approach because it is affected neither by scattering or reflection, the overall intensity of the light field, or by inhomogeneous thickness of the paint. Lifetime can be measured in the time domain or the frequency domain,^[74-80] as it is schematically depicted in *figure 2.2*.

In the frequency domain approach, the fluorophore is excited by sinusoidal modulated light. The luminescence of the probe follows the excitation frequency with a lifetime-dependent delay. This phase shift $\Delta\Phi$ is measured. Time-domain



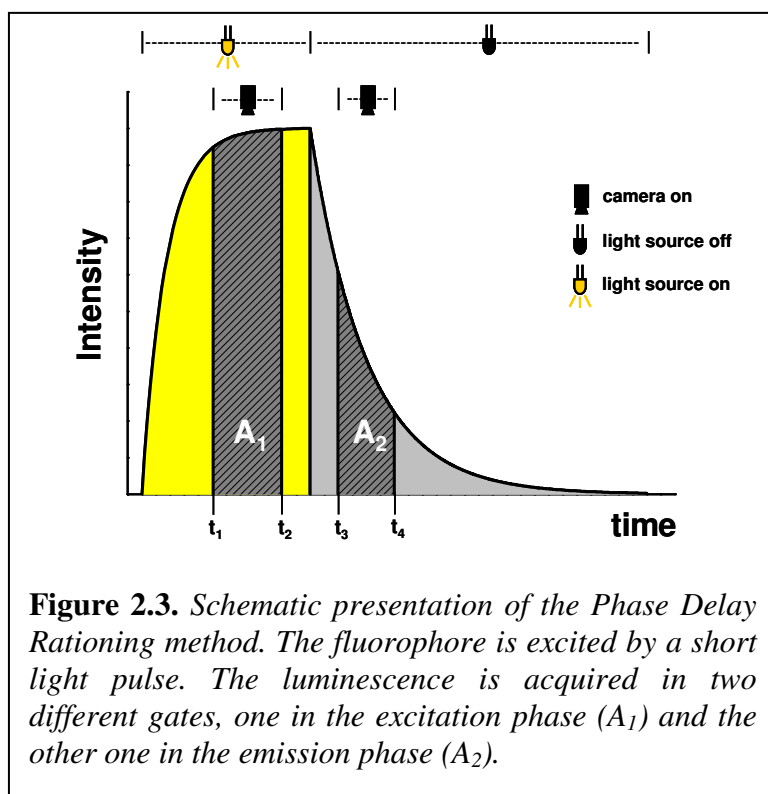
measurements require a square shaped light pulse for exciting the fluorophore. The sensor response rises and falls with a certain delay which is dependent on the luminescence decay time of the fluorophore. In principle, the two methods can be transferred into each other by Fourier transformation. The required setup for detecting lifetimes in the time domain is less complex and less expensive compared to the frequency domain approach. For example, when applying the frequency domain approach to CCD-based imaging, expensive image intensifiers

are mandatory, which can be sinusoidal modulated. Since the luminescence decay times of metal-ligand complexes (MLCs) are in the microsecond time scale, the time domain approach along with the use of MLCs is the method of choice for aerodynamic research and wind tunnel applications. They also enable for elimination of background fluorescence because it usually decays within max 100 nanoseconds and can thus be excluded by starting the measurements after a certain time delay.

There are various methods and schemes for measuring luminescence lifetime. The important methods for time domain imaging are presented and discussed in the following.

2.4.2.1. Phase Delay Rationing (PDR)

The Phase Delay Rationing (PDR) approach is a ratiometric and intrinsically referenced method. The luminescence is excited with a pulsed light source and measured in defined time gates. In the PDR method, schematically explained in figure 2.3., two gated images are taken. The first gate A_1 is located in the



excitation phase of the probe, the second gate A_2 in its emission phase. The ratio of the intensities acquired within the two different time gates is decay time-dependent and represent the intrinsically referenced sensor response.^[76,83,84]

For practical applications it is not essential to determine absolute values for the luminescence lifetime, because this

measurement method is mainly used for imaging of changes in lifetimes, making

the knowledge of absolute lifetime values needless. When applying the same parameters for different measurements, the data received are highly reproducible. One major drawback of the PDR method is the detection of background fluorescence in the first gate A_1 , because it is located in the excitation phase. This makes the method hardly applicable to biological or medicinal applications like for instance imaging tissue or blood samples.

2.4.2.2. Dual Lifetime Referencing (DLR)

This time-resolved imaging method is tightly related to the PDR method discussed above. The relative positions of the gates remain the same. The Phase Delay Rationing method is suitable for luminescence decay time measurements in the microsecond time regime (when applying LEDs as light sources). In practice, many indicators possess a nanosecond decaying fluorescence that is strongly affected by the analyte. The Dual Lifetime Referencing (DLR) calibration scheme is based on the conversion of the fluorescence intensity information into a time-dependent parameter. Therefore, a long decaying reference indicator is added to the system, being completely inert towards the analyte. Both probes are excited simultaneously. With the first gate A_1 (see *figure 2.3.*) the overall intensity is detected, that of the indicator as well as that of the reference dye. The second gate (A_2) is located in the emission phase of the system with an appropriate delay after the excitation pulse. In this way it gathers exclusively the intensity information of the long decaying phosphorescence of the reference dye, because the (short-lived) fluorescence of the indicator has already decayed at this time. It is “gated out”. Since the intensity of the indicator (gathered in A_1) contains the information about the analyte, whereas the phosphorescence is inert against the analyte, the ratio A_1/A_2 displays a referenced intensity distribution that reflects the analyte distribution.^[85,86]

Of course, the DLR calibration method has the same drawback as the PDR method. The intensity in the first gate A_1 is strongly influenced by the autofluorescence of the sample. Additionally, the sensor systems used for “DLR imaging” suffer from effects of photobleaching of the probes. When one of the

indicators bleaches to a certain extent over time, the mixed intensity recorded in the first gate A_1 varies. This results in falsified ratios of A_1/A_2 .

2.4.2.3. Rapid Lifetime Determination (RLD)

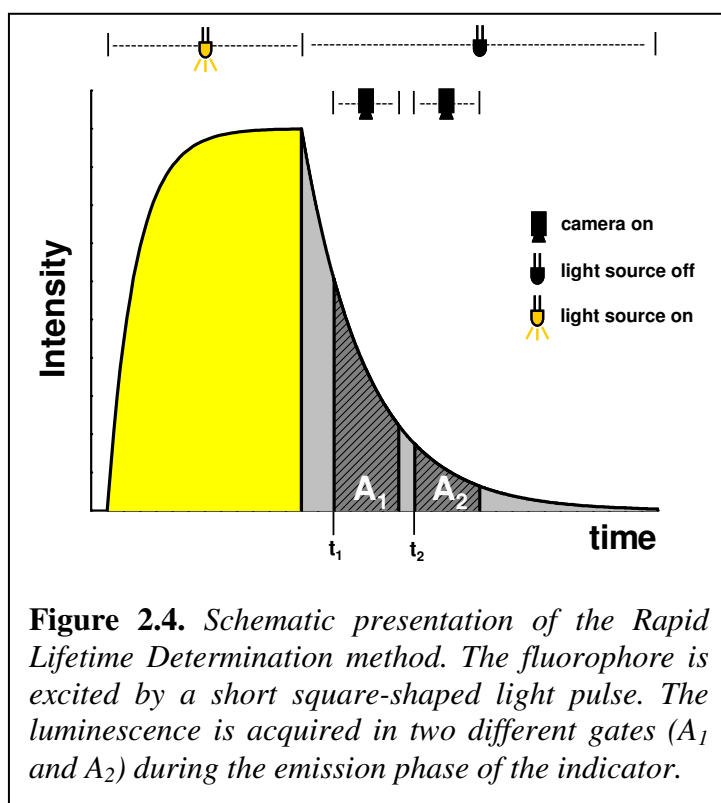
In the Rapid Lifetime Determination method, luminescence is detected in two different gates, both located in the emission phase of the indicator (A_1 and A_2 , see *figure 2.4.*) after a square-shaped excitation pulse. The lifetime-dependent ration of the two intensity images represents the intrinsically referenced sensor response which is thus empirically calibrated against the analyte concentration. The lifetime of the measured luminescence can be calculated according to:

$$\tau = \frac{t_2 - t_1}{\ln \frac{A_1}{A_2}} \quad \text{eq. 2.13}$$

with τ the lifetime, t_1 and t_2 as the times when the different gates start (relative to the end of the excitation pulse) and A_1 and A_2 the intensities gathered in the two gates, respectively. In other words, the lifetime-dependent ratio of the two intensity images represents the intrinsically referenced response of the paint. It is often empirically determined.^[76-78,87,88]

For calculating the lifetime according to *equation 2.13*, the two time windows A_1 and A_2 have to have the same length. As in the PDR method (see *chapter 2.4.2.1*), it is difficult to obtain true values for the decay time, because the equation is only valid for mono-exponentially decaying luminophores.^[89-91] However, for imaging applications it is often sufficient to detect relative changes in lifetime.

Furthermore, the RLD method is less prone to interferences. It is not necessary to correct the alignment of the light field because the luminescence decay time is independent of the overall intensity. On account of this, also effects of inhomogeneous indicator distribution within the sensor layer, coloration, turbidity, reflections, variations in the opto-electronic system, background fluorescence, and varying distance between surface and camera do not adversely affect accuracy. The method even tolerates low levels of ambient light and displacements in the optical setup between calibration and application measurements.^[76,87] In contrast to the DLR method, the Rapid Lifetime Determination is not affected by effects of photobleaching. Even if the fluorophore has lost e.g. 50% of its luminescence



intensity due to bleaching, the relative intensities in the two gates A_1 and A_2 are reduced to the same extent.

The RLD approach is a very powerful tool for the evaluation of luminescence lifetimes. However, their calculation (see *equation 2.13*) assumes monoexponential decay behaviour. The RLD method is often performed with metal-ligand complexes many of which exhibit an at least bi-

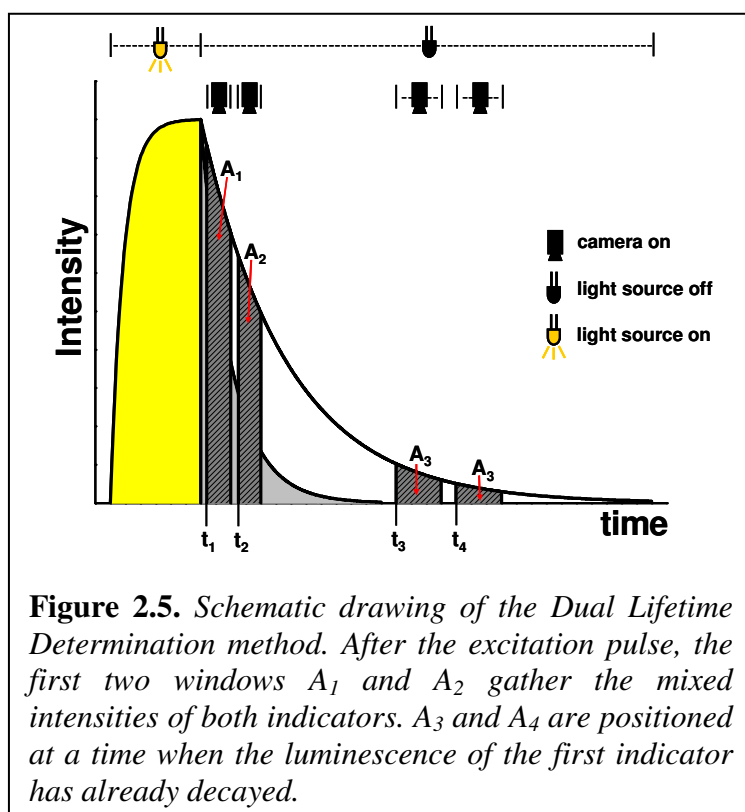
exponential decay. Hence, much effort was made in modifying the existing scheme to obtain more accurate data. This can be achieved by appropriate positioning of the gates. For bi-exponential decay, a 50% overlap of the two gates improves accuracy and precision of the resulting data enormously.^[92] Furthermore, the length of the gates and the relative position to each other play an important role for evaluating lifetimes.^[93] Two or more different τ -values are dominant for the slope of a multi-exponential decay curve at different times, respectively. Thus, the position of the gates may decisively influence the lifetime data obtained. A look at a bi-exponential decay curve reveals that positioning windows A_1 and A_2 in the initial part of the decay curve will result in a smaller τ than if placed at the end.

2.4.2.4. Dual Lifetime Determination (DLD)

In the majority of the cases, the signals obtained with dually sensing paints are separated via the spectral differences of the indicators, either by absorbance or emission, and are measured separately. A more elegant way consists in the acquisition of both signals within one measurement if they can be separated because of differences in the spectra and/or lifetimes.^[86,94] Herein, a measurement

method is presented, which was developed and improved within this work for characterisation of dual sensors, making spectral signal separation gratuitous (see *figure 2.5*). This method is applicable, if the luminescence decay time of one indicator is at least about 10 times higher than the luminescence decay time of the other indicator.

In this calibration scheme, four gated images are taken in the emission phase of the fluorophores. The first two gates (A_1 and A_2) have the same length (gate width) and are positioned in the luminescence phase of both indicators, monitoring a mixed intensity, and hence mixed lifetime, of both probes. The second two gates

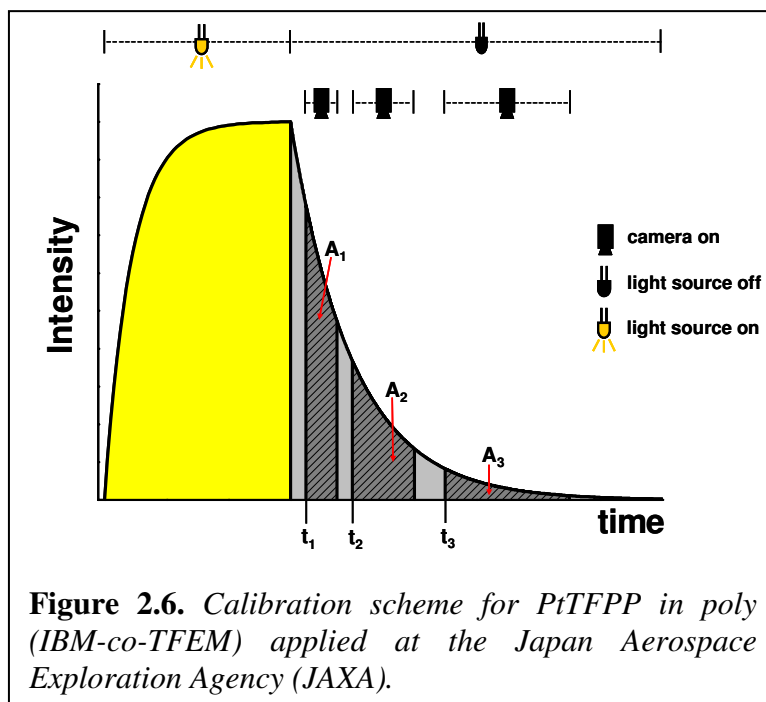


(A_3 and A_4) have also the same gate width and are positioned at a time when the luminescence of the first probe has already decayed. They acquire exclusively the luminescence of the long-decaying second indicator. The first two windows (acquiring the mixed lifetime) do not reflect the true decay time of the first indicator with the shorter lived emission. The intensity is influenced by the

luminescence of the long-lived probe. The luminescence information of the first (short-lived) probe, and thus of the analyte concentration, is monitored by the resulting variation of lifetime.^[95,96] They can be calculated according to *equation 2.13*. Actually, the DLD method is a two-fold RLD-method, capable of detecting the change of the lifetimes of two different indicators at the same time.

2.4.2.5. Alternative Schemes

Modified time-resolved imaging approaches that make use of multiple gating have been developed for both the DLR and RLD method. This also is the result of advances made in CCD, LED, and laser technologies. It is possible, at least in principle, to obtain the complete decay function of the luminescence of an indicator by subsequently opening a large number of gates. The more gates are used, the better the resolution and the more precise are the results, this leading (theoretically) to an infinite number of gates, all of an infinitesimally small width.^[93] In case of indicators of well known decay time, refining the parameter settings will



make the data more precise.^[90] With proper settings along with appropriate positions and widths of the gates it is even possible to monitor two parameters (O_2 , T) with one measurement. In Japanese aerodynamic and wind tunnel research at JAXA, a tailor made calibration scheme for the PSP probe platinum(II)

tetrakis(pentafluorophenyl)porphyrin (PtTFPP) in poly(isobutyl methacrylate-co-trifluoroethyl methacrylate) (poly(IBM-co-TFEM)) has been developed (see figure 2.6.).^[97]

This method accounts for the non-monoexponential luminescence decay of the porhyrin. The parameters are adjusted such that all three gates have the same intensity at reference conditions. The ratios of the intensities of the gates are evaluated applying the standard RLD method:

$$R_{12} = \frac{A_1}{A_2} = f(p, T) \quad \text{eq. 2.14}$$

$$R_{13} = \frac{A_1}{A_3} = f'(p, T) \quad \text{eq. 2.15}$$

Thus, it is possible to obtain two equations for two unknown parameters (pressure and temperature) by only one measurement. Accordingly, pressure and temperature can be measured simultaneously with just one single probe.

2.5. Requirements and Characteristics of the Imaging Setup

From what was explained in *chapter 2.4*, it is obvious that in order to determine luminescence lifetimes applying the time domain method, the components of the setup have to be well coordinated. The requirements and technical specification of the different components of an imaging setup are introduced and discussed in the following sections.

2.5.1 Camera Systems

Time-resolved measurements require the camera and the light source to be triggered synchronously in the nanosecond time regime. This can be achieved using an expensive image intensifier. When making use of metal-ligand complexes (decaying in microsecond time scale), a CCD or CMOS camera with a fast shutter will be sufficient and makes an image intensifier needless. It even tolerates interfering ambient light, which is highly practical in many applications. Cooled digital camera chips are adequate, due to their very low signal-to-noise ratio. Usually, computers control the trigger steps and the data acquisition.

Other systems are available for intensity signal detection but all have their merits and drawbacks. For example, photomultiplier tubes are capable of detecting weak signals, but they do not offer the possibility of imaging intensity distributions due to the non-selective multiplication of all incoming intensity information, resulting in a single overall intensity signal. Common techniques and configurations of the black-and-white digital cameras are specified and explained in the following sections. It has to be pointed out that the class of electron multiplying CCDs (EMCCDs) as well as the streak cameras technique are not discussed in the following, because they are not applicable for time-resolved imaging with high spatial resolution.

2.5.1.1 Interline Cameras

Every second serial pixel column of a interline chip is covered with a thin layer of a light-impermeable metal such as aluminum. The “dark” pixels do not register incoming photons. During the readout of the chip, the light intensity information is transferred from the active columns to the inactive columns, being thus protected from re-exposure. After the transfer, the columns are shifted to the output amplifier and are read out.^[98] The transfer of the pixels to the vicinal “dark” pixel is very fast. Once accomplished, the next image can be taken without the readout being completed. In other words, a second photo can be shot while the first one is still on the chip.

2.5.1.2. Frame Transfer Cameras

This kind of chip is also composed of active areas and a storage area. The active pixels register light intensity when exposed to light. The storage area – as in interline chips – is blinded. After image recording, the image information on the active area is transferred to the coated (inactive) region. The pixels are read, row by row, from this storage area. The active pixel array can be re-exposed already during readout.^[98] The process of transferring the information to the active area is not as fast as the analogue process in interline chips. Furthermore, the frame transfer technique is susceptible to cross-talk, because the transfer of the information over many lines takes more time.

2.5.1.3. Full Frame Cameras

Unlike interline and frame transfer chips, full frame arrays do not possess a storage area. All pixels are sensitive to light. The intensity information is read row by row after exposure. A new image can be taken as soon as the “old” image is completely read by the output amplifier. This limits the speed and performance of the system. In addition, the full frame technique is prone to image smearing. This

disadvantage can be widely eliminated by the application of shutters, but this necessitates fast and precise triggering steps.

2.5.1.4. Intensified CCD Cameras

The intensified CCD (ICCD) chip is suitable for detecting even weak signals. Before reaching the chip, the incoming photons are converted to electrons by a photocathode. Each electron is converted into a cloud of electrons (more than 1000 electrons per incident electron) by a multiplier, the so-called microchannel plate. The cloud hits an electroluminescent screen and causes the emission of much more photons than initially entered the photocathode. Light is then guided to a CCD chip by a tapered fiber-bundle.^[99,100]

2.5.1.5. Areas of Application of the Various Cameras

There are mainly four characteristics to be considered when selecting the most appropriate camera: visualization speed, resolution, sensitivity, and noise. A first differentiation has to be made between ordinary CCDs and ICCDs, because the different CCD techniques feature virtually the same main characteristics, however with differences in terms of speed.

CCD-based systems can acquire and process image data much faster than intensified cameras. However, for luminescence imaging applications, this advantage in speed has to be put into perspective. Luminescence usually is not of strong intensity. Thus, the exposure time has to be increased when using conventional CCD cameras, and this compromises the advantage of faster electronic processing. In case of low intensity, the CCDs are slower than the ICCDs. Intensified CCDs detect thousands of signals per incoming photon, and this results in better-quality images at a given exposure time. The ICCDs also are faster because they have fewer pixels, so less information has to be read out. Accordingly, the spatial resolution is not very high. On the other side, CCD cameras enable binning. In this process, a certain number of pixels is combined to form a single (combined) pixel. For example, when applying 4x4 binning, the

intensity will be higher by a factor of 16 but of course at only 1/16 of the spatial resolution. This is a very efficient way to speed up cameras.

The choice of the camera system also depends on the field of application. If the signal is low and the observed process is fast, an ICCD camera is preferable. However, for the bigger part of aerodynamic applications, a cooled CCD camera is more than adequate. The typical time needed for cooled CCD cameras to acquire a single image is ~100 ms (including parameter transfer from the computer to the camera and image readout), depending on the amount of pixels and number of bits. The intensity of the luminescence emitted by the indicator dye also depends on the brightness of the light source. However, in case of indicators with low absorbance and low quantum yield, in case of weak light sources, and of imaging over large distances, ICCD cameras are clearly preferable.

The performance of any camera system is limited by several noise sources. They can be divided into three main types: shot noise, dark current noise and readout noise. The shot noise is an inevitable effect based on the quantum nature of photons. It emerges from statistical variations in the overall number of photons emitted from the object (indicator). This noise source is the limit for any camera system in terms of signal-to-noise ratio (SNR).

CCD chips are made of silicone. In this kind of substrate, temperature can generate electrons. Hence, there is a temperature-dependent current in CCD chips causing the so-called dark current noise. Cooling the chip can significantly reduce the dark current. For example, a non-cooled chip might generate a dark current of approx. 300 e/s/pixel at 20 °C. This effect can be reduced to a value of 1 e/s/pixel when cooling the chip down to -40 °C. However, the dark current effect is reproducible for a given temperature and can thus be corrected by dark image subtraction.^[101]

After exposing the CCD chip to light, the generated charge on each pixel has to be digitalized and processed. Therefore, the charges have to be shifted and amplified. It may then happen that electrons are left behind or change their relative position. This effect causes the readout noise which is thus dependent on the frame rate.

The SNR of a CCD is limited by the readout noise, especially at low light intensity. Under these conditions, the SNR of ICCDs is shot-noise limited which is the ideal case for any camera system. As it was said before, ICCD outperforms

the cooled CCD at low light conditions, until the limit of approx. 400 photons per pixel is reached. At values greater than that, the cooled CCD is preferable.^[101]

2.5.2 Light Sources

Light sources are expected to have high output and – in case of time-resolved measurements – to allow for high pulse frequencies. Lasers represent the ideal form of such light sources. However, certain types of lasers are expensive, and the available wavelengths are limited. More seriously, the laser beam is rather focused. Thus, only a confined area of the paint is excited. For imaging a whole aircraft model, a scanning system has to be installed. This increases the complexity of the setup. Alternatively, the laser may be guided to the site of interest by applying lenses, mirrors, and/or fiber optics. This has become shown to work for pressure or temperature imaging using microplates or confocal microscopes.^[85,102,103] Laser diodes are particularly attractive in being compact, easy to drive, and (mostly) suitable for high frequency operation. They cover the wavelength range from 280 nm to above 2000 nm, but those of $\lambda < 370$ nm are expensive.

With a wavelength range from approx. 250 nm up to 600 nm, mercury lamps and xenon flash lamps are most useful. Almost any desired excitation wavelength can be chosen by using appropriate optical filters. These systems are rather compact.

Light emitting diodes (LEDs) are the light sources of choice due to their low costs, compactness, output, efficiency, pulse rates, and flexibility. LEDs can be triggered in the nanosecond timescale, are bright and easy to handle, thereby reducing the demands on the experimental setup. They are mostly employed in the form of LED arrays (“batteries”).

Given the number of possible combinations of materials for use in PSPs and TSPs, of possible spectroscopic schemes (from intensity to decay time resolution), of geometries, cameras, and light sources, it does not come as a surprise, that there is no generally applicable approach.

2.6. State of the Art

PSPs and TSPs have been, and are, widely applied to aerodynamic wind tunnel testing. In cooperation between NASA and the University of Washington, dual PSP systems were developed that make use of the platinum porphyrin PtTFPP or the platinum porpholactone PtTFPL (structures see *chapter 2.3.1.*) as oxygen-sensitive probes, and e.g. a magnesium meso(pentafluorophenyl)porphyrin as a reference probe. All components are incorporated in fluorinated block polymers such as FIB as binder.^[18,36,46,104,105]

Intense research also is being performed in Japan within the MOSAIC (molecular sensors for aerodynamic research) project and its subsequent programs. The PSPs are based on the use of ruthenium polypyridyl complexes and on platinum porphyrins. New binders and polymers with superior permeability for oxygen also were developed. New approaches like the anodized aluminum PSP and polymers acting as pressure-sensitive probes were elaborated, and the accuracy and performance of existing paints were improved.^[106-120]

Polycyclic aromatic hydrocarbons (PAHs) like pyrene, pyrene butyric acid, pyrene sulfonic acid and their derivatives have had a large impact on wind tunnel research. The PSPs used in Europe are mainly based on pyrene derivatives, and are applied in aerodynamic research facilities like those of DLR (Germany),^[121,122] ONERA (France),^[123,124] and BAE Systems (UK).^[125]

2.7. References

- [1] J. R. Lakowicz, *Principles of Fluorescence Spectroscopy*, 2nd edition, Kluwer Academic/Plenum Publishers, New York, Boston, Dordrecht, London, Moscow, **1999**
- [2] H. G. O. Becker, *Einführung in die Photochemie*, 3rd revised edn., Verlag der Wissenschaften, Berlin, **1991**
- [3] B. Valeur, *Molecular Fluorescence – Principles and Applications*, Wiley-VCH, Weinheim, **2002**
- [4] S. G. Schulman, *Fluorescence and Phosphorescence Spectroscopy: Physicochemical Principles and Practice*, Pergamon press, Oxford, **1977**
- [5] P. W. Atkins, J. dePaula, *Physical Chemistry*, 7th edn., Oxford University press, Oxford, **2002**
- [6] A. A. Alberty, R. J. Silbey, *Physical Chemistry*, 2nd edn., John Wiley & Sons, New York, Chichester, Brisbane, Toronto, Singapore, **1997**

- [7] S. H. Maron, J. B. Lando, *Fundamentals of Physical Chemistry*, Collier MacMillan Publishers, London, **1974**
- [8] V. Stern, M. Volmer, *Physik Z.* **1919**, 20, 183
- [9] E. R. Carraway, J. N. Demas, B. A. DeGraff, *Langmuir* **1991**, 7, 2991
- [10] S. Draxler, M. E. Lippitsch, *Anal. Chem.* **1996**, 68, 753
- [11] X. Lu, M. A. Winnik, *Chem. Mater.* **2001**, 13, 3449
- [12] J. N. Demas, B. A. DeGraff, *Anal. Chem.* **1991**, 63, 829A
- [13] T. Liu, B. T. Campbell, J. P. Sullivan, *Exp. Therm. Fluid Sci.* **1995**, 10, 101
- [14] M. A. Woodmansee, J. C. Dutton, *Exp. Fluid* **1998**, 24, 163
- [15] L. M. Coyle, M. Gouterman, *Sens. Actuators B* **1999**, 61, 92
- [16] G. Liebsch, I. Klimant, O. S. Wolfbeis, *Adv. Mater.* **1999**, 11, 1296
- [17] Y. Amao, K. Asai, I. Okura, *J. Porphyrin Phthalocyanine* **2000**, 4, 292
- [18] B. Zelelow, G. E. Khalil, G. Phelan, B. Carlson, M. Gouterman, J. B. Callis, L. R. Dalton, *Sens. Actuators B* **2003**, 96, 304
- [19] M. Kameda, T. Tabei, K. Nakakita, H. Sakaue, K. Asai, *Meas. Sci. Technol.* **2005**, 16, 2517
- [20] Y. Sakamura, M. Matsumoto, T. Suzuko, *Meas. Sci. Technol.* **2005**, 16, 759
- [21] W. J. Bowyer, W. Xu, J. Demas, *Anal. Chem.* **2004**, 76, 4374
- [22] E. R. Carraway, J. N. Demas, B. A. DeGraff, J. R. Bacon, *Anal. Chem.* **1991**, 63, 332
- [23] J. R. Bacon, J. N. Demas, *Anal. Chem.* **1987**, 59, 2780
- [24] O. S. Wolfbeis, H. E. Posch, H. W. Kroneis, *Anal. Chem.* **1985**, 57, 2556
- [25] J. I. Peterson, R. V. Fitzgerald, D. K. Buckhold, *Anal. Chem.* **1984**, 56, 63
- [26] Y. Amao, *Mikrochim. Acta* **2003**, 143, 1
- [27] M.-C. Merienne, Y. LeSant, J. Ancelle, D. Soulevant, *Meas. Sci. Technol.* **2004**, 15, 2349
- [28] C. Klein, R. H. Engler, U. Henne, W. E. Sachs, *Exp. Fluids* **2005**, 39, 475
- [29] J. B. Basu, K. S. Rajam, *Sens. Actuators B* **2004**, 99, 459
- [30] C. J. M. Brugman, P. J. van Scerpenzeel, R. P. H. Rettschnik, *J. Chem. Phys.* **1973**, 58, 3468
- [31] M. E. Cox, B. Dunn, *Appl. Optics* **1985**, 24, 2114
- [32] S.-K. Lee, I. Okura, *Spectrochim. Acta A* **1998**, 54, 91
- [33] Y. Amao, T. Miyashita, I. Okura, *J. Porphyrin Phthalocyanin* **2000**, 5, 433
- [34] S.-K. Lee, I. Okura, *Anal. Comm.* **1997**, 34, 185
- [35] C. M. McGraw, J. H. Bell, G. Khalil, J. B. Callis, *Exp. Fluids* **2006**, 40, 203
- [36] M. Gouterman, J. Callis, L. Dalton, G. Khalil, Y. Mebarki, K. R. Cooper, M. Grenier, *Meas. Sci. Technol.* **2004**, 15, 1986
- [37] M. Gouterman, R. J. Hall, G.-E. Khalil, P. C. Martin, E. G. Shankland, R. L. Cerny, *J. Am. Chem. Soc.* **1989**, 111, 3702
- [38] S.-W. Lai, Y.-J. Hou, C.-M. Che, H.-L. Pang, K.-Y. Wong, C. K. Chang, N. Zhu, *Inorg. Chem.* **2004**, 43, 3724
- [39] D. B. Papkovsky, G. V. Ponomarev, W. Trettnak, P. O'Leary, *Anal. Chem.* **1995**, 67, 4112
- [40] K. Asai, K. Nakakita, K. Teduka, *Proceedings of the 19th International Congress in Instrumentation in Aerospace Simulation Facilities (ICIASF)*, Cleveland, Ohio, USA, 27.-30. August, **2001**, 25
- [41] O. S. Wolfbeis, *Fiber Optic Chemical Sensors and Biosensors*, Vols. 1-2, CRC Press, Boca Raton, Florida, USA, **1991**
- [42] R. A. Potyrailo, *Angew. Chem.* **2006**, 118, 718
- [43] S. Pauly, *Permeability and Diffusion Data*, in: *Polymer Handbook*, 4th edn, (eds: J. Brandrup, E. H. Immergut, E. A. Grulke), John Wiley & Sons, New York, Chichester, Weinheim, Brisbane, Singapore, Toronto, **1999**
- [44] G. Liebsch, I. Klimant, B. Frank, G. Holst, O. S. Wolfbeis, *Appl. Spec.* **2000**, 54, 548
- [45] S. Gouin, M. Gouterman, *J. Appl. Polym. Sci.* **2000**, 77, 2805

- [46] E. Puklin, B. Carlson, S. Gouin, C. Costin, E. Green, S. Ponomarev, H. Tanji, M. Gouterman, *J. Appl. Polym. Sci.* **1999**, 77, 2795
- [47] K. Asai, Y. Amao, Y. Iijima, I. Okura, H. Nishide, *J. Thermophys. Heat Transfer* **2002**, 16, 109
- [48] Y. Amao, K. Asai, T. Miyashita, I. Okura, *Polym. Adv. Tech.* **2000**, 11, 705
- [49] S. Gouin, M. Gouterman, *J. Appl. Polym. Sci.* **2000**, 77, 2815
- [50] S. M. Borisov, O. S. Wolfbeis, *Anal. Chem.* **2006**, 78, 5094
- [51] Y. Amao, T. Komori, H. Nishide, *React. Funct. Polym.* **2005**, 63, 35
- [52] F. P. Reding, J. A. Faucher, R. D. Whitman, *J. Polym. Sci.* **1962**, 57, 483
- [53] R. Dedeurwaerder, J. F. M. Oth, *J. Chim. Phys.* **1959**, 56, 940
- [54] N. Yi-Yan, R. M. Felder, W. J. Koros, *J. Appl. Polym. Sci.* **1980**, 25, 1755
- [55] V. Compan, L. Lopez, A. Andrio, A. Lopez-Aleman, M. F. Refojo, *J. Appl. Polym. Sci.* **1998**, 72, 321
- [56] C.-W. Lim, C.-G. Kim, W.-Y. Kim, Y.-S. Jeong, Y.-S. Lee, *Bull. Korean. Chem. Soc.* **1999**, 20, 672
- [57] C. Weinmüller, C. Langel, F. Fornasiero, C. J. Radke, J. M. Prausnitz, *J. Biomed. Mat. Research* **2005**, 77A, 230
- [58] J. I. Eldridge, T. J. Benic, S. W. Allison, D. L. Beshears, *J. Therm. Spray. Tech.* **2004**, 13, 44
- [59] K. Nakakita, T. Yamazaki, K. Asai, N. Teduka, A. Fuji, M. Kameda, *Proceedings of the 21st AIAA Aerodynamic Measurements Technology and Ground Testing Conference*, Denver, CO, USA, 19.-22. June **2000**
- [60] H. Sakaue, J. P. Sullivan, Y. Egami, Y. Iijima, K. Asai, R. H. Engler, U. Beifuss, F. Doering, *Proceedings of the 19th International Congress in Instrumentation in Aerospace Simulation Facilities (ICIASF)*, Cleveland, Ohio, USA, 27.-30. August, **2001**, 186
- [61] M. Kameda, N. Tezuka, T. Hangai, K. Asai, K. Nakakita, Y. Amao, *Meas. Sci. Technol.* **2004**, 15, 489
- [62] M. E. Köse, A. Omar, C. A. Virgin, B. F. Carroll, K. S. Schanze, *Langmuir* **2005**, 21, 9110
- [63] A. Omrane, G. Särner, M. Alden, *Appl. Phys. B* **2004**, 79, 431
- [64] J. P. Feist, A. L. Heyes, S. Seefeldt, *Meas. Sci. Technol.* **2003**, 14, N17
- [65] L. M. Coyle, M. Gouterman, *Sens. Actuators B* **1999**, 61, 92
- [66] S. W. Allison, G. T. Gillies, *Rev. Sci. Instrum.* **1997**, 68, 2615
- [67] G. Liebsch, I. Klimant, O. S. Wolfbeis, *Adv. Mater.* **1999**, 11, 1296
- [68] Z. Wang, A. McWilliams, C. Evans, X. Lu, S. Chung, M. Winnik, I. Manners, *Adv. Funct. Mater.* **2002**, 12, 415
- [69] S. M. Borisov, T. Mayr, A. A. Karasyov, I. Klimant, P. Chojnacki, C. Moser, S. Nagl, M. Schäferling, M. I. Stich, G. S. Vasilevskaya, O. S. Wolfbeis, *Springer Series on Fluorescence, Vol. 4: Fluorescence of Supramolecules, Polymers, and Nanosystems* (ed. M. N. Berberan-Santos), Springer, Berlin, Heidelberg, **2008**
- [70] T. Liu, B. T. Campbell, S. P. Burns, J. P. Sullivan, *Appl. Mech. Rev.* **1997**, 50, 227
- [71] R. Erausquin, C. Cunningham, J. P. Sullivan, K. Asai, H. Kanda, T. Kunimasu, Y. Iijima, *AIAA Paper*, **1998**, 98-0588
- [72] C. Yang, L.-M. Fu, Y. Wang, J.-P. Zhang, W.-T. Wong, X.-C. Ai, Y.-F. Qiao, B.-S. Zou, L.-L. Gui, *Angew. Chem. Int. Ed.* **2004**, 43, 5009
- [73] Y. Le Sant, M. Marchand, P. Millan, J. Fontaine, *Aerospace Sci. Technol.* **2002**, 6, 355
- [74] D. S. Miller, S. Letcher, D. M. Barnes, M. David, *Am. J. Physiol.* **1996**, 271, 508
- [75] L. Paglario, *Adv. Mol. Cell Biol.* **1995**, 11, 93
- [76] G. Liebsch, *Ph.D. thesis*, **2000**, University of Regensburg, Regensburg, Germany
- [77] G. Marriott, R. M. Clegg, D. J. Arndt-Jovin, T. M. Jovin, *Biophys. J.* **1991**, 60, 1374

- [78] X. F. Wang, T. Uchida, D. M. Coleman, S. Minami, *Appl. Spec.* **1991**, 45, 360
- [79] C. G. Morgan, A. C. Mitchel, *Chromosome Res.* **1996**, 4, 261
- [80] J.W. Holmes, *The Aeronautical Journal* **1998**, Paper 2306, 189
- [81] K. König, S. Böhme, N. Leclerc, R. Ahuja, *Cell. Mol. Biol.* **1998**, 44, 763
- [82] T. W. J. Gadella, A. van Hoek, A. J. W. G. Visser, *J. Fluoresc.* **1997**, 7, 35
- [83] P. Hartmann, W. Ziegler, *Anal. Chem.* **1996**, 68, 4512
- [84] P. Hartmann, W. Ziegler, G. Holst, D. W. Lübbers, *Sens. Actuators B* **1997**, 38, 110
- [85] T. Mayr, C. Igel, G. Liebsch, I. Klimant, O. S. Wolfbeis, *Anal. Chem.* **2003**, 75, 4389
- [86] G. Liebsch, I. Klimant, C. Krause, O. S. Wolfbeis, *Anal. Chem.* **2001**, 73, 4345
- [87] J. N. Demas, W. M. Jones, R. A. Keller, *Anal. Chem.* **1986**, 58, 1717
- [88] R. J. Woods, S. Scypinski, L. J. Cline Love, H. A. Ashworth, *Appl. Spec.* **1984**, 45, 360
- [89] R. Ballew, J. N. Demas, *Anal. Chem.* 1989, 61, 30
- [90] S. P. Chan, Z. J. Fuller, J. N. Demas, B. A. DeGraff, *Anal. Chem.* **2001**, 73, 4486
- [91] S. P. Chan, Z. J. Fuller, J. N. Demas, F. Ding, B. A. DeGraff, *Appl. Spec.* **2001**, 55, 1245
- [92] K. K. Sharman, A. Periasamy, H. Ashworth, J. N. Demas, N. H. Snow, *Anal. Chem.* **1999**, 71, 947
- [93] C. Moore, S. P. Chan, J. N. Demas, B. A. DeGraff, *Appl. Spec.* **2004**, 58, 603
- [94] C. M. Schroeder, L. Polerecky, I. Klimant, *Anal. Chem.* **2007**, 79, 60
- [95] S. Nagl, M. I. J. Stich, M. Schäferling, O. S. Wolfbeis, *Anal. Bioanal. Chem.* **2008**, available online
- [96] M. I. J. Stich, S. Nagl, O. S. Wolfbeis, U. Henne, M. Schäferling, *Adv. Funct. Mater.* **2008**, 18, 1399
- [97] K. Mitsuo, K. Asai, A. Takahashi, H. Mizushima, *Meas. Sci. Technol.* **2006**, 17, 1282
- [98] J. C. Feltz, M. A. Karim, *Appl. Opt.* **1990**, 29, 717
- [99] A. Frenkel, M. A. Sartor, M. S. Wlodawski, *Appl. Opt.* **1997**, 36, 5288
- [100] J. L. A. Fordham, C. F. Moorhead, R. F. Galbraith, *Mon. Not. R. Astron. Soc.* **2000**, 312, 83
- [101] D. Dussault, P. Hoess, *Proceedings of SPIE* **2004**, 5563, 195
- [102] M. Schäferling, M. Wu, J. Enderlein, H. Bauer, O. S. Wolfbeis, *Appl. Spec.* **2003**, 57, 1386
- [103] R. Cubeddu, D. Comelli, C. D'Andrea, P. Taroni, G. Valentini, *J. Phys. D: Appl. Phys.* **2002**, 35, R61
- [104] G. E. Khalil, C. Costin, J. Crafton, G. Jones, S. Grenoble, M. Gouterman, J. B. Callis, L. R. Dalton, *Sens. Actuators B* **2004**, 97, 13
- [105] R. J. Morris, J. K. Donovan, J. T. Kegelmann, S. D. Schwab, R. L. Levy, R. C. Crites, *AIAA Journal* **1993**, 31, 419
- [106] Y. Amai, K. Asai, I. Okura, *J. Porphyrin Phthalocyanine* **2000**, 4, 179
- [107] Y. Amai, K. Asai, T. Miyashita, I. Okura, *J. Porphyrin Phthalocyanine* **2000**, 4, 19
- [108] Y. Amai, K. Asai, T. Miyashita, *Chem. Letters* **1999**, 10, 1031
- [109] M. Obata, Y. Tanaka, N. Araki, S. Hirohara, S. Yano, K. Mitsuo, K. Asai, M. Harada, T. Kakutchi, C. Ohtsuki, *J. Polym. Sci. A : Polym. Chem.* **2005**, 43, 2997
- [110] Y. Fujiwara, Y. Amai, *Sens. Actuators B* **2004**, 99, 130
- [111] Y. Fujiwara, Y. Amai, *Sens. Actuators B* **2003**, 89, 187
- [112] Y. Fujiwara, Y. Amai, *Sens. Actuators B* **2003**, 89, 58
- [113] Y. Amai, I. Okura, *Sens. Actuators B* **2003**, 88, 162
- [114] Y. Fujiwara, Y. Amai, *Sens. Actuators B* **2002**, 85, 175
- [115] Y. Amai, Y. Tabuchi, Y. Yamashita, K. Rimura, *Europ. Polym. J.* **2002**, 38, 675
- [116] Y. Amai, Y. Ishikawa, I. Okura, *Anal. Chimica Acta* **2001**, 445, 177
- [117] Y. Amai, T. Miyashita, I. Okura, *React. Funct. Polym.* **2001**, 47, 49

- [118] Y. Amao, I. Okura, T. Miyashita, *Chem Letters* **2000**, 29, 934
- [119] Y. Amao, I. Okura, T. Miyashita, *Chem. Letters* **2000**, 29, 1286
- [120] Y. Amao, K. Asai, T. Miyashita, *Anal. Commun.* **1999**, 36, 367
- [121] R. H. Engler, C. Klein, O. Trinks, *Meas. Sci. Technol.* **2000**, 11, 1077
- [122] U. Fey, R. H. Engler, Y. Egami, Y. Iijima, K. Asai, U. Jansen, J. Quest, *20th International Congress on Instrumentation in aerospace Simulation Facilities (ICIASF) 2003 Record*, Göttingen, Germany, 25.-29. August **2003**, 77
- [123] R. H. Engler, M.-C. Merienne, C. Klein, Y. Le Sant, *Aerospace Sci. Technol.* **2002**, 6, 313
- [124] Y. Le Sant, M.-C. Merienne, *Aerospace Sci. Technol.* **2005**, 9, 285
- [125] J. R. Kingsley-Rowe, G. D. Lock, A. G. Davies, *Royal Aeronautical J.* **2003**, 107, 1

CHAPTER 3

Dual Pressure-Sensitive and Temperature-Sensitive Paint for Wind Tunnel Applications

As mentioned in *chapter 2*, there is no ideal pressure- or temperature-sensitive paint suitable for all kinds of wind tunnel applications. There are several types of wind tunnels with certain specifications and setups, designed and built for different areas of research, respectively. Thus, it is obvious that pressure-sensitive and temperature-sensitive paints have to be prepared and optimized for various types of applications. The different wind tunnel systems and their specifications along with complementary possibilities for analyzing the surface of interest (e.g. aircraft models) are discussed in the following chapter.

3.1. Wind Tunnels and Model Analysis

Wind tunnels are facilities to investigate the aerodynamic and aeroacoustic properties and effects when air is moving around or over solid objects. The heart of a wind tunnel is the fan (or arrays of fans), a nozzle to accelerate the air flow, one or more flow rectifiers to guarantee laminar air flow, and the measurement section where the model is mounted. Wind tunnel tests are most often applied for aircraft or car models, turbo machines, and rotors. However, other objects such as skyscrapers, chimneys, or bridges gained in importance during the last years. It is obvious that different flow velocity and experimental setups are needed for all these different systems of interest.

Table 3.1. *Different types of wind tunnels and the speed of air flow they generate.*

type of wind tunnel	flow velocity [Mach]
low speed: <i>subsonic</i>	$0 < Ma < 0.3$
high speed: <i>high subsonic</i>	$0.4 < Ma < 0.75$
<i>transonic</i>	$0.75 < Ma < 1.2$
<i>supersonic</i>	$1.2 < Ma < 5$
<i>hypersonic</i>	$5 < Ma < 15$

Even if considering aircraft models only, there are different types of wind tunnels depending on the type of aircraft. The different types of wind tunnels can be classified due to the flow velocity they generate (see *table 3.1*).^[1] No matter which air flow speed is applied, the model of interest as well as its influence on the air flow has to be analyzed. Therefore, optical methods are preferred, because they itself do neither interfere with the air flow nor the model. Important parameters to be analyzed during a wind tunnel test are e.g. air flow field around the model, changes in the object itself, temperature and heat transfer, and of course absolute pressure and pressure changes on the surface of the model. Some of the methods applied are given in *table 3.2*.

Table 3.2. *Optical methods for determining important parameters in aerodynamic wind tunnel research*

Parameter	Method	Ref.
flow field	particle image velocimetry (PIV)	[2] [3]
	background oriented schlieren method (BOS)	[3] [4]
	temperature-sensitive paints (TSP)	[5]
deformation	Moiré interferometry	[6] [7]
	image pattern correlation technique (IPCT)	[8]
pressure	pressure-sensitive paints (PSP)	[9] [10] [11]
temperature	temperature-sensitive paints (TSP)	[11] [12] [13] [14]
	IR thermography	[15] [16] [17]

The methods mentioned in *table 3.2* are only the optical approaches for quantifying important parameters like e.g. deformation or translation of parts of the model (IPCT, Moiré), absolute pressure/temperature and pressure/temperature gradients (PSP/TSP, IR-thermography) on the surface or transition from laminar to turbulent flow (PIV, BOS), just to mention a few. They are often combined with non-optical methods like e.g. pressure determination with pressure taps. Furthermore, the different techniques often are combined in order to obtain maximum data precision or to compensate for undesired side-effects.

One of the most important variables in aerodynamic research is the so called Reynolds number Re . It specifies the ratio of inertial forces to viscous forces and can be written as:^[18]

$$\text{Re} = \frac{\text{inertial forces}}{\text{viscous forces}} = \frac{\rho \cdot v \cdot L}{\eta} \quad \text{eq. 3.1.}$$

with ρ as the density of the medium, v the velocity of flow, L the length of the object, and η the dynamic viscosity. This dimensionless number describes the relation between size and speed of an object in a given medium (air, water,...). More precisely, a definite Reynolds number can be assigned to e. g. a passenger plane travelling in cruising altitude at a certain speed. Studying a model of this passenger plane in a wind tunnel at the same speed will result in erroneous data. This is due to a) the smaller size of the model and b) the different density of the air flow in the wind tunnel and in the plane's cruising attitude. In other words, the Reynolds numbers of both systems differs.^[18,19] To overcome this effect, it is possible to decrease the temperature and to increase the density (and therewith decrease viscosity) of the air in the wind tunnel. The latter is accomplished in cryogenic wind tunnels by cooling down the air with liquid nitrogen.

It becomes obvious, that the different methods for analysing an aircraft model (see *table 3.2*) are not applicable to all wind tunnel systems. IR-cameras for example can not be used in cryogenic wind tunnels, due to their very poor performance at low temperatures. PSPs and TSPs are very versatile systems for optical sensing. Existing paints can be tuned or new systems can be invented to meet the requirements of given aerodynamic tasks. In other words, by choosing appropriate indicator molecules, materials for particles, and polymer binders, new paints can be tailor-made for certain areas of application.

3.2. The System PtTFPL and Ru(phen)₃(TMS)₂/PAN in FIB

As mentioned above, every single component of a PSP/TSP system has to be chosen such, that it meets the requirements of the aerodynamic problem. They have to be fine-tuned to exhibit maximum accuracy and precision in the given area of application. In the course of this dissertation, a new approach for a dual PSP/TSP for subsonic and/or transonic wind tunnel applications was elaborated. The choice of the components and their optical and chemical properties are explained and discussed in the following chapters.

3.2.1. Choice of Materials

The materials applied in the paints have to fulfil certain prerequisites. They have to be sensitive in the desired pressure and temperature range, be photostable, and exhibit high extinction coefficients and quantum yields. The response time has to be very short and the paint has to be sprayable with excellent adhesion on the model.

3.2.1.1. PtTFPL

Pt²⁺ and Pd²⁺ porphyrins are well established indicators for gaseous and dissolved oxygen (DO).^[20] They have distinct opto-chemical advantages compared to other metal porphyrins or their free base.^[21,22] Thus, various platinum and palladium porphyrin species were invented and applied for optical oxygen sensing. The most successful compounds are summarized in *table 3.3*.

Table 3.3. *Platinum(II) and palladium(II) porphyrin complexes applied for optical oxygen sensing*

porphyrin system (<i>acronym</i>) ^{a)}	metal
octaethyl porphyrin (<i>OEP</i>)	Pt ²⁺ , Pd ²⁺
octaethyl porphyrin ketone (<i>OEPK</i>)	Pt ²⁺ , Pd ²⁺
tetrakis(pentafluorophenyl) porphyrin (<i>TFPP</i>)	Pt ²⁺ , Pd ²⁺

tetrakis(pentafluorophenyl) porpholactone (TFPL)	Pt ²⁺
tetraphenyl tetrabenzo porphyrin (TPTBP)	Pd ²⁺
a) for exact IUPAC nomenclature, please see chapter “Abbreviations, Acronyms, and Symbols”	

All the metallo-porphyrins mentioned in *table 3.3* exhibit some extraordinary properties. They show, besides at least one Q-Band, an intense absorption band around 400 nm, the so-called B-band or Soret-Band, where the molecule can be excited directly into the S₂-state. Therefore, the absorption coefficients are very high. They all possess a large Stokes'-shift, facilitating the separation of excitation light from the luminescence. Typical luminescence lifetimes are in the range from 50 μs – 150 μs for the Pt-porphyrins and 250 – 1600 μs for the analogous palladium complexes. The optical properties of the different porphyrins are summarized in *table 3.4*.

Table 3.4. Photoluminescence properties of Pt²⁺ and Pd²⁺ porphyrins applied for optical oxygen sensing

compound	λ _{abs} (max) [nm]	λ _{em} (max) [nm]	φ [%]	τ [μs]	Ref.
PtOEP	381, 535	646	~ 50 ^{a)}	100 ^{a)}	[20] [23]
PdOEP	393, 512, 546	663	~ 50 ^{a)}	770 ^{a)}	[20] [24]
PtOEPK	398, 592	758	12 ^{a) b)}	60 ^{a) b)}	[25] [26]
PdOEPK	410, 603	790	1 ^{a) b)}	455 ^{a) b)}	[25] [26]
PtTFPP	395, 541	648	9 ^{a) b)}	50 ^{a) b)}	[27] [28]
PdTFPP	406, 518, 552	653	21 ^{c)}	1650 ^{c)}	[29]
PtTFPL	392, 527	745	60 ^{c)}	70 ^{c)}	[30] [31]
PdTPTBP	450, 625	795	8 ^{a) d)}	250 ^{a) d)}	[32] [33] [34]

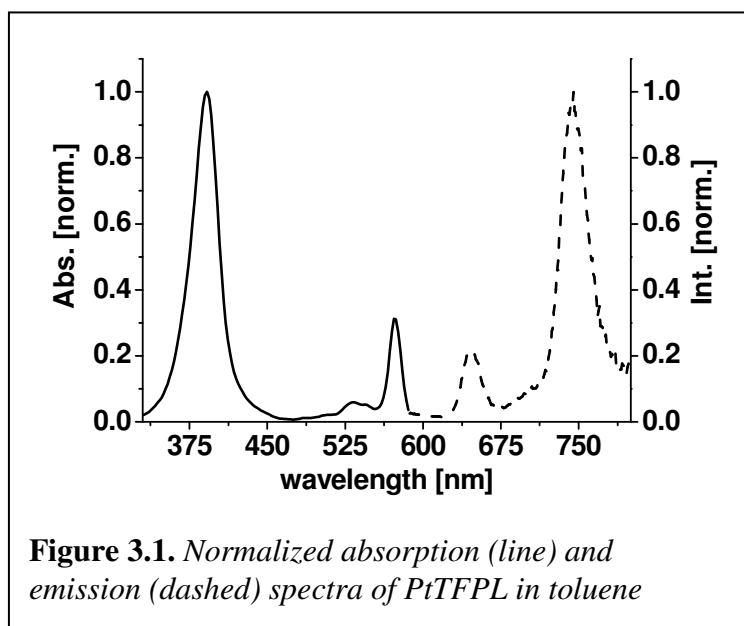
a) room temperature b) ambient air c) at 77 K d) absence of oxygen

One prerequisite set by us was that the indicators had to be excitable with LEDs, preferably at 405 nm. The pressure-sensitive probe should exhibit good sensitivity and precision in the range from ~700 mbar up to ~1300 mbar. Particularly, the palladium porphyrins are almost fully quenched in this region. This effect can be compensated for by embedding the probes into polymer particles with a medium oxygen permeability coefficient *P*, thus extending the dynamic range of pressure determination. However, the encapsulation of the dyes in these kinds of polymers

will increase the response time of the system, which is not desirable for possible unsteady measurements.

From the group of Pt-compounds, the octaethyl porphyrin (PtOEP) suffers from substantial photobleaching and is therefore not feasible for wind tunnel applications. Further developments of these porphyrin systems yielded in the octaethyl porphyrin ketones (PtOEPK, PdOEPK).^[25,26] They are 10 times more photostable than the OEP analogues.^[20]

The highly fluorinated complexes PtTFPP and the corresponding lactone PtTFPL are the most stable metalloporphyrins. Their perfluorophenyl substituents



represent strong electron-withdrawing groups and therefore raise the redox potential of the system and diminish the electron density of the porphyrin ring.^[20,27,35] These effects render the pentafluorophenyl substituted complexes PtTFPP, PdTFPP, PtTFPL) not susceptible for photooxidation and -reduction. One

crucial advantage of the PtTFPL compared to PtTFPP is the red-shifted emission (~ 100 nm, see *table 3.4*). Absorption and emission spectra of PtTFPL are depicted in *Fig 3.1*. The NIR emission of the porpholactone offers more possibilities for the combination with temperature probes, because most of them emit in the red region of the spectrum.

3.2.1.2. Ru(phen)₃(TMS)₂ in Poly(acrylonitrile)

Unlike probes for optical oxygen sensing, indicators for temperature are not very numerous. There are mainly two types of compounds suitable for temperature sensing besides the inorganic thermographic phosphors: Eu³⁺ and Ru²⁺ complexes. Many of the Eu metal-ligand complexes are only excitable in the UV and are therewith not compatible with 405 nm LED excitation. They all show the typical narrow Eu emission at 614 nm (⁵D₀). Special compounds were designed during the last 5 years that extend the absorption range into the visible part of the spectrum.^[30,36,37] However, they all are not easy to synthesize and are somewhat chemically instable (e.g. towards polar solvents), making them hard to apply in aerodynamic research.

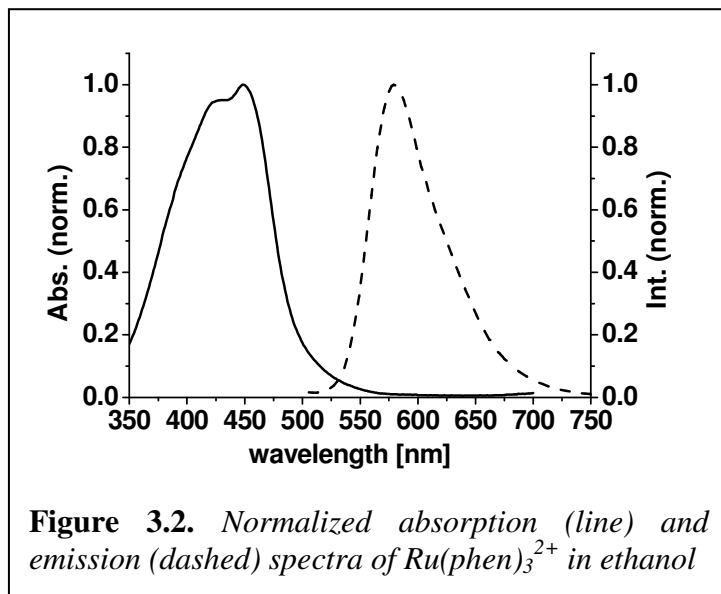
Ruthenium(II)-imine complexes are very attractive compounds for optical sensing. They exhibit fairly large extinction coefficients, good luminescence quantum yields, and are photostable. Their typical brightness *B*s is between 1,000 and 20,000. On this account, they are well established in the area of optical sensing of various compounds.^[38-40] As it can be seen, the Ru-imine complexes often respond to more than one analyte, which is not very desirable for application. For example, the ruthenium tris(4,7-diphenyl-1,10-phenanthroline) (Ru(dpp)₃²⁺) also is a common probe for oxygen sensing.^[41-45] The related ruthenium tris(1,10-phenanthroline) (Ru(phen)₃²⁺) exhibits more or less the same spectral properties, but its oxygen sensitivity is reduced to a certain extent. The major advantage of these kinds of Ru-complexes is the possibility to block possible interferents (e.g. oxygen) by the choice of appropriate polymer matrices.^[46] On this account, Ru(II)-imine complexes are common probes for temperature. Some of the ruthenium complexes applied for temperature sensing are summarized in *table 3.5*.

Table 3.5. *Some of the Ru(II)-imine complexes applied in TSP formulations. These are the basic structures from which a huge variety of derivatives was introduced for T-sensing.*

compound ^{a)}	binder	T-range	Ref.
Ru(bpy) ₃ ²⁺	shellac	0 °C to 80 °C	[5]
Ru(trpy) ₂ ²⁺	DuPont ChromaClear	- 175 °C to -85 °C	[47]
Ru(phen) ₃ ²⁺	poly(acrylonitrile)	0 °C to 60 °C	[36] [46] [48]

a) *for exact IUPAC nomenclature, please see chapter "Abbreviations, Acronyms, and Symbols"*

The Ru(phen)_3^{2+} complex shows a broad absorption band between 300 and 500 nm and is therefore fully compatible with 405 nm LED excitation. The broad



emission band between 550 and 700 nm does not interfere with the emission of the oxygen indicator PtTFPL, and its luminescence is temperature-dependent in the range from 0 °C to 60 °C. It can be easily encapsulated into poly(acrylonitrile) (PAN) particles in a very straightforward procedure. Amongst

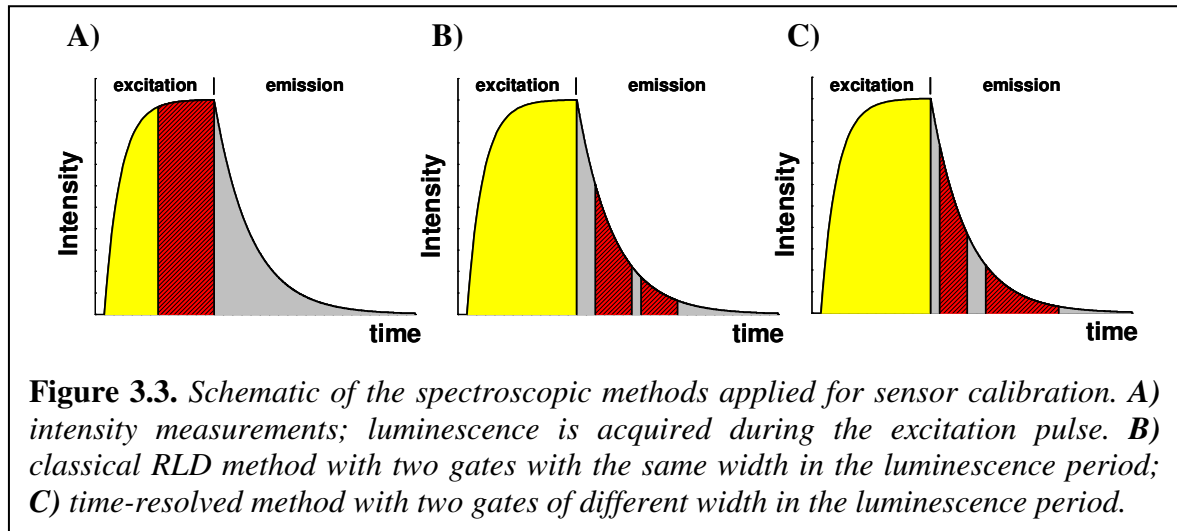
the group of gas-blocking polymers, PAN possesses the lowest gas permeability coefficient P of $1.5 \cdot 10^{-17} \text{ cm}^2 \cdot \text{Pa} \cdot \text{s}^{-1}$.^[49] The normalized absorption and emission spectra of Ru(phen)_3^{2+} are depicted in figure 3.2.

3.2.1.3. FIB Matrix Polymer

Ever since the early days of optical sensing, improving matrix polymer systems required strong development efforts.^[50] From poly(styrene) as standard polymer, over sol-gel materials^[46,51] and silicones,^[52,53] the scientist discovered and improved more and more oxygen-permeable binders. They soon realized the benefits of fluorinated poly(methacrylate) block polymers. Polymers like poly(isobutyl methacrylate-co-trifluoroethyl methacrylate) (poly(IBM-co-TFEM)) or poly(hexafluoroisopropyl methacrylate-co-heptafluoro-n-butyl methacrylate) (FIB) exhibit extraordinary oxygen permeability, are chemically and mechanically stable, and, unlike many of the silicones, are feasible for unsteady measurements.^[54-57]

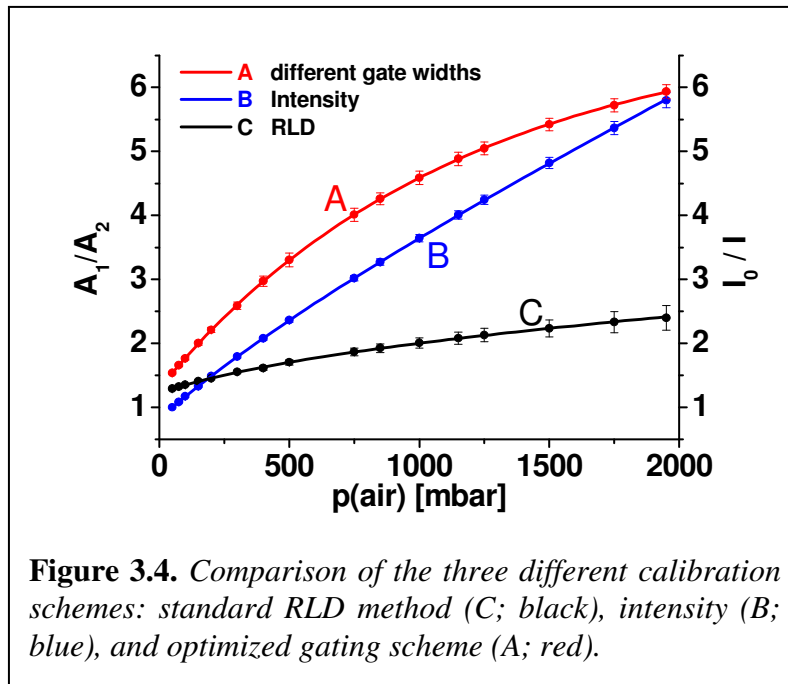
3.2.2. Intensity versus Time-Resolved Imaging

As outlined in *Chapter 2*, lifetime-based imaging offers substantial benefits compared to intensity-based imaging. Time-resolved imaging schemes like the Rapid Lifetime Determination or the Dual Lifetime Determination are self-referenced methods. They are independent of external influences (e.g. ambient light) or intrinsic interference factors (e.g. autofluorescence, dye concentration, photobleaching etc.).^[58,59] At a closer look the question arises, if these spectroscopic methods are comparable in terms of signal deconvolution and resolution. A sensor layer consisting of PtTFPL in poly(IBM-co-TFEM) was calibrated applying different calibration schemes to evaluate these effects (see *sections 3.5.3 and 3.5.4* in the Experimental Part). The sensor was mounted in the calibration chamber (see Experimental Part) and calibrated using a) intensity measurements, b) the classical RLD method, and c) time-resolved imaging with different gate widths. The gate settings applied are schematically depicted in *figure 3.3*.



The luminescence of the system is recorded during the excitation pulse, when measuring intensity (see *Fig 3.3 A*). Therefore, the intensity is very strong. Due to the proneness to errors like uneven dye distribution in the sensor, the intensity signal I is referenced against a standard intensity value I_0 or I_{ref} . In case of aerodynamic research, these reference pictures are often the so-called wind-off images (see *chapter 2*). Two gates A_1 and A_2 are taken in the luminescence period of the system in case of the Rapid Lifetime Determination (RLD) scheme (see *Fig. 3.3 B*). The ratio of the intensities in these two gates is used to calculate

luminescence lifetimes (see *eq. 2.13*). When the intensity of the indicator is reduced (e.g. due to oxygen quenching), the intensity in both gates is reduced to a certain extent. The signal change is further “mathematically” reduced when calculating A_1/A_2 . An overlap of the gates of 50% to 75% is proposed for maximum lifetime precision when dealing with unknown lifetimes.^[60,61] However, these settings are inadequate for determining lifetime changes over a wider range (see figure 3.4). Several optimized gating schemes were proposed in order to overcome the drawbacks of the standard RLD method.^[10,62] Gates with different



widths are set during the luminescence time of the indicator (e.g. $A_1=15 \mu\text{s}$, $A_2=30 \mu\text{s}$) to get rid of the poor signal change (see *Fig. 3.3 C*). This is of particular advantage, because the signal change is much higher than in the standard RLD method and the parameters can be easily adjusted to the

dynamic range of interest. The calibration data of the sensor applying the different spectroscopic schemes are depicted in *figure 3.4*. As it can be seen, the results obtained with the optimized gating approach are comparable with those of the intensity measurements. The RLD method on the other hand is hardly applicable over a large pressure range. The optimized time-resolved method furthermore entails the benefits of intrinsically referenced methods, and is therefore superior to intensity measurements. It turned out, that the best results can be achieved, when the first gate A_1 is opened during the excitation pulse (data not shown).

3.3. Application of the Paint

The feasibility of the system PtTFPL as oxygen probe and Ru(phen)₃(TMS)₂/PAN as temperature probe in FIB as matrix polymer was investigated in the facilities of the German Aerospace Center (Deutsches Zentrum für Luft- und Raumfahrt, DLR), from March 6. -14. 2008 at the Institute of Aerodynamics and Flow Technology in Göttingen, Germany.

3.3.1. Composition and Coating Tests

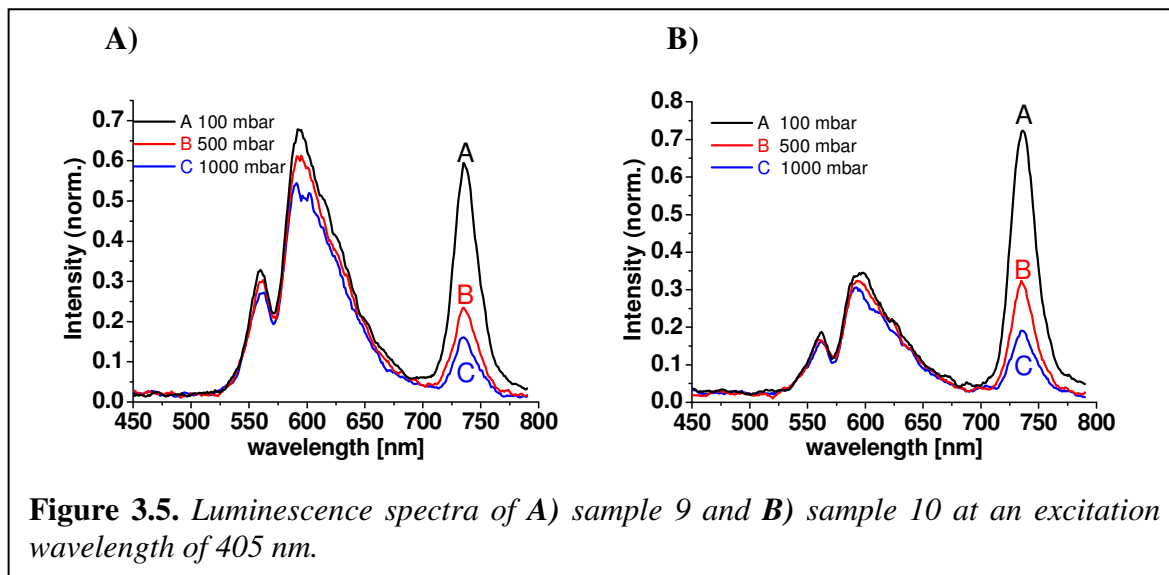
In order to study the adhesion properties of the system, 3x3 cm² aluminum plates were coated with different compositions of the paint (see *table 3.6*). The aluminium supports were pre-coated with a Cloucryl[®] / titanium dioxide screenlayer. Tests were conducted with poly(IBM-co-TFEM) and later with FIB (both provided by Dr. V. Ondrus from the University of Hohenheim, Germany). Different solvents for spraying were tested in order to improve spraying results and to minimize the toxicity. Some of the paint compositions are given in *table 3.6*. The samples were prepared in an analogous procedure like described in *section 3.5.3* in the Experimental Part.

Table 3.6. *Composition of the paints applied for coating tests on alumina plates*

sample No.	content [mg/mL]		
	particles	PtTFPL	polymer
1	3.040	0.100	101.060
2	3.020	0.050	100.140
3	3.040	0.025	100.220
4	1.520	0.050	100.140
5	1.040	0.050	100.080
6	0.680	0.050	101.320
7	1.980	0.050	50.420
8	2.040	0.050	26.020
9	1.014	0.100	100.114
10	1.040	0.100	50.400

It turned out that the solvents ethylacetate, tetrahydrofurane, toluene, and 4-chloro- α,α,α -trifluorotoluene (4-chlorobenzotrifluoride) were appropriate for spraying. Other solvents like methanol or chloroform did dissolve the components of the paint as well, but were not well sprayable.

The samples 9 and 10 were also prepared with FIB as matrix polymer and 4-chloro- α,α,α -trifluorotoluene as solvent. Again, the paints were sprayed onto pre-coated aluminum plates. The samples were then mounted in a calibration chamber and the luminescence spectra were taken at different air pressures (see figure 3.5). The paints just differ in the amount of matrix polymer (FIB). However, the signal of the $\text{Ru(phen)}_3(\text{TMS})_2/\text{PAN}$ particles in sample 9 is much higher than that in sample 10. This is most probably due to the better adhesion of the particles



because of the higher amount of binder in sample 9. The pressure range in the planned wind tunnel test is expected to be between approx. 800 mbar and 1100 mbar. Hence, the composition of sample 10 was adapted for the coating of the aircraft model, because the ratio of the signals of $\text{Ru(phen)}_3(\text{TMS})_2/\text{PAN}$ and PtTFPL is more advantageous at higher pressures.

3.3.2. Wind Tunnel Test

The coating of the aircraft model is described in the following section. Furthermore, the wind tunnel and its specifications are presented. The experimental setup for time-resolved imaging, along with the aerodynamic measurements are presented and discussed.

3.3.2.1. Aircraft Model and Experimental Setup

A classical delta wing (see *figure 3.6*) was chosen as a model system for the aerodynamic measurements. This wing configuration is well known and the flow effects on this system are fully explored and understood.^[63] The delta wing model

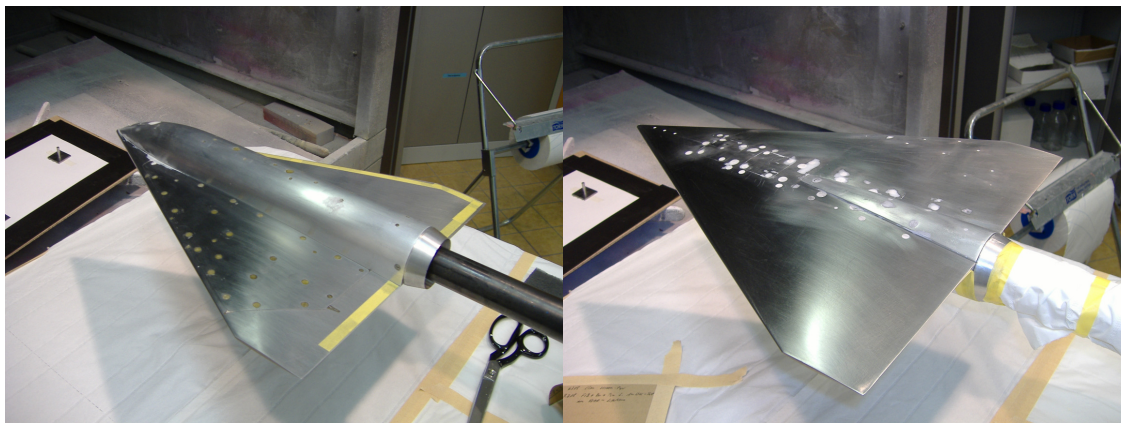


Figure 3.6. *The delta wing model applied for aerodynamic measurements; left: bottom side, right: upper surface;*

is equipped with 48 pressure taps for pointwise pressure determination. The taps as well as three PT-100 temperature sensors are mounted on the right half of the delta wing. The required components were installed inside the wing for not altering the surface properties (and therewith the air flow over it).

The delta wing was pre-coated with a Cloucryl[®] / titanium dioxide screenlayer to increase the luminescence intensity during the measurements. The dual PSP/TSP was deposited onto this highly reflective basecoat. A total amount of 11 mg of PtTFPL, 110 mg of the Ru(phen)₃(TMS)₂ / PAN particles, and 5.5 g of the FIB polymer, altogether in 110 mL of 4-chloro- α,α,α -trifluorotoluene was sprayed onto the upper side of the model. All spraying steps – coating with screenlayer as well as spraying the binary paint – were performed by Dr. Christian Klein from the

Institute of Aerodynamics and Flow Technology of the DLR in Göttingen. The paint was allowed to dry over night. Markers were set onto the delta wing (see *figure 3.7*) in order to guarantee an unambiguous data evaluation after the measurements. The different probes of the paint are imaged with two different

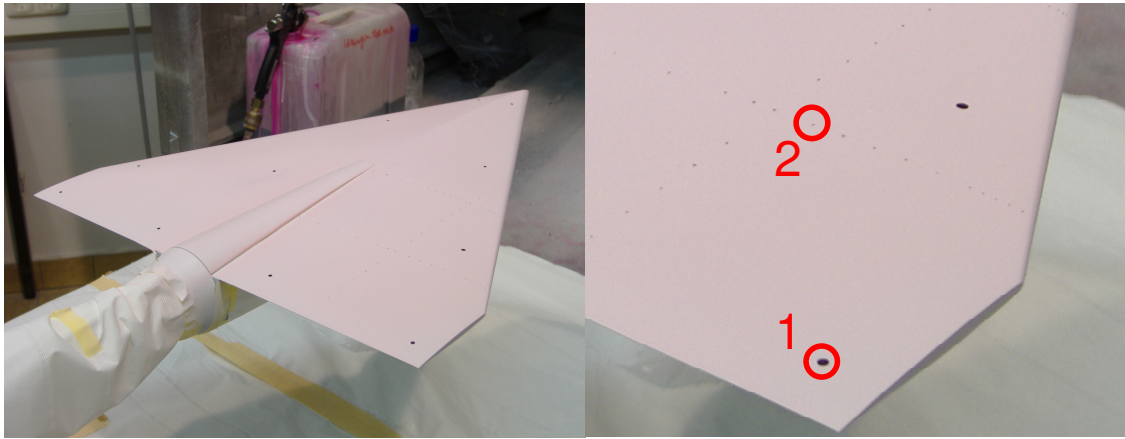


Figure 3.7. *Left: the completely coated delta wing (screenlayer and paint); Right: part of the right wing with the markers (1) and the pressure taps (2)*

cameras, both of them in a slightly different angle towards the model. The markers allow the evaluation software to compensate automatically for this effect.

The measurements were conducted at the 1 meter low-speed wind tunnel in Göttingen. This facility is an open wind tunnel with a one meter test section (see *figure 3.8*, left panel). The maximum flow velocity is 65 m/s. The delta wing model



Figure 3.8. *Left: the 1-meter low-speed open wind tunnel at the Institute of Aerodynamics and Flow Technology of the German Aerospace Center (DLR) in Göttingen. Right: the delta wing attached on the angle transmitter and mounted in the measurement section of the wind tunnel.*

was attached to an angle transmitter and mounted in the test section of the wind tunnel (see *figure 3.8*, right panel). The angle transmitter allows for remote changing of the angle of attack relating to the air flow in the wind tunnel. All

components of the delta wing (pressure taps, PT-100...) were connected to the read-out electronics for online monitoring of pressure and temperature.

Time-resolved luminescence measurements were performed applying two high power LED pods mounted directly above the delta wing aircraft model (see *figure 3.9*). The luminescence was perceived with two PCO 4000 digital black-and-white CCD cameras. They were equipped with two optical filters for separating the signal of interest (PtTFPL for pressure and $\text{Ru}(\text{phen})_3^{2+}$ particles for temperature), respectively. They were also mounted above the test section, in close vicinity to the light sources (see *figure 3.9*). Additionally, an IR-camera was installed to verify

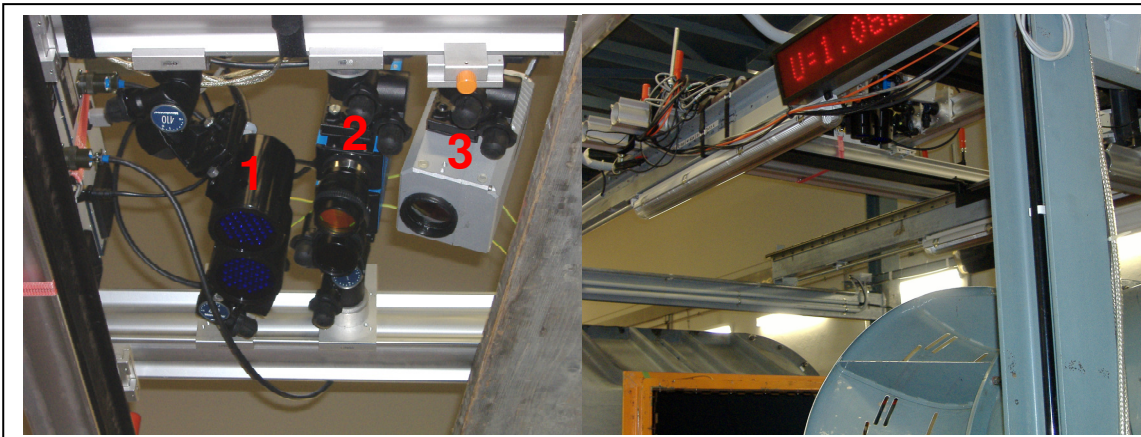


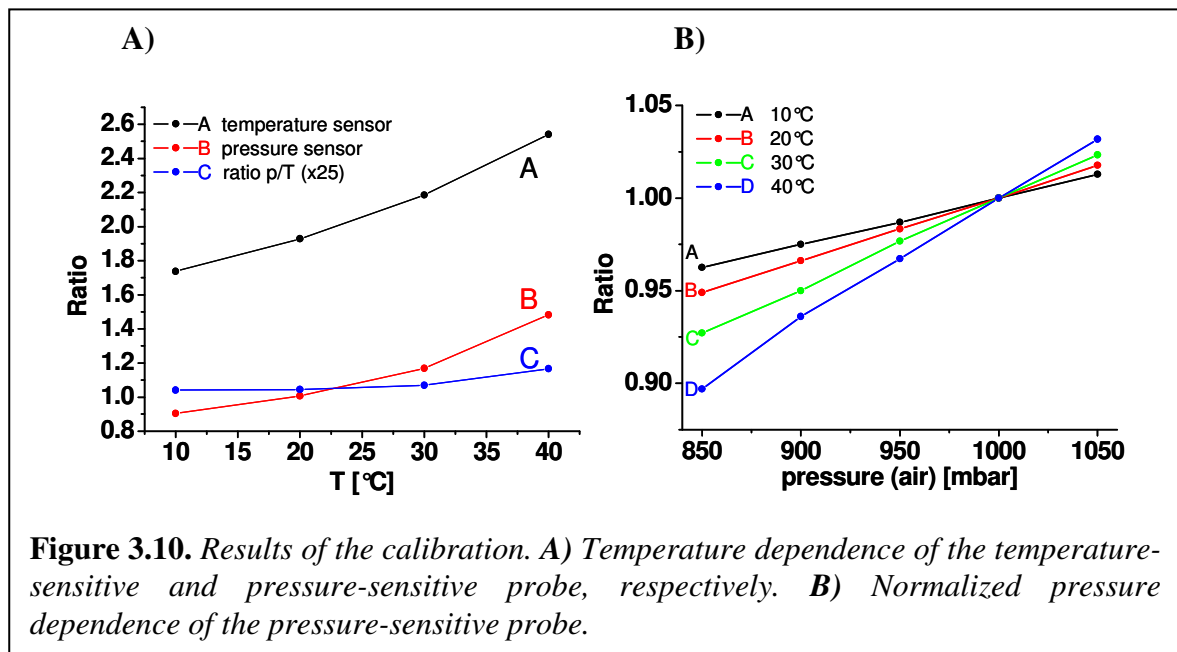
Figure 3.9. *Left: experimental setup for time-resolved imaging with (1) two high power LED pods, (2) two PCO 4000 CCD cameras, and (3) one IR-camera. Right: the complete setup mounted directly above the measurement section.*

the temperature data received from the temperature probe of the dual paint. All components were connected to the electronics in the measurement and control station for triggering the components and for remote data acquisition.

3.3.2.2. Results

3.3.2.2.1. Calibration

The prepared paint composition (see *section 3.5.3*) was additionally sprayed on aluminum plate (pre-coated with a screenlayer) and was calibrated in a pressure cell. The same cameras and filters as applied in the wind tunnel test were used. All calibration results were performed by Dr. Ulrich Henne from the Institute of Aerodynamics and Flow Technology of the German Aerospace Center (DLR) in Göttingen. The calibration data reveal that both the temperature and pressure probe exhibit the same temperature dependence (except for a factor) between 10 °C and 30 °C (see *figure 3.10*). This is advantageous for the application, because the compensation for temperature effects of the pressure probe can be accomplished by simply dividing the data from the pressure probe by those of the temperature probe. The temperature dependence between 10 °C and 30 °C is



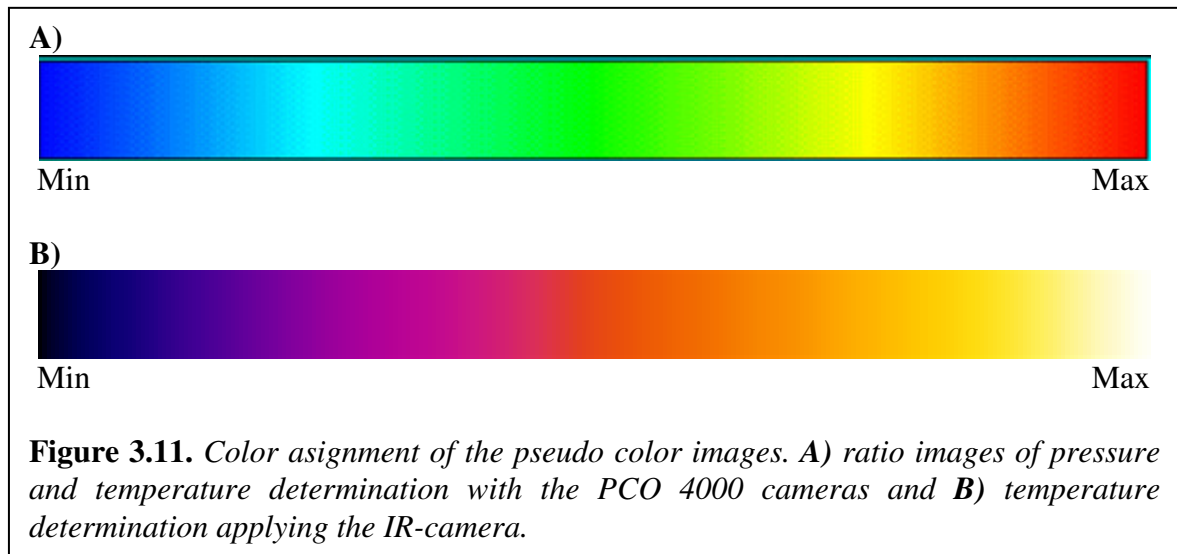
1.2%/K. All the calibration measurements were repeated several times and a deviation in the results of 0.6% was found. This corresponds to a reproducibility of 0.5 K. The pressure cross-sensitivity of the temperature probe is rather low. The signal change in a range of 200 mbar is only 1%, between 10 °C and 30 °C only 0.5%.

The pressure dependence of the pressure probe is 25, 35, 50, and 70%/bar at 10 °C, 20 °C, 30 °C, and 40 °C, respectively. In other words, the data show a very high temperature cross-sensitivity of the pressure probe PtTFPL. This is a

drawback in terms of application for pressure determination on aerodynamic wind tunnel models. First of all, the easy temperature compensation method mentioned above can not be applied. Furthermore, a very precise determination of the absolute temperature is essential. The most severe problem is the reproducibility of pressure determination. Repeating the measurements after calibration at 10 °C and 30 °C, respectively, result in a deviation up to 3.2%. Hence, the reproducibility of pressure determination is worse than 120 mbar. It seems as if the paint is affected by an aging process, caused either by heating the system to 40 °C or by the excitation light.

3.3.2.2.2. Image Design

The results of the wind tunnel test are presented and discussed in the following. All figures of the measurements are pseudo color images of the ratio of the different gates. These ratio values are used for determining pressure and temperature on the surface of the aircraft model. In all the figures of pressure and



temperature measurements applying the dual paint, the minimum values are displayed in blue color, and the maximum values in red (see *figure 3.11*). For the temperature measurements with the IR-camera, the minimum temperature is displayed in dark blue, whilst the maximum temperature is bright yellow / white (see *figure 3.11*). The temperature and ratio value ranges are denoted in the respective figure captions.

3.3.2.2.3. Raw Images

The ratio images are used for the evaluation of the results of time-resolved

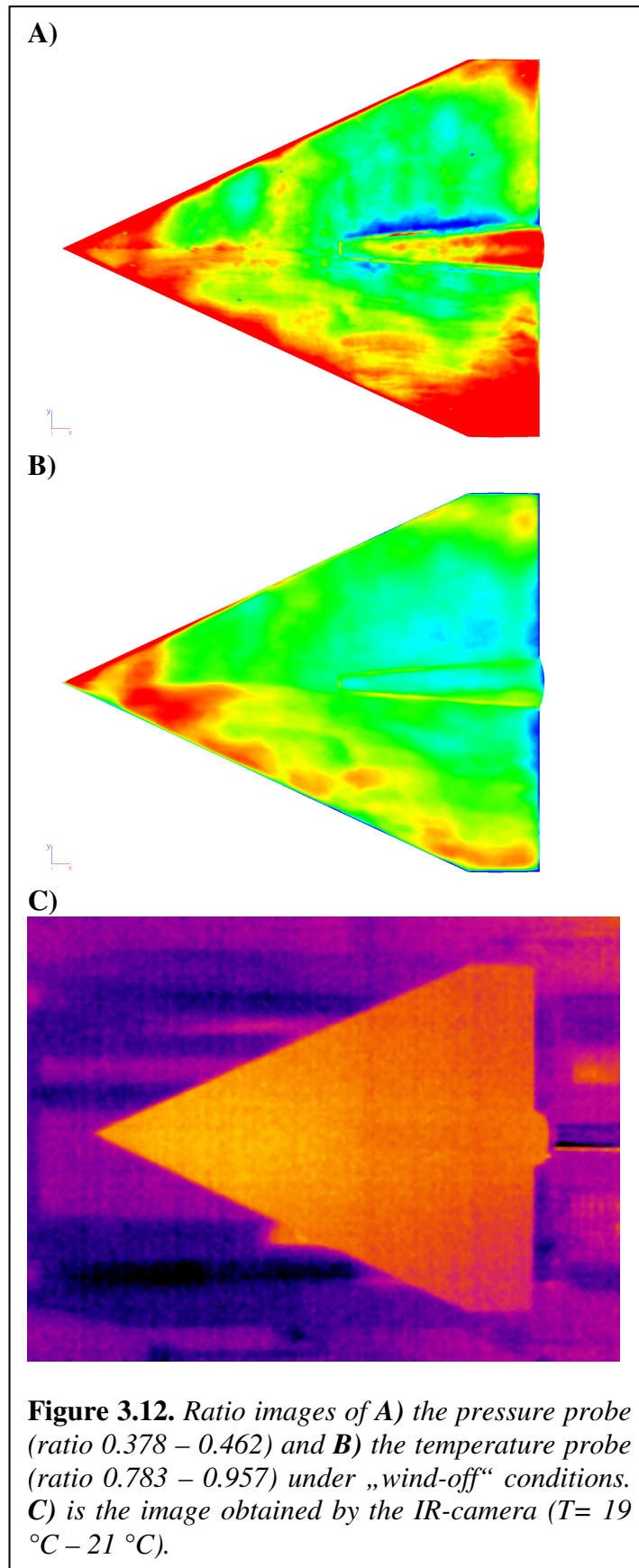
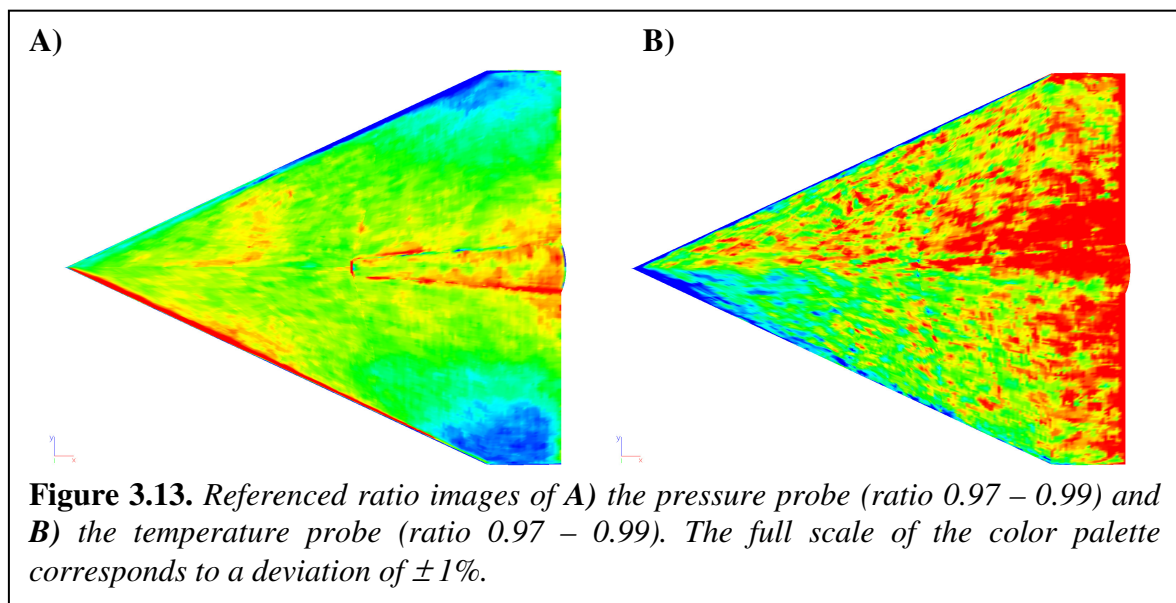


Figure 3.12. Ratio images of **A)** the pressure probe (ratio 0.378 – 0.462) and **B)** the temperature probe (ratio 0.783 – 0.957) under „wind-off“ conditions. **C)** is the image obtained by the IR-camera ($T = 19\text{ }^{\circ}\text{C} - 21\text{ }^{\circ}\text{C}$).

measurements. The background is already subtracted from these images. The exact determination of luminescence lifetime is not of interest for aerodynamic research. The pseudo color images shown in the following sections display the surface structure on a 3D model, and not the raw pixel based images. This enables for comparison and evaluation of results obtained for different angles of attack.

When evaluating the data from the pressure probe of the “wind-off” images, a clear structure is visible on the surface of the delta wing (see *figure 3.12 A*)). This effect is very exceptional, because, – obviously – there is no air flow applied for acquiring these “wind-off” images. A constant ratio value over the whole surface area is expected, due to the absence of pressure gradients. The data from the temperature probe also show an inhomogeneous distribution over the surface (see

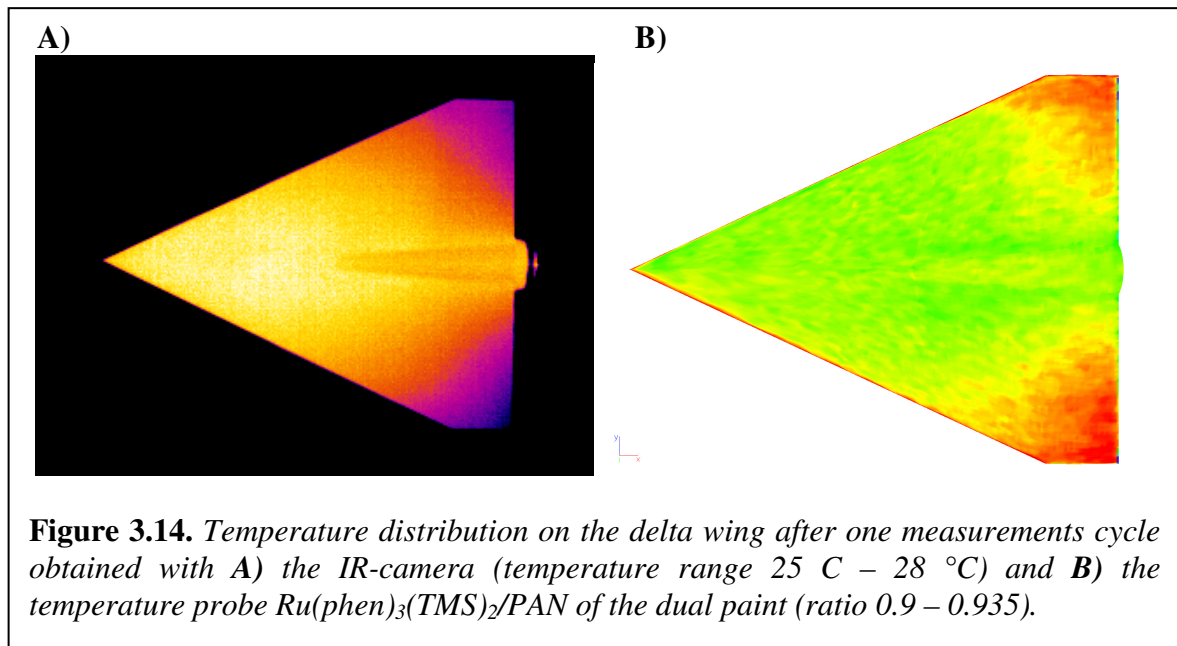
figure 3.12 B)), even though there is nearly no difference in temperature on the aircraft model, as it is proven by the IR-camera (see figure 3.12 C)). The deviations from homogeneity are more pronounced on the left part of the model. This is the area where the model was cleaned with toluene before the coating with the paint. The deviations cause changed ratio values in the images and falsify the pressure and temperature measurement. The calculated deviations in the ratio image of the pressure probe are $\pm 10\%$. This corresponds to a pressure deviation of ± 285 mbar at 1000 mbar and 20 °C. Deviations of this dimension render the system not feasible for aerodynamic measurements, if it is not possible to compensate for these effects. Furthermore, the deviations in the ratio images of the temperature probe are also very high. At 1000 mbar and 20 °C, a deviation of ± 8 K is found, which also is insufficient for any application. Unfortunately, the structures are different in the two ratio images, so it is not possible to compensate by simply dividing the two ratio images. However, using the “wind-off” images as a reference for the “wind-on” images, like it is done when applying the intensity method, it is possible to compensate for these effects. This can be shown when regarding the results from the measurements at different angles of attack (α). In figure 3.13, the ratios of two different ratio images, one at $\alpha = 10^\circ$ and the other at $\alpha = 26^\circ$, are displayed. Evaluation of these images reveals that the deviations are ten times smaller than they are in the unreferenced ratio images. In other words, the paint is applicable for aerodynamic measurements when the results are referenced with “wind-off” images.



In contrast to intensity imaging, the reference image has to be taken only once. This means that one reference “wind-off” image has to be taken before starting the measurements, which is then applicable to all measurements at any angle of attack. However, the signal-to-noise ratio (SNR) is worse compared to intensity measurements (see *figure 3.17*), due to the lower overall intensity.

3.3.2.2.4. Temperature-Sensitive Probe

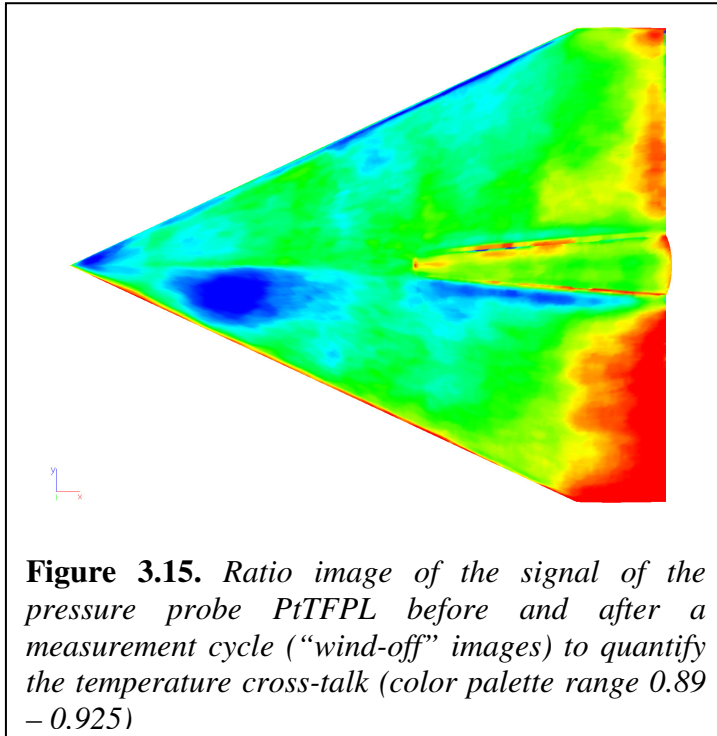
To test the correct operation of the temperature probe, the reference image of the “wind-off” image before and after a measurements cycle was compared with the respective data of the IR-camera. The images show the same surface temperature distribution (see *figure 3.14*). The wing tips in the rear of the model are the coolest areas, because they cool down more quickly than the rest of the model after being heated up during the measurement cycle. The ratio image shows a variation of 9%, which corresponds to a temperature change of 7.5 K. These results are in good agreement with the values obtained by the IR-camera. In fact, the



temperature of the model has risen from 20 °C to 27 °C. There is a deviation of only 0.5 K between the results obtained by the temperature probe of the dual paint and those of the IR-camera.

3.3.2.2.5. Pressure-Sensitive Probe

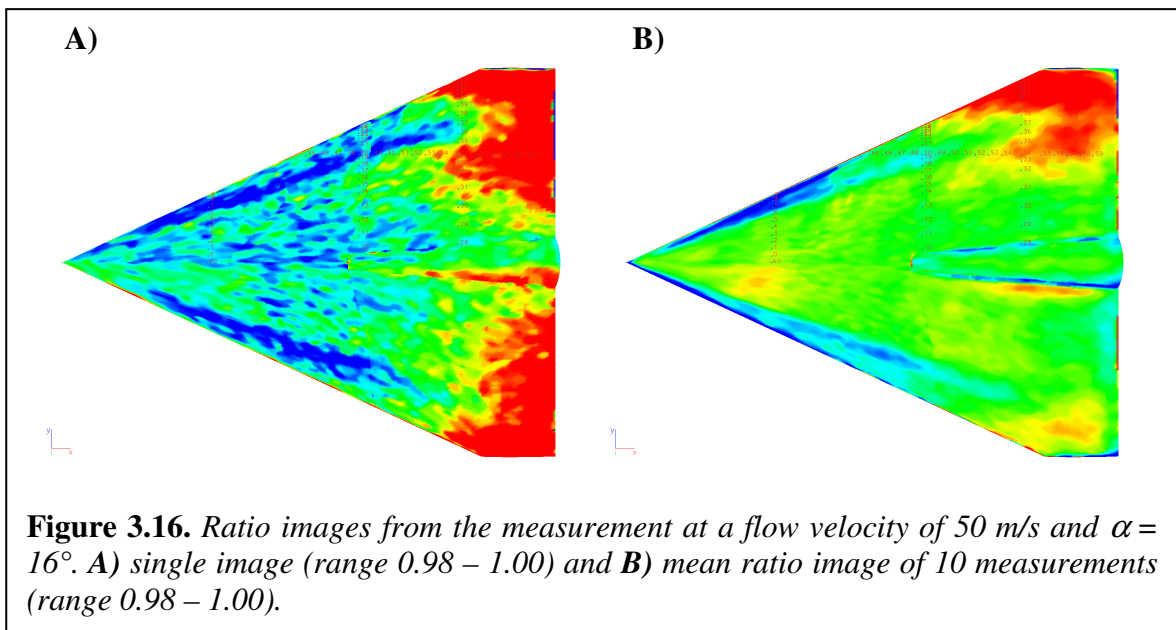
An operational test was also performed with the pressure probe PtTFPL of the dual paint. To check the temperature cross-talk, the same data points as



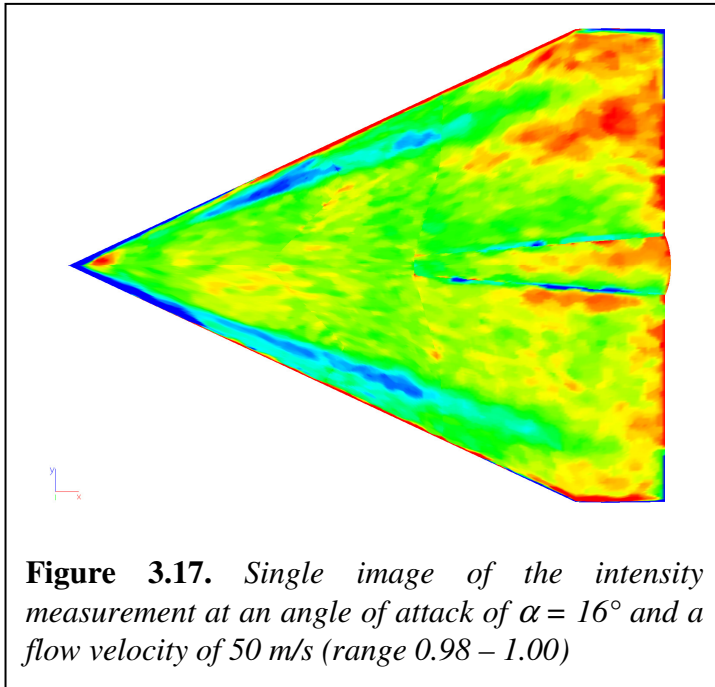
mentioned above were evaluated (“wind-off” images before and after a measurement cycle). There is a mean ratio of 0.90 between the two images. Surprisingly, this deviation is not only an effect of temperature. As it can be seen in figure 3.15, there are substantial inhomogeneities in the ratio image. Especially in the middle of the rear part, there is an asymmetric spatial distribution as well as on the

left side of the front. The latter was formed during the measurement cycles. This indicates either a non-uniform aging of the pressure probe or a partial damage of the paint (these effects are discussed later).

However, when applying the “ratio-approach” as mentioned above, many of the effects are referenced out. The results of the measurements at an angle of



attack of 16° and a flow velocity of 50 m/s are shown in *figure 3.16*. In order to enhance the signal-to-noise ratio, the measurement cycle was repeated 10 times. The results obtained are in good agreement with the data from conventional pressure tap measurements. The expected vortices can be visualized with the binary paint. However, an offset correction (in the range of 5 to 20 mbar) is mandatory – like it is the case when measuring intensity – in order to obtain



unambiguous results. The same measurement was conducted applying intensity imaging (see *figure 3.17*). The images of both measurements show the same topology and give the same result. However, in contrast to intensity imaging the time-resolved measurements have to be repeated several times in order to enhance the SNR. The

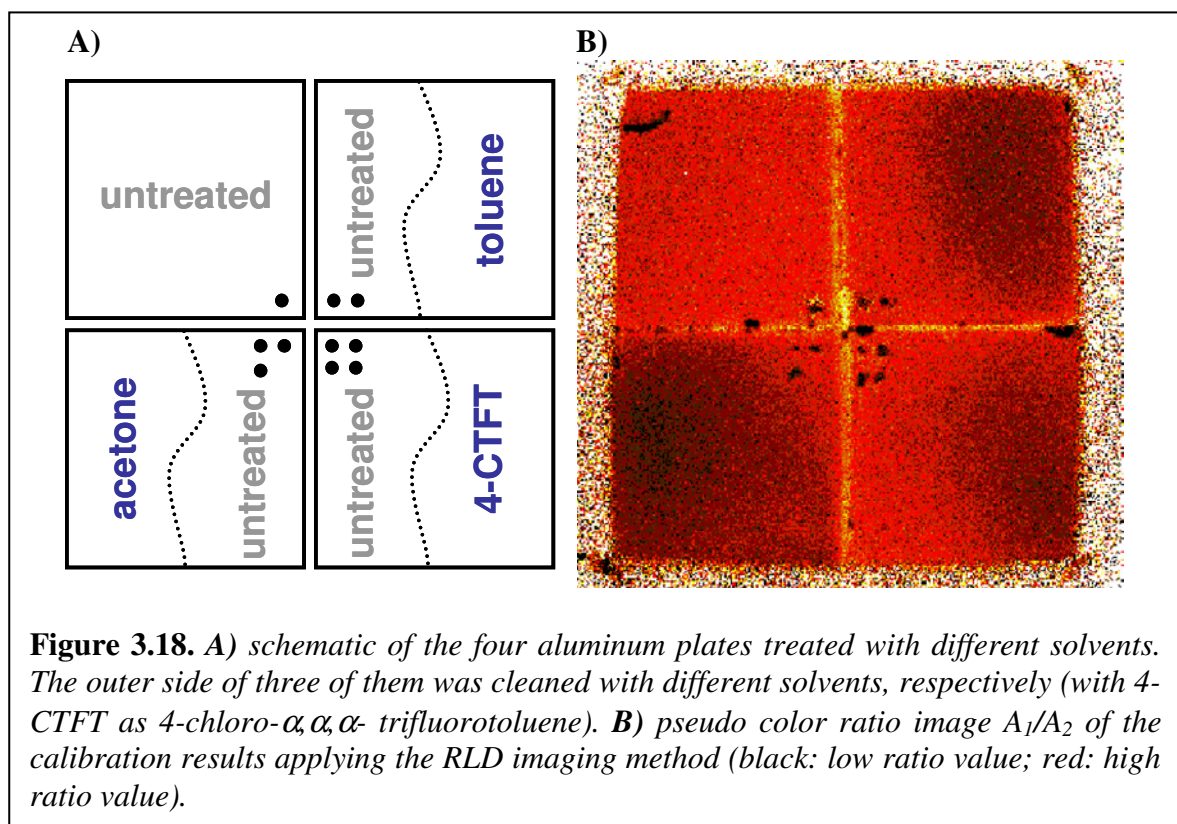
results of all pressure measurements reveal an unsymmetrical distribution of the pressure on the surface of the delta wing. This is most probably due to a non ideal adjustment of the aircraft model in the test section of the wind tunnel. This slight displacement can cause a non-symmetrical air flow over the surface that can be seen in all images when determining pressure.

3.3.2.2.6. Further Investigations

The unexpected effects of uneven surface distribution and/or different aging of the paint on the aircraft model were studied in more detail. An inhomogeneous spraying of the dual PSP/TSP on the surface of the model will cause serious problems when measuring intensity. However, the time-resolved imaging methodology applied is not affected by this kind of effect, because it is a self referencing technique. Furthermore, ageing of the paint - in terms of photobleaching – would not falsify the data for the same reason. If a certain

fraction of e.g. PtTFPL undergoes photobleaching, the overall intensity is decreased. However, this effect would be the same in both gates A_1 and A_2 , respectively, not influencing the ratio of the two gates (and accordingly the calculated lifetime).

When regarding the unexpected structures on the images, e.g. in *figure 3.15* and *figure 3.16 B*), the topology reminds of patterns resulted by wiping the surface. In fact, before spraying the surface with the binary paint, the surface was cleaned with toluene. In order to confirm this suspicion, four $1.5 \times 1.5 \text{ cm}^2$ aluminum plates were coated with the binary paint (see *section 3.5.3*) in the same way the model was sprayed (see *section 3.5.4*). The plates were pre-coated with the identical

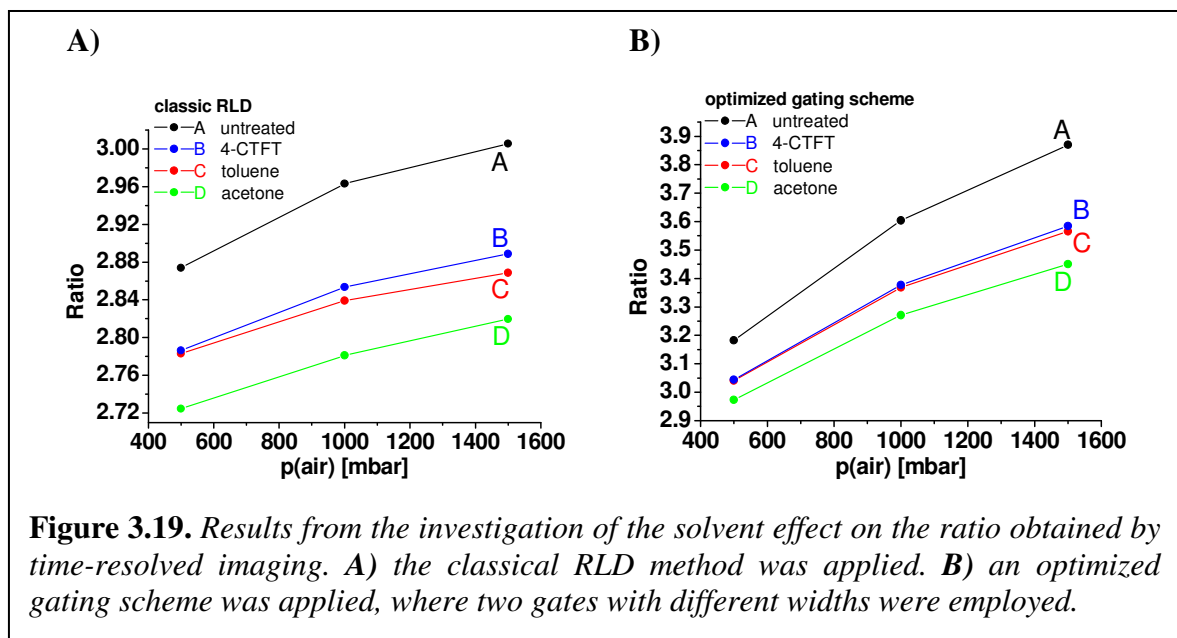


Cloucryl[®] screenlayer as used in the wind tunnel test. To investigate the effect of the solvents applied for cleaning, one half of the pre-coated aluminium plate was treated with different solvents, respectively (see *figure 3.18*). For referencing and for quantifying the effect, one plate was left untreated. Acetone, toluene, and 4-chloro- α,α,α -trifluorotoluene (4-CTFT) were used as cleaning solvents. The four plates were mounted in a pressure chamber and calibrated at three different pressures (see experimental part), once applying the classical RLD method and once with the optimized gating scheme (see *figure 3.3*) similar to the one applied

in the wind tunnel test. For all the parameters applied, see *section 3.5.4* in the experimental part.

The results from this experiment clearly show that the paint is somehow chemically altered by cleaning the pre-coated surface with organic solvents (see *figure 3.18*). The untreated aluminum plate shows a homogeneous distribution over the whole surface. The cleaned areas exhibit a reduced ratio value when interrogated via time resolved measurements. Surprisingly, these patterns are virtually not visible when regarding the intensity in the respective gates. This means that the lifetime and not the PtTFPL itself is altered. The chemical structure of the porphyrin seems to stay intact.

The system shown in *figure 3.18 A)* was calibrated applying two different sets of parameters to investigate how the parameter settings influence the results and if the solvent effects can be somehow reduced. Therefore, each treated surface was evaluated twice after calibration. The ratio once was calculated for a ROI (region of interest) in a solvent-treated area and compared with the result of ROI with the same size in a non-treated area. The results of this measurement are given in *figure 3.19*. As it can be seen, every organic solvent changes the resulting ratio somehow. Toluene and 4-CTFT cause the effect to the same extent. Acetone as

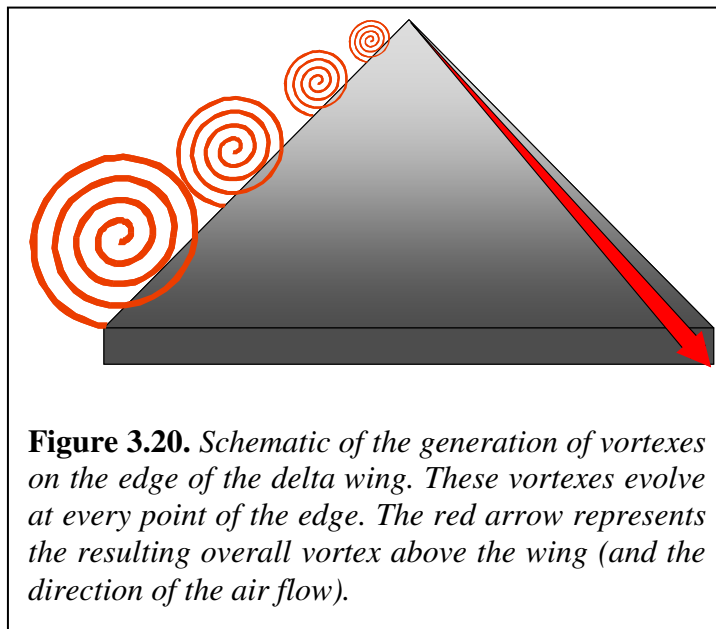


solvent for cleaning the basecoat extensively alters the properties of the binary paint. This “solvent effect” is more pronounced when applying the classic RLD method.

3.3.2.3. Discussion

The results of temperature probe of the binary paint (see *section 3.5.3*) are in very good agreement with the results obtained by reference measurements applying an IR-camera. Surprisingly, fine structures of temperature gradients cannot be seen in the ratio image A_1/A_2 , not until this ratio image is referenced with the “wind-off” image. The images from the temperature sensor exhibit a higher signal-to-noise ratio compared to the results from the IR-camera. This is due to the comparatively low overall intensity (especially in the second gate A_2).

The results of the pressure probe suffer from the same problems as the temperature probe. Without the “wind-off” images, no significant and unambiguous results can be obtained and the overall intensities are rather low as well. However,



the results obtained with the pressure probe are consistent with the theoretical behaviour of a delta wing in an air stream. On this kind of wing, the lifting forces emerge from vortices that are generated on the leading edge of the wing (see *figure 3.20*).^[63] They are located slightly above the surface, thus generating a low pressure

area on the upper side and lifting the wing. These vortices can be seen in the evaluated images of the wind tunnel test (see *figure 3.16*, blue regions). In order to obtain reliable results, averaging of several images is necessary.

The effects on the lifetime of the pressure-sensitive probe after cleaning the pre-coated screenlayer with organic solvents are a major problem. All the three tested solvents toluene, 4-chloro- α,α,α -trifluorotoluene, and acetone influence the system. The latter causes the most severe effect. The origin or the mechanism of this interference cannot be explained or proven. One theory is that the solvent changes the properties of the basecoat, thus providing a different microenvironment for the pressure probe PtTFPL. It is still unexplained why two

gates (A_1 and A_2) are not sufficient for resolving spatial distributions of pressure or temperature fluctuations. The need for a “wind-off” image to reference with is a substantial drawback and is somehow inconsistent with the theory of time-resolved imaging. Even if there are some surface effects like inhomogeneities or solvent interactions, they should a) be visible in each single gate and b) be referenced out especially when determining temperature cross-sensitivity. Because even if a microenvironment with different oxygen accessibility to the pressure probe is formed, it should not influence the response of the PtTFPL towards temperature (unless the “new” environments exhibit a drastically different thermal conductivity).

3.4. Conclusion

The dual pressure-sensitive and temperature-sensitive paint consisting of PtTFPL and $\text{Ru(phen)}_3(\text{TMS})_2/\text{PAN}$ in the matrix polymer FIB was applied in an aerodynamic wind tunnel test for the first time. The paint is well sprayable and exhibits an excellent adhesion on the surface of the aircraft model. The system can be applied for time-resolved imaging methods. The overall intensities are low compared to existing systems with PAHs as indicators, worsening the signal-to-noise ratio. The necessity to reference the ratio image with “wind-off” images is a drawback. However, the “wind-off” images have to be recorded only once unlike when measuring intensity. The whole measurement cycle can be performed without the need for other “wind-off” images with this reference image.

The results obtained from the temperature probe $\text{Ru(phen)}_3(\text{TMS})_2$ in PAN particles exhibit a good agreement with those from the IR-camera. Absolute temperature determination on the aircraft model is consistent with the calibration of the system. The rather low intensity of the particle system requires longer integration times or more numbers of cycles.

The barometric pressure probe PtTFPL is applicable for air pressure determination in combination with time-resolved imaging methodologies. Again, the ratio images from the measurement have to be referenced with the “wind-off” image. The results obtained are in good agreement with the data from the conventional pressure taps. Unfortunately, there are some unexplained surface effects, limiting its feasibility. Obviously, the solvent used for cleaning the

PDMS/TiO₂ screenlayer before spraying the paint also influences the results. Despite these drawbacks, the results of the pressure probe are consistent with the theory. The evaluated surface pressure topology coincides with the reference data for the delta wing. Due to the low intensity of the PtTFPL at the considered pressure ranges, averaging of several repetitions is necessary.

In principle, the dual PSP/TSP system is applicable to aerodynamic measurements in wind tunnels. The encountered negative effects require further analysis and improvements. They diminish the advantages of time-resolved imaging compared to intensity measurements. Once the problems are solved, this system and methodology is superior to intensity-based approaches.

3.5. Experimental

3.5.1. Materials and Methods

Poly(styrene-*co*-acrylonitrile) (PSAN, 30 wt% of acrylonitrile, $M_w=185000$), dichlorotris(1,10-phenanthroline)ruthenium(II) ($\text{Ru}(\text{phen})_3\text{Cl}_2$), and 3-(trimethylsilyl)-1-propanesulfonic acid sodium salt (NaTMS) were obtained from Sigma-Aldrich (www.sigmaaldrich.com). Platinum(II)-5,10,15,20-tetrakis(2,3,4,5,6-pentafluorophenyl)porpholactone was purchased from Frontier Scientific Inc. (www.frontiersci.com). All solvents (*N,N*-dimethylformamide, ethanol, acetone, ethylacetate, toluene, methanol, chloroform, 4-chloro- α,α,α -trifluorotoluene) were from Fluka (www.sigmaaldrich.com) and used in analytical purity. All chemicals were used without further purification. The Cloucryl[®] / titanium dioxide coated aluminum plates were received from the Institute of Aerodynamics and Flow Technology of the DLR Göttingen. Poly(IBM-*co*-TFEM) and FIB were provided by Dr. V. Ondus from the Institute of Chemistry of the University of Hohenheim.

3.5.2. Preparation of Temperature-Sensitive Particles

150 mg (0.21 mmol, 1 eq.) of dichlorotris(1,10-phenanthroline)ruthenium(II) were dissolved in approx. 4 mL of doubly distilled water and a solution of 96 mg (0.44 mmol, 2.1 eq.) of 3-(trimethyl-silyl)-1-propanesulfonate in 4 mL of doubly distilled water was added dropwise under vigorous stirring. After 30 minutes, the solution was extracted 5 times with chloroform. The gathered organic fractions were removed on the rotary evaporator. The remaining $\text{Ru}(\text{phen})_3(\text{TMS})_2$ was dried in vacuum (yield approx. 80%).

250 mg of poly(acrylonitrile) were dissolved in 50 mL of DMF and 15 mg of PtTFPL were added. 150 mL of doubly distilled water were added dropwise under vigorous stirring. The precipitated particles were centrifuged and washed with water and ethanol four times, respectively. Subsequent freeze drying yielded in a yellow powder. The diameter of the beads was determined by fluorescence microscopy to be $\sim 1 \mu\text{m}$.

3.5.3. Paint Composition and Coating

For the calibration test (see *section 3.2.2*), 0.4 mg PtTFPL were dissolved in a solution of 40 mg poly(IBM-co-TFEM) dissolved in 3 mL of toluene. This dye/polymer mixture was ultrasonicated for at least 10 minutes and was then immediately sprayed on an aluminum plate using a “Walther Pilot Mini” air gun (www.walther-pilot.de), with a nozzle diameter of 1 mm and an applied air pressure of ~ 2.5 bar. The paint was allowed to dry over night.

For coating the aircraft model and the aluminum plates, the binary paint consisted of 1.0 mg/mL $\text{Ru}(\text{phen})_3(\text{TMS})_2$ /PAN particles, 0.1 mg/mL PtTFPL, and 50.5 mg/mL FIB, relating to the final overall volume of 4-chloro- α,α,α -trifluorotoluene. For the coating of the aircraft, a total volume of 110 mL of the solvent was used. For coating aluminum plates, the volume was downscaled to 4 mL. The readily prepared particle/dye/polymer mixture was ultrasonicated for at least 10 minutes and was then immediately sprayed using a “Walther Pilot Mini” air gun (www.walther-pilot.de), with a nozzle diameter of 1 mm and an applied air

pressure of ~ 2.5 bar. The paint was allowed to dry over night. Its characteristics are described in the *sections 3.3.2.2 and 3.3.2.3*.

3.5.4. Experimental Setup and Parameters

Absorption and emission spectra were recorded on a Lambda 14 p Perkin-Elmer UV-vis spectrophotometer (Waltham, MA, USA, www.perkinelmer.com) and an Aminco AB 2 luminescence spectrometer (Thermo Scientific Inc., Waltham, MA, USA, www.thermo.com), respectively. The coated aluminum plates were calibrated in a pressure chamber where air pressure can be changed in the range from 50 mbar to 2000 mbar, equipped with a peltier element and water cooling for thermostating the chamber. All time-resolved measurements were performed with a PCO SensiCam 12 bit b/w CCD camera (PCO, Kelheim, Germany, www.pco.de) equipped with a Schneider-Kreuznach Xenon 0.95/17 lens (www.schneiderkreuznach.com, Jos. Schneider Optische Werke, Bad Kreuznach, Germany) and a 405-66-60 405 nm LED sold by Roithner Lasertechnik (Vienna, Austria, www.roithner-laser.com). The excitation light was focussed by a PCW 18 x 18 MgF2 TS lens from Edmund Optics (www.edmundoptics.com, Karlsruhe, Germany) and hit the sensor layer at an angle of approximately 20° . Light was filtered through a BG 12 filter (Schott, Mainz, Germany, www.schott.com) with a thickness of 2 mm. Emission of the temperature probe $\text{Ru(phen)}_3(\text{TMS})_2/\text{PAN}$ was detected through a D580/60M band pass filter (Chroma, Rockingham, VT, USA, www.chroma.com). For the pressure probe PtPFL, a RG 695 high-pass filter was used. The parameters applied for calibration of the samples as well as for investigating the solvent effects on the basecoat (see *chapter 3.3.2.2.6*.) are given in *table 3.7*.

Table 3.7. *Parameters applied for time-resolved measurements. The times t_1 and t_2 are related to the end of the excitation pulse*

method	excitation pulse [μs]	gate width [μs]		t_1	t_2
		A_1	A_2		
classic RLD	160	60	60	0.5	30.5
optimized gating scheme	160	30	50	-20	10

The experimental setup at the DLR Göttingen and the parameters applied for the wind tunnel test were slightly different from those applied at the University of Regensburg for calibrating the paint. The emission of the temperature probe $\text{Ru(phen)}_3(\text{TMS})_2/\text{PAN}$ was detected through a combination of a FH550 high pass filter and a FL630 low pass filter. For the pressure probe PtTFPL a 695FG07-50 band pass filter was used. The respective filter systems were directly mounted in front of the PCO4000 CCD cameras (PCO, Kelheim, Germany, www.pco.de). The parameters applied for the wind tunnel test are given in *table 3.8*.

Table 3.8. Parameters applied for the measurements in the wind tunnel. The times t_1 and t_2 are related to the end of the excitation pulse

	excitation pulse [μs]	gate width [μs]		t_1	t_2
		A_1	A_2		
pressure probe	14.5	10.0	25.0	-8.5	15.5
temperature probe	4.0	3.5	6.0	-2.0	1.0

3.6. References

- [1] D. D. Baals, W. R. Corliss, *Wind Tunnels of NASA*, Scientific and Technical Information Branch, National Aeronautics and Space Administration (NASA), USA, **1981**
- [2] S. Funatani, N. Fujisawa, H. Ikeda, *Meas. Sci. Technol.* **2004**, 15, 983
- [3] C. J. Kähler, U. Scholz, *PIV'03 Paper* **2003**, 3223, 1, 5th International Symposium on Particle Image Velocimetry, Busan, Korea, Sept. 22-24, **2003**
- [4] H. Richard, M. Raffel, *Meas. Sci. Technol.* **2001**, 12, 1576
- [5] T. Lui, B.T. Campbell, S. P. Burns, J. P. Sullivan, *Appl. Mech. Rev.* **1997**, 50, 227
- [6] P. H. Baumann, K. A. Butefisch, *Proc. SPIE* **1995**, 2546, 16
- [7] G. A. Flemming, A. W. Burner, *Proc. SPIE* **1999**, 3783, 228
- [8] E. Germain, J. Quest, *AIAA Journal* **2005**, 458, 1
- [9] C. Klein, R. H. Engler, U. Henne, W. E. Sachs, *Exp. Fluids* **2005**, 39, 475
- [10] K. Mitsuo, K. Asai, A. Takahashi, H. Mizushima, *Meas. Sci. Technol.* **2006**, 17, 1282
- [11] T. Liu, J. P. Sullivan, *Pressure and Temperature Sensitive Paints. Springer Series on Fluid Mechanics* (eds: R. J. Adrian, M. Gharib, W. Merzkirch, D. Rockwell, J. H. Whitelaw), Springer, Berlin, **2004**
- [12] T. Liu, J.P. Sullivan, *Int. J. Heat Mass Transfer* **1996**, 39, 3695
- [13] K. Asai, H. Kanda, T. Kunimasu, T. Liu, J. P. Sullivan, *J. of Aircraft* **1997**, 34, 34
- [14] Y. Egami, U. Fey, J. Quest, *Conference Proceedings online (AIAA-2007-1062)* (ed. American Institute of Aeronautics and Astronautics): *Development of New Two-*

- Component TSP for Cryogenic Testing*, pp. 1 – 11, 45th AIAA Aerospace Sciences Meeting and Exhibit, Reno, Nevada, USA, 8th – 11th Jan. **2007**
- [15] A. S. Roberts, *J. of Aircraft* **1992**, 29, 161
 - [16] L. de Luca, G. Cardone, G. M. Carlomagno, D. A. de la Chevalerie, T. A. de Roquefort, *Exp. Heat Tran.* **1992**, 5, 65
 - [17] M. Mori, L. Novak, M. Sekavčnik, *Exp. Therm. Fluid Sci.* **2007**, 32, 387
 - [18] J. H. Spurk, N. Aksel, *Fluid Mechanics*, 2nd edition, Springer Berlin, **2007**
 - [19] S. Tavoularis, *Measurement in Fluid Mechanics*, 1st edition, Cambridge University Press, **2005**
 - [20] Y. Amao, *Microchim. Acta* **2003**, 143, 1
 - [21] M. Gouterman, L. K. Hanson, G. – E. Khalil, J. W. Buchler, K. Rohbock, D. Dolphin, *J. Am. Chem. Soc.* **1975**, 97, 3142
 - [22] M. Gouterman, *J. Mol. Spec.* **1961**, 6, 138
 - [23] S. – K. Lee, I. Okura, *Spectrochim. Acta A* **1998**, 54, 91
 - [24] Y. Amao, T. Miyashita, I. Okura, *J. Porphyrin. Phthalocyanine* **2000**, 5, 433
 - [25] D. B. Papkovsky, G. V. Ponomarev, W. Trettnak, P. O'Leary, *Anal. Chem.* **1995**, 67, 4112
 - [26] P. Hartmann, W. Trettnak, *Anal. Chem.* **1996**, 68, 2615
 - [27] S. – K. Lee, I. Okura, *Anal. Commun.* **1997**, 34, 185
 - [28] S. – W. Lai, Y. – J. Hou, C. – M. Che, H. – L. Pang, K. – Y. Wong, C. K. Chang, N. Zhu, *Inorg. Chem.* **2004**, 43, 3724
 - [29] P. J. Spellane, M. Gouterman, A. Antipas, S. Kim, Y. C. Liu, *Inorg. Chem.* **1980**, 19, 386
 - [30] B. Zelelow, G. E. Khalil, G. Phelan, B. Carlson, M. Gouterman, J. B. Callis, L. R. Dalton, *Sens. Actuators B* **2003**, 96, 304
 - [31] G. E. Khalil, C. Costin, J. Crafton, G. Jones, S. Grenoble, M. Gouterman, J. B. Callis, L. R. Dalton, *Sens. Actuators B* **2004**, 97, 13
 - [32] J. E. Rogers, K. A. Nguyen, D. C. Hufnagle, D. G. McLean, W. Su, K. M. Gossett, A. R. Burke, S. A. Vinogradov, R. Pachter, P. A. Fleitz, *J. Phys. Chem.* **2003**, 107, 11331
 - [33] S. A. Vinogradov, D. F. Wilson, *J. Chem. Soc. Perkin Trans.* **1995**, 1, 103
 - [34] S. A. Vinogradov, D. F. Wilson, *Adv. Exp. Med. Biol.* **1997**, 411, 597
 - [35] K. Asai, K. Nakakita, K. Teduka, *Proceedings of the 19th International Congress in Instrumentation in Aerospace Simulation Facilities (ICIASF)*, Cleveland, Ohio, USA, 27.-30. August, **2001**, 25
 - [36] S. M. Borisov, T. Mayr, A. A. Karasyov, I. Klimant, P. Chojnacki, C. Moser, S. Nagl, M. Schäferling, M. I. J. Stich, G. S. Vasilevskaya, O. S. Wolfbeis, *Springer Series on Fluorescence, Vol. 4: Fluorescence of Supramolecules, Polymers, and Nanosystems* (ed. M. N Berberan-Santos), Springer, Berlin, Heidelberg, **2008**
 - [37] C. Yang, L.-M. Fu, Y. Wang, J.-P. Zhang, W.-T. Wong, X.-C. Ai, Y.-F. Qiao, B.-S. Zou, L.-L. Gui, *Angew. Chem. Int. Ed.* **2004**, 43, 5009
 - [38] G. Holst, R. Glud, M. Kühl, I. Klimant, *Sens. Actuators B* **1997**, 38-39, 122
 - [39] I. Klimant, O. S. Wolfbeis, *Anal. Chem.* **1995**, 67, 3160
 - [40] O. S. Wolfbeis, I. Klimant, T. Werner, C. Huber, U. Kosch, C. Krause, G. Neurauter, A. Dürkop, *Sens. Actuators B* **1998**, 51, 17
 - [41] M. Kameda, T. Tabei, K. Nakakita, H. Sakaue, K. Asai, *Meas. Sci. Technol.* **2005**, 16, 2517
 - [42] Y. Sakamura, M. Matsumoto, T. Suzuko, *Meas. Sci. Technol.* **2005**, 16, 759
 - [43] W. J. Bowyer, W. Xu, J. Demas, *Anal. Chem.* **2004**, 76, 4374
 - [44] E. R. Carraway, J. N. Demas, B. A. DeGraff, J. R. Bacon, *Anal. Chem.* **1991**, 63, 332
 - [45] J. R. Bacon, J. N. Demas, *Anal. Chem.* **1987**, 59, 2780
 - [46] G. Liebsch, I. Klimant, O. S. Wolfbeis, *Adv. Mater.* **1999**, 11, 1296
 - [47] R. Erausquin, C. Cunningham, J. P. Sullivan, K. Asai, H. Kanda, T. Kunimasu, Y. Iijima, *AIAA Paper*, **1998**, 98-0588

- [48] S. M. Borisov, A. S. Vasylevska, C. Krause, O. S. Wolfbeis, *Adv. Funct. Mater.* **2006**, 16, 1536
- [49] *Polymer Handbook* (Eds : J. Brandrup, E. H. Immergut, E. A. Grulke), Wiley-VCH, New-York **1999**
- [50] O. S. Wolfbeis, *J. Mater. Chem.* **2005**, 15, 2657
- [51] A. K. McEvoy, C. McDonagh, B. D. MacCraith, *J. Sol-Gel Sci. Technol.* **1997**, 8, 1121
- [52] S. M. Borisov, M. C. Waldhier, I. Klimant, O. S. Wolfbeis, *Chem. Mater.* **2007**, 19, 6187
- [53] X. Lu, M. A. Winnik, *Chem. Mater.* **2001**, 13, 3449
- [54] M. Gouterman, J. Callis, L. Dalton, G. Khalil, Y. Mébarki, K. R. Cooper, M. Grenier, *Meas. Sci. Technol.* **2004**, 15, 1986
- [55] E. Puklin, B. Carlson, S. Gouin, C. Costin, E. Green, S. Ponomarev, H. Tanji, M. Gouterman, *J. Appl. Polym. Sci.* **2000**, 77, 2795
- [56] Y. Amao, T. Miyashita, I. Okura, *J. Porphyrin. Phthalocyanine* **2001**, 5, 433
- [57] A. Amao, T. Miyashita, I. Okura, *React. Funct. Polym.* **2001**, 47, 49
- [58] M. I. J. Stich, O. S. Wolfbeis, *Springer Series on Fluorescence, Vol. 5, Part 1: Fluorescence Sensing and Imaging Using Pressure-Sensitive Paints and Temperature-Sensitive Paints*, (ed.: U. Resch-Genger), Springer, Berlin, Heidelberg, **2008**
- [59] J. N. Demas, W. M. Jones, R. A. Keller, *Anal. Chem.* **1986**, 58, 1717
- [60] S. P. Chan, Z. J. Fuller, J. N. Demas, B. A. DeGraff, *Anal. Chem.* **2001**, 73, 4486
- [61] K. K. Sharman, A. Periasamy, H. Ashworth, J. N. Demas, N. H. Snow, *Anal. Chem.* **1999**, 71, 947
- [62] C. Moore, S. P. Chan, J. N. Demas, B. A. DeGraff, *Appl. Spec.* **2004**, 58, 603
- [63] D. Hummel, *Conference Proceedings online (AIAA-2008-377)* (ed. American Institute of Aeronautics and Astronautics): *Review of the Second International Vortex Flow Experiment*, pp. 1 – 21, 46th AIAA Aerospace Sciences Meeting and Exhibit, Reno, Nevada, USA, 7th – 10th Jan. **2008**

CHAPTER 4

A Dual Luminescent Sensor Material for Simultaneous Imaging of Pressure and Temperature on Surfaces

A novel kind of composite material for simultaneous luminescent determination of air pressure and temperature is presented. The dual sensor consists of a fluorinated platinum porphyrin complex (PtTFPP) as an oxygen sensitive probe, and of the highly temperature-sensitive europium complex $\text{Eu}(\text{tta})_3(\text{dpbt})$ as temperature probe. Both are incorporated into different polymer microparticles to control response characteristics and to avoid interferences. Encapsulation of PtTFPP in poly(styrene-co-acrylonitrile) (PSAN) results in a broad dynamic range from 0.05 to 2.00 bar for pressure measurements. The europium complex was incorporated into poly(vinyl chloride) to reduce the cross-sensitivity towards oxygen. This system represents a new class of luminescent sensor systems, where the signals are separated via the different luminescent lifetimes of the indicators. It is possible to monitor the emission of the temperature-sensitive probe by means of time-resolved fluorescence imaging without interferences, because the luminescence lifetime of the temperature indicators is tenfold longer than that of the oxygen indicator. The temperature image can then be used to compensate the cross-sensitivity of the pressure indicator towards temperature. In combination with an appropriate time-resolved measurement technique, this material enables simultaneous imaging of pressure (or oxygen partial pressure) and temperature distributions on surfaces. It is distinguished from other approaches of dual pressure- and temperature-sensitive paints because it avoids the need of signal separation by application of different cameras or by use of different optical filters or light sources.

4.1. Introduction

Oxygen or air pressure can be imaged instantly and in high spatial resolution by means of luminescent oxygen-sensitive materials.^[1-5] Generally, optical sensors are based on materials responding to an analyte by changing their optical properties like absorption, intensity or wavelength of luminescence emission, or their luminescence lifetime. The indicators can be encapsulated into polymer particles to control response characteristics or, in case of multi-indicator systems, to minimize interferences. These beads are incorporated into a matrix polymer and can be applied in different systems like fiber optics^[6] or sensor foils.^[7,8] Finally, they can also be sprayed or painted on surfaces to cover areas of any shape. By means of pressure-sensitive or temperature-sensitive paints (PSPs/TSPs) these basic factors in fluid mechanics can be imaged and quantified noninvasively with an unsurpassed spatial resolution.^[9-11] An ubiquitous problem consists in the fact that probes for oxygen also respond to temperature (and vice versa). Therefore, the obtained pressure data have to be corrected to compensate temperature effects. This can be accomplished by incorporation of temperature-sensitive indicators as a reference fluorophore to the sensor system. Therefore, dual PSP/TSP formulations have found increasing interest in the past years.^[12-15]

In dual sensor systems, the luminescent signals of the indicators applied have to be separated in order to obtain unambiguous data. This is achieved in most cases by different optical emission filters. This requires clearly separable emission wavelengths of the probes with almost no spectral overlap. In practice, it is a high challenge to select such a combination of indicators. A new principle of dual sensor material composition is presented here. Unlike in previous systems, the signals are not separated via their different emission wavelengths but by different luminescence decay times. The basis of this approach is a dual lifetime determination scheme (DLD).^[16]

Time-resolved (“gated”) luminescence lifetime imaging outmatches standard intensity detection techniques in terms of accuracy and reliability. Sources of error like an inhomogeneous sensor layer, photobleaching of the fluorophores, variable distances and angles of light source and detectors, or a non-ideal alignment of the excitation light are eliminated by this intrinsically reference technique.^[17] The fluorescent probes are excited by LEDs or laser diodes and the subsequent light

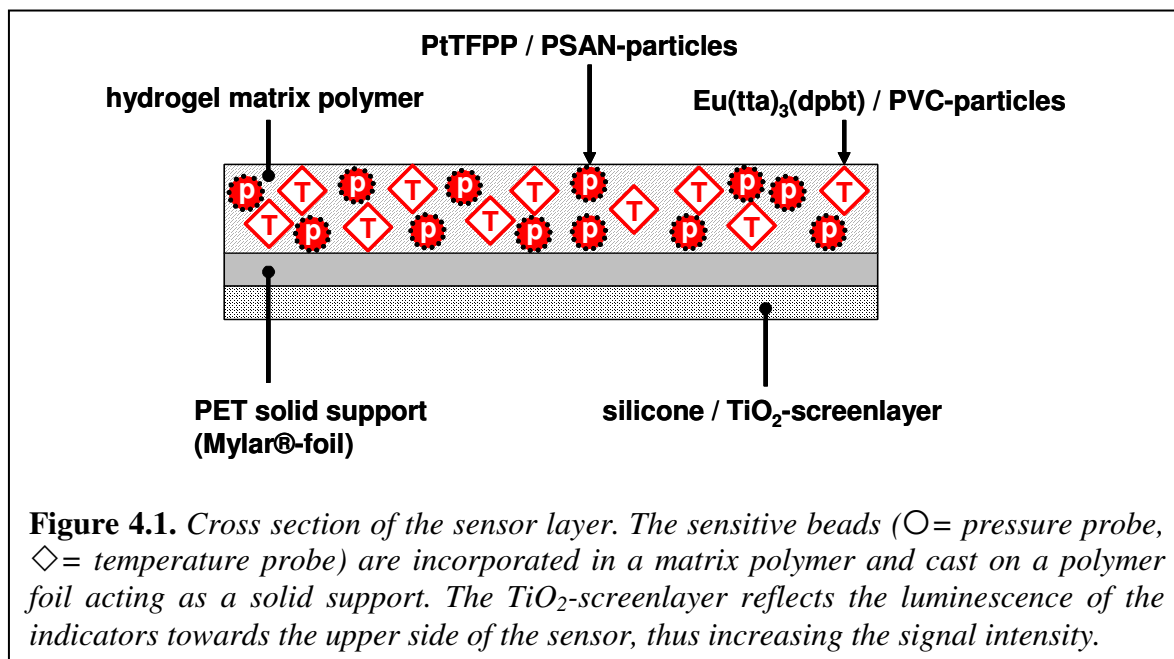
emission is detected by means of a CCD camera. In most cases, two time gated images with different delay times are taken in the luminescence emission phase of the dye (see *chapter 2.4.2.3*).^[4,18] From these two intensity images the luminescence lifetime τ can be calculated according to *equation 2.13* (assuming monoexponential decay of the luminescence). Four images are taken in this novel DLD approach, like it is explained in *chapter 2.4.2.4*. The first two match the mixed intensity of both indicators. The second gate pair is set with a lag time at which the emission of the pressure indicator is completely decayed. Thus, the luminescence signal of the long-decaying temperature-sensitive dye is exclusively detected.^[16] This information can be used to subtract the temperature-fraction of the pressure data obtained from the first two gates. This dual sensor material is also extremely useful if the two parameters pressure (or oxygen partial pressure) and temperature are to be analyzed in parallel, e.g., in biomedical imaging or aerodynamic measurements.

4.2. Results and Discussion

4.2.1. Sensor Composition

The dual sensor paint consists of an oxygen-sensitive probe and a temperature-sensitive probe, both encapsulated into different polymer particles. These particles are then incorporated into a matrix polymer that is cast onto a solid support. A schematic drawing of the cross-section of the sensor is given in *Figure 4.1*, and the preparation is described in detail in *section 4.4*. The particle system was chosen to adjust the sensitivity of the system and to reduce cross-sensitivity effects.^[19,20] The phosphorescence of the oxygen (= pressure) sensitive indicator Pt(II)-5,10,15,20-tetrakis(2,3,4,5,6-pentafluorophenyl)porphyrin (PtTFPP) is almost completely quenched at ambient air pressure.^[21] With poly(styrene-co-acrylonitrile) as particle material it is possible to extend the dynamic range of pressure determination beyond atmospheric pressure. The luminescence of the temperature indicator Eu(III)-tris(thenoyltrifluoroacetyl-acetonato) - (2-(4-diethylaminophenyl) - 4,6-bis(3,5-dimethylpyrazol-1-yl)-1,3,5-triazine)^[22] (Eu(tta)₃ (dpbt), structure see *table 2.3*) is also strongly affected by oxygen

quenching, as it is the case with most metal-ligand complexes. This interference can be minimized by shielding the fluorophores with gas-blocking polymers like



poly(vinyl chloride). The encapsulation of both indicator dyes also inhibits possible resonance energy transfer processes between the two chromophores. Furthermore, encapsulation in polymer beads warrants a sufficient solubility of the indicator molecules in the matrix polymer, which enables preparation of homogeneous one-layer paints.

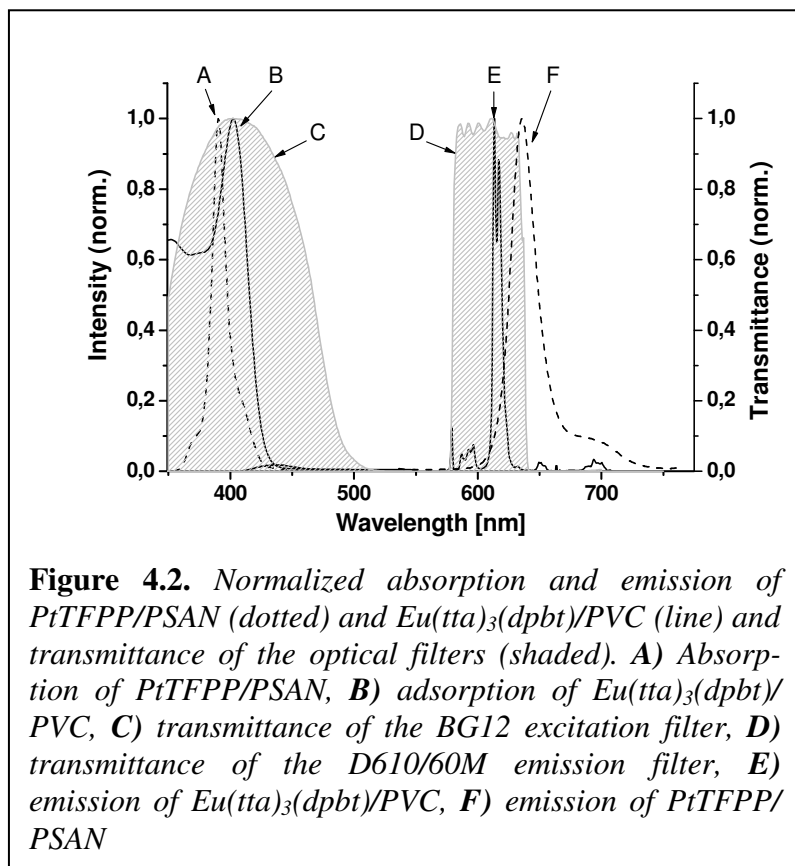
Among the large variety of pressure-sensitive luminescent probes, we decided to utilize PtTFPP because of its spectral properties like a large “Stokes’ shift”, a phosphorescence lifetime in the microsecond time regime, and the large extinction coefficient of $323,000 \text{ dm}^3 \text{ mol}^{-1} \text{ cm}^{-1}$ of the Soret band,^[23] resulting in a brightness of $\sim 30,000$ at ambient atmosphere and room temperature. This is much higher than any of the Ru-probes. It is one of the most photostable compounds in the group of metalloporphyrins. The highly fluorinated phenyl substituents in the molecule make the compound less susceptible towards photooxidation.^[24]

The platinum porphyrin exhibits very high quantum yields in the absence of oxygen, which drops to a value of approximately 8% at ambient air pressure.^[23] Hence, the luminescence is almost quenched at standard atmospheric pressure.^[21,25] In order to increase the effective dynamic range of pressure determination, the dye was incorporated into a moderately gas-permeable copolymer (poly(styrene-co-acrylonitrile) (PSAN), with 30 wt% acrylonitrile). This polymer possesses a reduced oxygen permeability coefficient P of $3.5 \cdot 10^{-14}$

$\text{cm}^2\cdot\text{Pa}\cdot\text{s}^{-1}$,^[26] and therefore retards the rapid quenching of luminescence intensity (and accordingly lifetime) of PtTFPP by oxygen. The polymer microspheres were prepared according to literature.^[19] The synthetic procedures were slightly modified and adjusted to the properties of the compounds. PSAN microparticles were obtained by precipitation from a polymer/dye/DMF-solution under ultrasonication (see *section 4.4.2*).^[27] The size of the beads does not exceed 5 μm .

$\text{Eu}(\text{tta})_3(\text{dpbt})$ exhibits an extraordinary strong temperature dependency of its luminescence, with a luminescence quantum yield of 75% in toluene solution at room temperature^[22] and a lifetime of approximately 600 μs . In most cases, luminescence of europium metal-ligand complexes occurs after energy transfer (ET) from the triplet excited state of the ligand to the metal centre.^[28] Due to energetic reasons, excitation is restricted to wavelengths below 390 nm for effective and irreversible ET to the Eu^{3+} -ion.^[29] By combination of $\text{Eu}(\text{III})$ β -diketonates with push-pull sensitizers (e.g. diaryl ketones) it is possible to extend the excitation range into the area of visible light.^[30] The triazine ligand in $\text{Eu}(\text{tta})_3(\text{dpbt})$ acts as an “antenna” chromophore with the *N,N*-diethylaniline group as the electron donor and the dipyrzolyltriazine as the acceptor. In this system, the energy transfer between ligand and Eu^{3+} -ion occurs via the singlet pathway, thus additionally extending the excitation window to longer wavelengths.^[22,31] The distinct temperature sensitivity of the $\text{Eu}(\text{III})$ β -diketonates is caused by thermal deactivation of the 5D_1 and 5D_2 energy levels of europium. In these processes, electronic energy levels are coupled to the environment through molecular vibration energy levels.^[32,33] On this account, the materials applied as sensor matrix affect the temperature dependency of the indicators. High molecular weight poly(vinyl chloride) as encapsulating material for $\text{Eu}(\text{tta})_3(\text{dpbt})$ was chosen due to its low oxygen permeability coefficient P of $3.4\cdot 10^{-15} \text{ cm}^2\cdot\text{Pa}\cdot\text{s}^{-1}$ and for the positive effects on the temperature sensitivity of the indicator.^[26] The sub-micrometer sized $\text{Eu}(\text{tta})_3(\text{dpbt})/\text{PVC}$ particles were prepared by a combined precipitation/solvent stripping procedure as described in detail in *section 4.4.3*. The pressure-sensitive PtTFPP/PSAN particles and the temperature-sensitive $\text{Eu}(\text{tta})_3(\text{dpbt})/\text{PVC}$ particles were suspended in a solution of the hydrogel D4 matrix polymer. This “cocktail” was then cast on a poly(ethylene terephthalate) (PET) solid support to give a sensor layer of 12 μm thickness after drying (see *section 4.4.4*). The hydrogel binder (D4) is a highly oxygen- permeable matrix polymer, soluble in a

mixture of ethanol and water. The particles do not interact with these solvents by swelling and give very homogeneous suspensions. A highly reflective TiO_2 /silicone screenlayer (Elastosil® A07 rubber, 30wt% TiO_2 in hexane) was spread on the back of the solid support to increase the luminescence intensity from the sensor



layer. The spectral characteristics of both probes and the transmittance of optical filters applied are shown in Figure 4.2. Both fluorophores can be excited at 405 nm and are therefore compatible with (low cost) violet LEDs or the 405 nm laser diode as light sources. The excitation light passes a BG12 filter to cut off undesired light emission from the

LED. The emission of both dyes is within the same wavelength window and can be imaged through a D610/60M band-pass filter.

4.2.2. Calibration of the Dual Sensor Material

In usual dual sensor systems, the signals of the two indicators are separated via optical emission filters. A widely used decay time-based sensing approach is based on the “Rapid Lifetime Determination” (RLD) method, where two time gated images are taken in the luminescence decay period of the fluorophore. Presuming monoexponential luminescence decay and provided that the two time gates are of the same length, the luminescence decay time can be calculated according to equation 2.13 in chapter 2.4.2.3., with t_1 and t_2 as the starting times of the gates related to the end of the excitation pulse and A_1 and A_2 as the intensity values

gathered in the two different gates. The single intensity images as well as the corresponding background images are acquired in subsequent exposure cycles.^[34]

In our new approach, referred to as “Dual Lifetime Determination” (DLD) method,^[16] the sensor signals are not separated via different emission filters but by means of the different luminescence decay times of the indicators (see *figure 2.5* in *chapter 2.4.2.4*). This method is applicable if the luminescence decay time of the temperature-sensitive probe (here: $\text{Eu}(\text{tta})_3(\text{dpbt})/\text{PVC}$) is at least about 10 times higher than the luminescence decay time of the pressure-sensitive material ($\text{PtTFPP}/\text{PSAN}$). In *figure 2.5*, the different luminescence decay curves are depicted in grey and white, respectively. The temperature-dependent lifetime

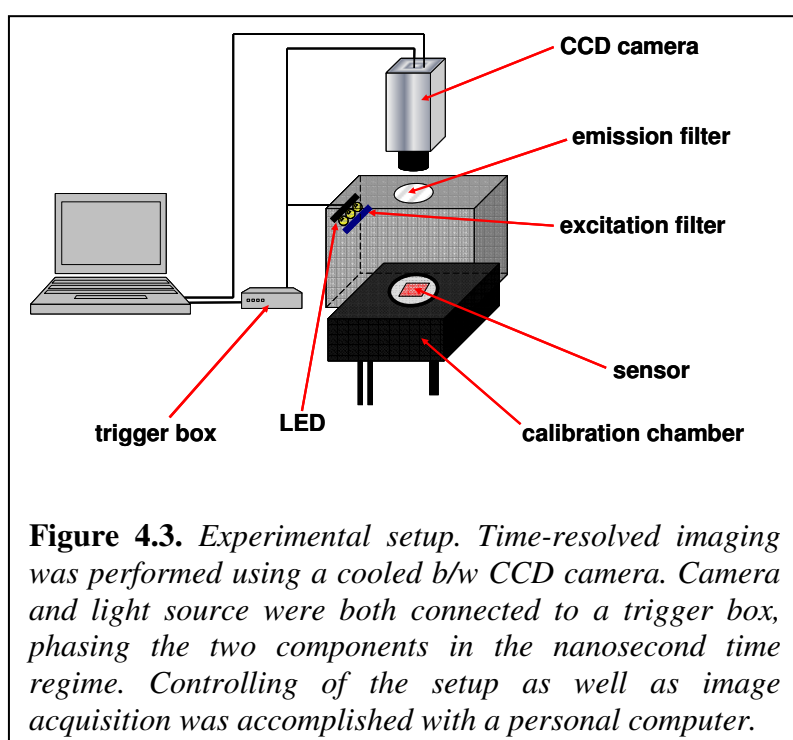


image calculated from A_3 and A_4 can be used to compensate the temperature effect on the lifetime of the pressure probe determined from A_1 and A_2 . Moreover, the Dual Lifetime Determination method is a twofold RLD method, capable of detecting the change of the lifetimes of two different probes at the

same time.^[16,35] The resulting lifetimes can be calculated from the respective pair of gates (A_1 and A_2 , A_3 and A_4 , respectively) according to *equation 2.13*. Decay time based imaging is preferable to imaging of luminescence intensity, because it is free of interferences and sources of error like inhomogeneous excitation light fields, photobleaching of fluorophores, effects of varying distances, light scattering, inhomogeneous dye concentrations in the sensor layer, or turbidity. The dual sensing material was calibrated using a 405 nm LED as the light source. The sensor (9 cm^2) was mounted in a calibration chamber in which pressure and temperature can be adjusted in the range of 50 – 2000 mbar and 1 °C – 50 °C, respectively (see *figure 4.3*).

The dual sensor material was imaged and calibrated by the DLD method. Following an excitation pulse of the LED, four images are taken subsequently during the luminescence decay period of the fluorophore mixture (see *table 4.1.*). Two different sensors of the same composition were calibrated five times each. The standard deviations of data points from the mean value of these ten measurements do not exceed 3.5%. The last two gates exclusively detect the

Table 4.1. *Parameters applied for calibration of the dual sensor material. The times t refer to the end of the excitation pulse with a duration of 2000 μs*

	A_1	A_2	A_3	A_4
t [μs]	0	20	400	500
width [μs]	50	50	400	400

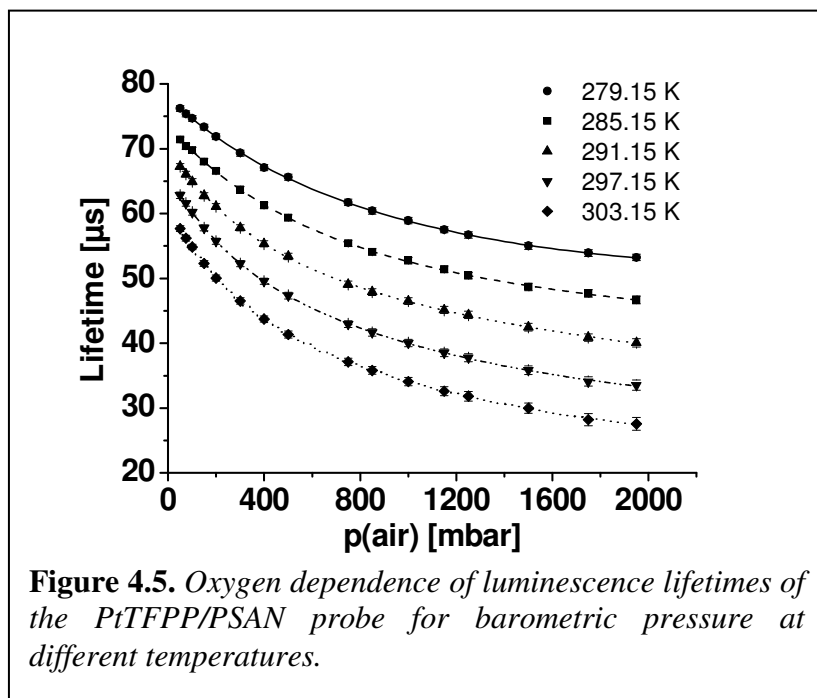
luminescence of the temperature indicator $\text{Eu}(\text{tta})_3(\text{dpbt})$. The dual sensor as well as the single sensors (referred to as reference sensors) containing only PtTFPP/PSAN and $\text{Eu}(\text{tta})_3(\text{dpbt})/\text{PVC}$, respectively, were calibrated and compared. The luminescence of the $\text{Eu}(\text{III})$ -complex particle system is highly temperature dependent, as in can be seen from *figure 4.4*. Both the reference sensor and the dual sensor system gave the same results for the temperature indicator. This proves the effective signal separation in the dual sensor. The luminescence of PtTFPP does not affect the lifetime signal of the $\text{Eu}(\text{tta})_3(\text{dpbt})$ because it is gated off.

The temperature dependency of the temperature sensor is linear at low pressure ranges. The devolution of the calibration curves starts to change above approximately 500 mbar of air pressure. At higher pressures, the decay of the luminescence lifetime by virtue of temperature changes can be described by an Arrhenius-type equation:^[36-38]

$$\frac{1}{\tau} = k_0 + k_1 \cdot \exp\left(-\frac{\Delta E}{R \cdot T}\right) \quad \text{eq. 4.1.}$$

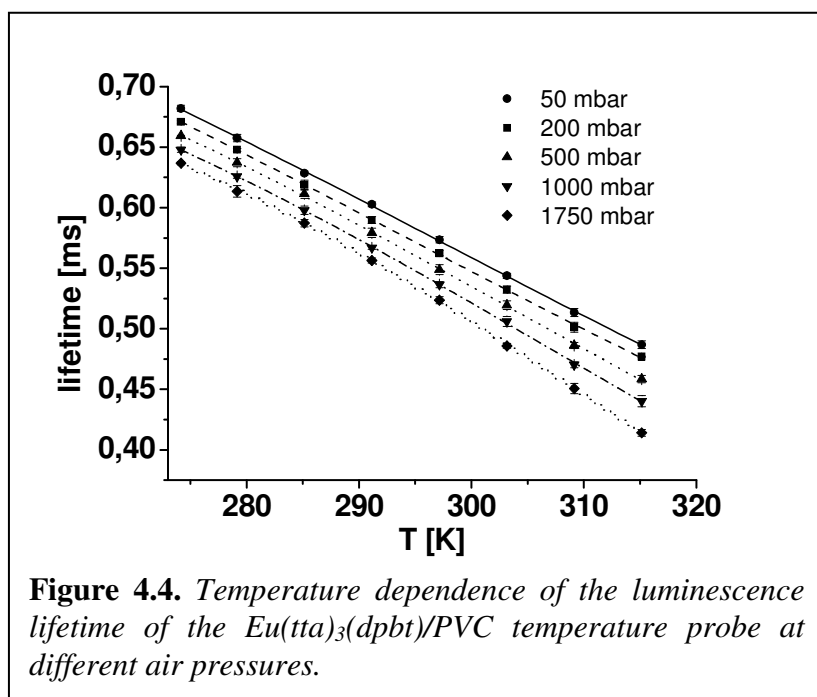
where τ is the lifetime, k_0 the temperature-independent decay rate for the deactivation of the excited state (the sum of radiative and nonradiative decay constants from the emitting state to the ground state), k_1 the preexponential factor, ΔE the energy gap between the emitting level and an upper deactivating excited state, R the gas constant, and T the absolute temperature. The T -dependency of the $\text{Eu}(\text{tta})_3(\text{dpbt})/\text{PVC}$ particles can be fitted using the following parameters (at 1000 mbar air pressure): $k_0=1.6 \text{ s}^{-1}$, $k_1=5.6 \cdot 10^3 \text{ s}^{-1}$, and $\Delta E=22.6 \text{ kJ} \cdot \text{mol}^{-1}$ with an

correlation coefficient (r^2) of 0.9998. The maximum cross-sensitivity of the temperature sensor towards O_2 - quenching is between 7% and 15%. This means,



at a temperature of 274 K the lifetime drops from 0.682 ms to 0.637 ms only (decrease by 7%) when pressure is increased from 50 mbar to 1750 mbar. Oxygen diffusion is more pronounced at higher temperatures. Thus, the cross-sensitivity at 315 K towards O_2 - quenching

raises to 15%. These are satisfactory values for indicators with luminescence decay times of several hundred μs . Besides its gas-blocking properties, the encapsulation in PVC microparticles has a positive effect on the temperature response of the Eu-complex. It linearizes the shape of the calibration curve. This is very desirable for application. In many other polymer matrices, the Arrhenius-type response characteristics is much more pronounced, resulting a smaller lifetime



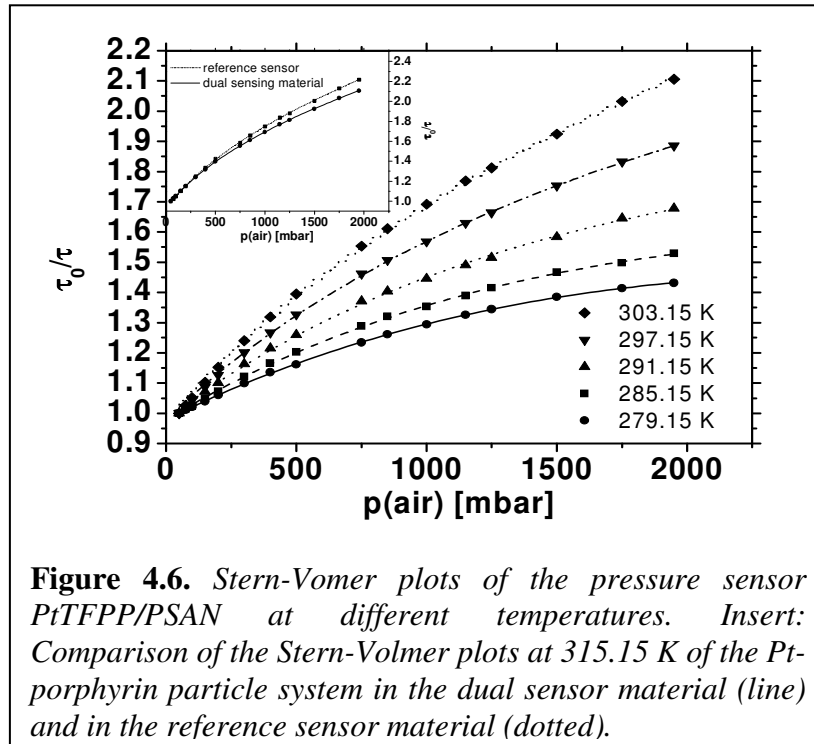
changes at low temperatures.

The response of the pressure sensor material PtTFPP / PSAN (see section 4.4.2) is calculated from the first two gates A_1 and A_2 . Calibration plots for pressure imaging with the new sensor material are presented in figure 4.5.

The mixed intensities of the two indicator systems gathered in A_1 and A_2 result in lower ratio values (and thus higher τ -values) for the Pt-porphyrin compared to the reference system. The ratio of the two intensity images is influenced by the longer decaying luminescence of the $\text{Eu}(\text{tta})_3(\text{dpbt})$. This is very pronounced in the second gate, thus decreasing the intensity ratio A_1/A_2 increases the calculated lifetime. This effect is not eminent, because its influence on the data is not very distinct when considering the relative signal change in the image ratio A_1/A_2 (see figure 4.6. insert). The response to oxygen can be described by the Stern-Volmer equation. In solid state systems, the deviation from linearity is expressed by the so-called “two-site model”,^[39] which accounts for the different chemical and physical environments in polymer matrices and particles.^[40]

$$\frac{\tau}{\tau_0} = \frac{I}{I_0} = \frac{f_1}{1 + k_{SV}^{(1)} \cdot [O_2]} + \frac{f_2}{1 + k_{SV}^{(2)} \cdot [O_2]} \quad \text{eq. 4.2.}$$

with f_1 and f_2 being the emissive fraction of the molecules in the different environment, k_{SV} the Stern-Volmer quenching constants in the different environments, and $[O_2]$ as the oxygen partial pressure. Assuming the constant proportion of oxygen in atmospheric air, the amount of oxygen quenching can be used for pressure determination. The Stern-Volmer type plots of the pressure sensor are depicted in figure 4.6. The response to oxygen of the dual sensing material is slightly decreased compared to the PtTFPP / PSAN reference sensor



(see figure 4.6. insert). This is the result of the non exclusive detection of the emission from the pressure indicator in the first two gates A_1 and A_2 . As described above, the second gate is influenced to a higher extent. Hence, the intensity of A_2 does not decrease to the same value compared with

the reference sensor. Consequently, the changes in the intensity ratio A_1/A_2 (and accordingly the calculated lifetimes) are reduced. This deviation from the reference sensor characteristics decreases with increasing temperature. The data obtained can be fitted by the Stern-Volmer equation (eq. 4.2.) with the factors $f_1=f_2=0.5$ and with r^2 values of greater than 0.9998. The main Stern-Volmer constant $k_{SV}^{(1)}$ increases with increasing temperature. The more efficient dynamic O_2 - quenching at higher temperatures agrees very well with theory. Higher temperature causes a more effective O_2 diffusion in the polymer. Accordingly, the secondary Stern-Volmer constants $k_{SV}^{(2)}$ increase just as well, but are negligible compared with the value of the main Stern-Volmer constant (see table 4.2.).

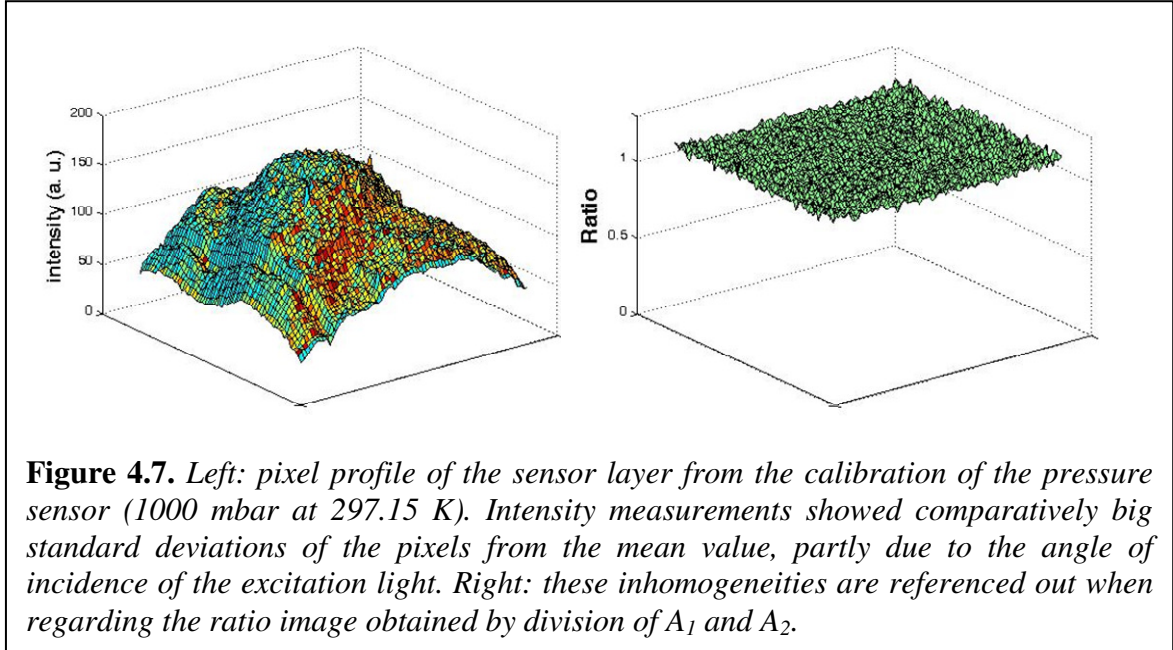
Table 4.2. Stern-Volmer constants from the calibration of the pressure sensor. Fitting parameters were set to $f_1=f_2=0.5$.

T [K]	$k_{SV}^{(1)}$ [10^{-3} mbar $^{-1}$]	$k_{SV}^{(2)}$ [10^{-3} mbar $^{-1}$]
279.15	1.13 ± 0.02	0.01 ± 0.003
285.15	1.33 ± 0.02	0.01 ± 0.002
291.15	1.64 ± 0.01	0.05 ± 0.002
297.15	1.95 ± 0.03	0.12 ± 0.004
303.15	2.22 ± 0.06	0.20 ± 0.006

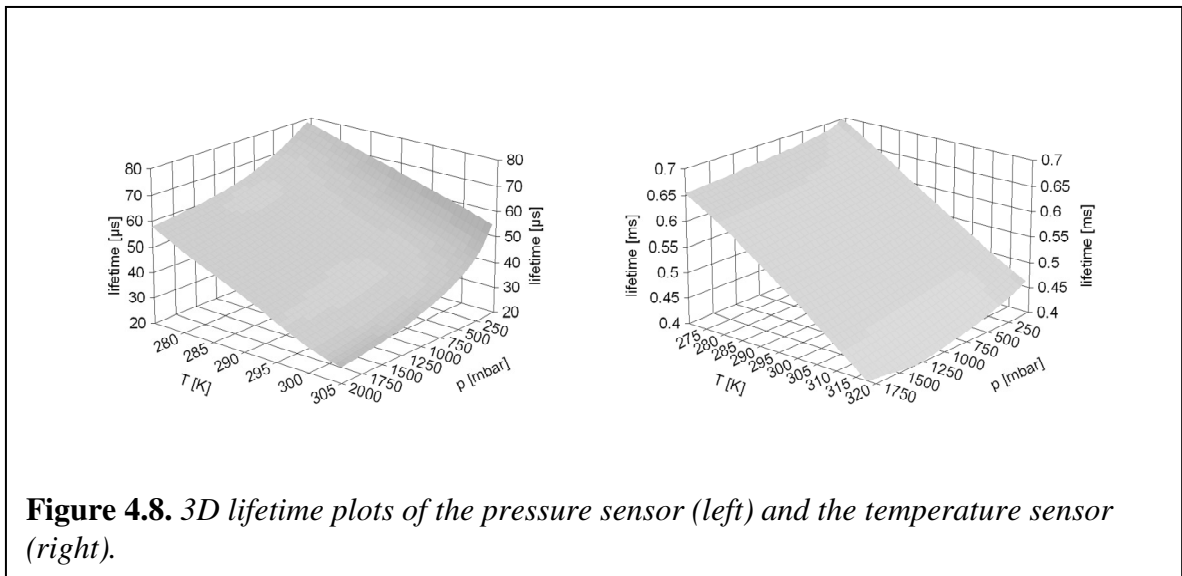
4.2.3. Sensor Validation

The novel dual sensor paint along with the DLD calibration method was tested regarding performance and accuracy. The intensity distribution of the sensor compared to the resulting image ratio, in which inhomogeneities are referenced out, is presented in figure 4.7. The DLD method in combination with the high homogeneity of the sensor layer enables simultaneous determination of pressure and temperature (p/T) in high spatial resolution. Lifetime results remained constant after ten times calibration over the full p/T range as well as after three months of storage of the sensor material. This demonstrates the good photostability and shelf life of the sensor system. In particular, photobleaching of one of the components would cause significant changes in the results obtained from the first two gates, where the mixed emission intensity of both indicators is recorded.

The accuracy of the system was investigated by imaging the lifetime of some randomly selected p/T data pairs not coinciding with data points from the calibration measurements. For that purpose, calibration data of the combined p/T



sensor were plotted in 3D and fitted polynomial surface equations (see figure 4.8.). The resulting image ratios of the selected p/T values were used to determine the corresponding p/T values. Pressure determination by using only the first two gates resulted in rather imprecise pressure values in the first step, covering the range from 700 mbar to 1500 mbar at different temperatures. Data from the temperature sensor were then used to compensate the large deviation in the pressure determination. For example the image data for the randomly selected point $p=1155$ mbar, $T=294$ K reveals a temperature of (294 ± 0.6) K and a pressure of



(1153.9 ± 3.1) mbar after three iteration steps in very good agreements with the chosen values for temperature and pressure. Similar results were obtained for other data points (900 mbar at 307 K, 750 mbar at 288 K). At air pressures lower than 400 mbar, the uncertainty of its determination increases rapidly. Accordingly, the novel dual sensing material is suitable for simultaneous determination of pressure and temperature in the range between 0.5 and 2.0 bar from 273 to 320 K with an average accuracy of 3.5 bar for pressure, and 0.7 K for the temperature.

Simultaneous optical sensing of two parameters such as oxygen, temperature, small organic molecules or gases, and biological relevant compounds like glucose gained much interest over the last 20 years.^[7,28,41,42,43] Temperature and pressure sensors were successfully applied to aerodynamic research^[5,10,44] and dermatology.^[3] Most of the approaches are based on the measurement of luminescence intensity instead of lifetime. Regardless of the method applied, temperature correction of the pressure measurement is necessary, because both analytes cause a response.^[36] This is accomplished in most of the cases by dual-luminophore pressure-sensitive paints where the signal of a reference dye is set into relation to the signal of the pressure indicator in order to compensate the temperature effect. The emission of the luminescence probes has to be separated via different optical filters and/or cameras. These methods are in contrast to the novel dual sensing technique used in this approach. Most of the PSPs reported in literature were evaluated via the intensity signal, which is very prone to errors. This effect can be minimized by addition of the reference dye, which however provides no information about the absolute temperature.^[36,45] The DLD method is a self-referenced technique, revealing absolute p/T values over large surface areas without the need of extensive calibration. The particle/matrix polymer suspension can be sprayed on surfaces, being therefore applicable as a dual PSP/TSP for aerodynamic measurements in wind tunnels. Unlike other approaches, this sensor system is exclusively based on luminescence lifetime determination and does not require any changes of the optical setup or the application of different cameras for signal separation.

4.3. Conclusion

A novel composite material for simultaneous p/T sensing was prepared which consists of two different metal-ligand complexes as fluorescent probes. These are incorporated into different polymer microspheres to control sensitivity, dynamic range of response, and to avoid interferences. These particles are mixed in a polymer binder and can be cast (or sprayed) on a solid support to give a dual sensor layer with high homogeneity. Signals were successfully separated via the distinct luminescence decay times of the applied fluorophores which differ by one order of magnitude. The binary sensor layer was calibrated and evaluated by means of the recently introduced dual lifetime determination method. The high homogeneity of the sensor paint along with the benefits of time-resolved imaging techniques makes the system suitable for simultaneous pressure and temperature determination with a very high spatial resolution. The accuracy and stability of the sensor material promises application in fluid mechanics as a dual PSP/TSP.

4.4. Experimental

4.4.1. Materials and Methods

Poly(styrene-*co*-acrylonitrile) (PSAN, 30 wt% of acrylonitrile, $M_w=185000$), high molecular poly(vinyl chloride) (PVC), and titanium dioxide were obtained from Aldrich (www.sigmaaldrich.com). Platinum(II)-5,10,15,20-tetrakis(2,3,4,5,6-penta-fluorophenyl)porphyrin (PtTFPP) was purchased from Porphyrin Systems (www.porphyrin-systems.de), Elastosil A07 silicone from Wacker (www.wacker.com), PET foil (Mylar) from Goodfellow (www.goodfellow.com), and the polymer hydrogel D4 (linear polyurethane) from Cardiotech (www.cardiotech-inc.com). All solvents (ethanol, tetrahydrofuran, hexane, heptane, and dimethylformamide) were from Fluka (www.sigmaaldrich.com) and used in analytical purity. All chemicals were used without further purification.

Europium(III)-tris(thenoyltrifluoroacetylacetonato)-(2-(4-diethylaminophenyl)-4,6-bis(3,5-dimethylpyrazol-1-yl)-1,3,5-triazine) ($\text{Eu}(\text{tta})_3(\text{dpbt})$) was synthesized according to Yang's procedure.^[31]

In the DLD calibration scheme, four gated images are taken in the emission phase of the fluorophores. The first two gates (A_1 and A_2) have the same length and are positioned in the luminescence phase of both indicators. The second two gates (A_3 and A_4) have also the same length and are positioned at a time, when the first (short living) luminescence has already completely decayed. They exclusively acquire the luminescence of the long-decaying temperature-sensitive probe ($\text{Eu}(\text{tta})_3(\text{dpbt})/\text{PVC}$). The first two images acquire a mixed lifetime of both indicators. The lifetime of the faster decaying pressure-sensitive probe ($\text{PtTFPP}/\text{PSAN}$) can be deduced from these data by iteration processes.

4.4.2. Preparation and Characterization of Oxygen-Sensitive Particles

250 mg of poly(styrene-co-acrylonitrile) were dissolved in 50 mL of DMF and 15 mg of PtTFPP were added. 150 mL of doubly distilled water were added dropwise under ultrasonication. The precipitated particles were centrifuged and washed with water and ethanol respectively. The size of the particles was determined by fluorescence microscopy.

4.4.3. Preparation and Characterization of Temperature-Sensitive Particles

300 mg of poly(vinyl chloride) were dissolved in 60 mL tetrahydrofuran (THF) and 12 mg $\text{Eu}(\text{tta})_3(\text{dpbt})$ were added. 320 mL of heptane was added dropwise under vigorous stirring to pre-precipitate the polymer. Afterwards, the THF was removed slowly at the rotary evaporator to stabilize the formed particles. After centrifugation, the precipitate was washed three times with ethanol and taken up in doubly distilled water. Freeze-drying yielded the particles as a slightly yellow powder. The size of the particles was determined by fluorescence microscopy.

4.4.4. Sensor Preparation

30 mg of the $\text{Eu}(\text{tta})_3(\text{dpbt})/\text{PVC}$ particles and 20 mg of the $\text{PtTFPP}/\text{PSAN}$ particles were suspended in 1300 mg hydrogel D4 solution (5 wt% in $\text{EtOH}:\text{H}_2\text{O}$ 9:1 v:v). This sensor cocktail was stirred overnight and then cast on the PET solid support (thickness: 125 μm) with a knife-coating device to give a sensor layer of 12 μm thickness after drying in ambient atmosphere. A highly reflective screenlayer (1 g silicone and 300 mg TiO_2 in hexane) was cast on the back side of the solid support and left drying over night.

4.4.5. Acquisition of Spectra and Experimental Setup

Absorption and emission spectra were recorded on a Lambda 14 p Perkin-Elmer UV-vis spectrophotometer (Waltham, MA, USA, www.perkinelmer.com) and an Aminco AB 2 luminescence spectrometer (Thermo Scientific Inc., Waltham, MA, USA, www.thermo.com), respectively. All time-resolved measurements were performed with a PCO SensiCam 12 bit b/w CCD camera (PCO, Kelheim, Germany, www.pco.de) equipped with a Schneider-Kreuznach Xenon 0.95/17 lens (www.schneiderkreuznach.com, Jos. Schneider Optische Werke, Bad Kreuznach, Germany) and a 405-66-60 405 nm LED sold by Roithner Lasertechnik (Vienna, Austria, www.roithner-laser.com). The excitation light was focussed by a PCW 18 x 18 MgF2 TS lens from Edmund Optics (www.edmundoptics.com, Karlsruhe, Germany) and fell onto the sensor through an angle of approximately 20°. It was filtered through a BG 12 filter (Schott, Mainz, Germany, www.schott.com) with a thickness of 2 mm. Emission was detected through a D610/60M band pass filter (Chroma, Rockingham, VT, USA, www.chroma.com).

4.5. References

- [1] C. Preiniger, I. Klimant, O. S. Wolfbeis, *Anal. Chem.* **1994**, *66*, 1841
- [2] K. Kellner, G. Liebsch, I. Klimant, O. S. Wolfbeis, T. Blunk, M. B. Schulz, A. Göpferich, *Biotechnol. Bioeng.* **2002**, *80*, 73
- [3] P. Babilas, V. Chacht, G. Liebsch, O. S. Wolfbeis, M. Landthaler, R. – M. Szeimies, C. Abels, *Br. J. Cancer* **2003**, *88*, 1462
- [4] A. E. Baron, J. D. S. Danielson, J. R. Wan, J. B. Callis, B. MacLachlan, *Rev. Sci. Instrum.* **1993**, *63*, 3394
- [5] C. Klein, R. H. Engler, U. Henne, W. E. Sachs, *Exp. Fluids* **2005**, *39*, 475
- [6] Z. Rosenzweig, R. Kopelman, *Anal. Chem.* **1995**, *67*, 2650
- [7] S. M. Borisov, C. Krause, S. Arain, O. S. Wolfbeis, *Adv. Mater.* **2006**, *18*, 1511
- [8] M. Schäferling, M. Wu, J. Enderlein, H. Bauer, O. S. Wolfbeis, *Appl. Spectrosc.* **2003**, *57*, 1386
- [9] R. H. Engler, C. Klein, O. Trinks, *Meas. Sci. Technol.* **2000**, *11*, 1077
- [10] B. G. MacLachlan, J. L. Kavandi, J. Callis, M. Gouterman, E. Green, G. Khalil, D. Burns, *Exp. Fluids* **1993**, *14*, 33
- [11] K. Mitsuo, K. Asai, A. Takahashi, H. Mizushima, *Meas. Sci. Technol.* **2006**, *17*, 1282
- [12] B. Zelelow, G. E. Khalil, G. Phelan, B. Carlson, M. Gouterman, J. B. Callies, L. R. Dalton, *Sens. Actuators B* **2003**, *96*, 304
- [13] J. Hradil, C. Davies, K. Mongey, C. McDonagh, B. D. MacCraith, *Meas. Sci. Technol.* **2002**, *13*, 1552
- [14] K. Nakakita, M. Kurita, K. Mitsuo, S. Watanabe, *Meas. Sci. Technol.* **2006**, *17*, 359
- [15] M. Kameda, N. Tezuka, T. Hangai, K. Asai, K. Nakakita, Y. Amao, *Meas. Sci. Technol.* **2004**, *15*, 489
- [16] S. Nagl, M. I. Stich, M. Schäferling, O. S. Wolfbeis, *Anal. Bioanal. Chem.* **2008**, available online
- [17] M. E. Lippitsch, J. Pusterhofer, M. J. P. Leiner, O. S. Wolfbeis, *Anal. Chim. Acta* **1988**, *205*, 1
- [18] R. E. Ballew, J. N. Demas, *Anal. Chem.* **1989**, *61*, 30
- [19] J. M. Kürner, I. Klimant, C. Krause, H. Preu, W. Kunz, O. S. Wolfbeis, *Bioconjugate Chem.* **2001**, *12*, 883
- [20] D. R. Walt, *Science* **2000**, *287*, 451
- [21] I. Klimant, M. Köhl, R. N. Glud, G. Holst, *Sens. Actuators B* **1997**, *38*, 29
- [22] L. – M. Fu, X. – F. Wen, X. – C. Ai, Y. Sun, Y. – S. Wu, J. – P. Zhang, Y. Wang, *Angew. Chem. Int. Ed.* **2005**, *44*, 747
- [23] S. – W. Lai, Y. – J. Hou, C. – M. Che, H. – L. Pang, K. – Y. Wong, C. K. Chang, N. Zhu, *Inorg. Chem.* **2004**, *43*, 3724
- [24] S. – K. Lee, I. Okura, *Anal. Comm.* **1997**, *34*, 185
- [25] Y. Amao, K. Asai, I. Okura, J. Porphyrins Phthalocyanines **2000**, *4*, 292
- [26] *Polymer Handbook* (Eds : J. Brandrup, E. H. Immergut, E. A. Grulke), Wiley-VCH, New-York **1999**
- [27] S. M Borisov, A. S. Vasylevska, C. Krause, O. S. Wolfbeis, *Adv. Funct. Mater.* **2006**, *16*, 1536
- [28] G. A. Crosby, *Mol. Cryst.* **1966**, *1*, 37
- [29] F. J. Steemers, W. Verboom, D. N. Reinhoudt, E. B. van der Tol, J. W. Verhoeven, *J. Am. Chem. Soc.* **1995**, *117*, 9408
- [30] M. H. V. Werts, M. A Duin, J. W. Hofstraat, J. W. Verhoeven, *Chem. Commun.* **1999**, 799
- [31] C. Yang, L. – M. Fu, Y. Wang, J. – P. Zhang, W. – T. Wong, X. – C. Ai, Y. – F. Qiao, B. – S. Zou, L. – L. Gui, *Angew. Chem. Int. Ed.* **2004**, *43*, 5009
- [32] M. L. Bhaumik, *J. Chem. Phys.* **1964**, *40*, 3711
- [33] G. E. Khalil, K. Lau, G. D. Phelan, B. Carlson, M. Gouterman, J. B. Callis, L. R. Dalton, *Rev. Sci. Instrum.* **2004**, *75*, 192

- [34] G. Liebsch, I. Klimant, B. Frank, G. Holst, O. S. Wolfbeis, *Appl. Spectrosc.* **2000**, *54*, 548
- [35] J. Hradil, C. Davis, K. Mongey, C. McDonagh, B. D. MacCraith, *Meas. Sci. Technol.* **2002**, *13*, 1552
- [36] L. M. Coyle, M. Gouterman, *Sens. Actuators B* **1999**, *61*, 92
- [37] G. Liebsch, I. Klimant, O. S. Wolfbeis, *Adv. Mater.* **1999**, *11*, 1296
- [38] J. N. Demas, B. A. DeGraff, *Anal. Chem.* **1991**, *63*, 829A
- [39] E. R. Carraway, J. N. Demas, B. A. DeGraff, J. R. Bacon, *Anal. Chem.* **1991**, *63*, 337
- [40] S. Draxler, M. E. Lippitsch, *Anal. Chem.* **1996**, *68*, 753
- [41] O. S. Wolfbeis, H. E. Posch, *Anal. Chem.* **1985**, *57*, 2556
- [42] O. S. Wolfbeis, E. Urbano, *Anal. Chem.* **1983**, *55*, 1994
- [43] J. W. Parker, O. Laksin, C. Yu, M. – L. Lau, S. Klima. R. Fisher, I. Scott, B. W. Atwater, *Anal. Chem.* **1993**, *65*, 2329
- [44] J. Gallery, M. Gouterman, J. Callis, G. Khalil, B. McLachlan, J. Bell, *Rev. Sci. Instrum.* **1994**, *65*, 712
- [45] G. E. Khalil, C. Costin, J. Crafton, G. Jones, S. Grenoble, M. Gouterman, J. B. Callis, L. R. Dalton, *Sens. Actuators B* **2004**, *97*, 13

CHAPTER 5

Read-Out of Multiple Optical Chemical Sensors by Means of Digital Color Cameras

Cooled black-and-white CCD-cameras are well-established devices to monitor the signal response of probes and sensors in imaging applications. When two (or even three) analytes are considered, the signals of interest have to be separated from each other. Generally, this is accomplished by using filter wheels or, in case of time-resolved imaging, by evaluating the different luminescence decay times of the indicators. Here a novel approach for signal separation of multiple sensors is presented. It utilizes the basic setup of color CCD and CMOS cameras. The principle of color cameras is based on the application of three different types of pixels (CCD/CMOS) or layers (FOVEON X3-type). These are sensitive towards different wavelength ranges. In other words, the intensity of the different colors is detected and processed in different areas on the camera chip. This information is transported in three different channels and is then combined, resulting in a colored image. The idea was to utilize this technique for the separation of multiple sensor signals. Due to the spatial distribution of three different types of pixels, it is possible to monitor the intensity of three different colors from the different analyte-sensitive probes with one single image.

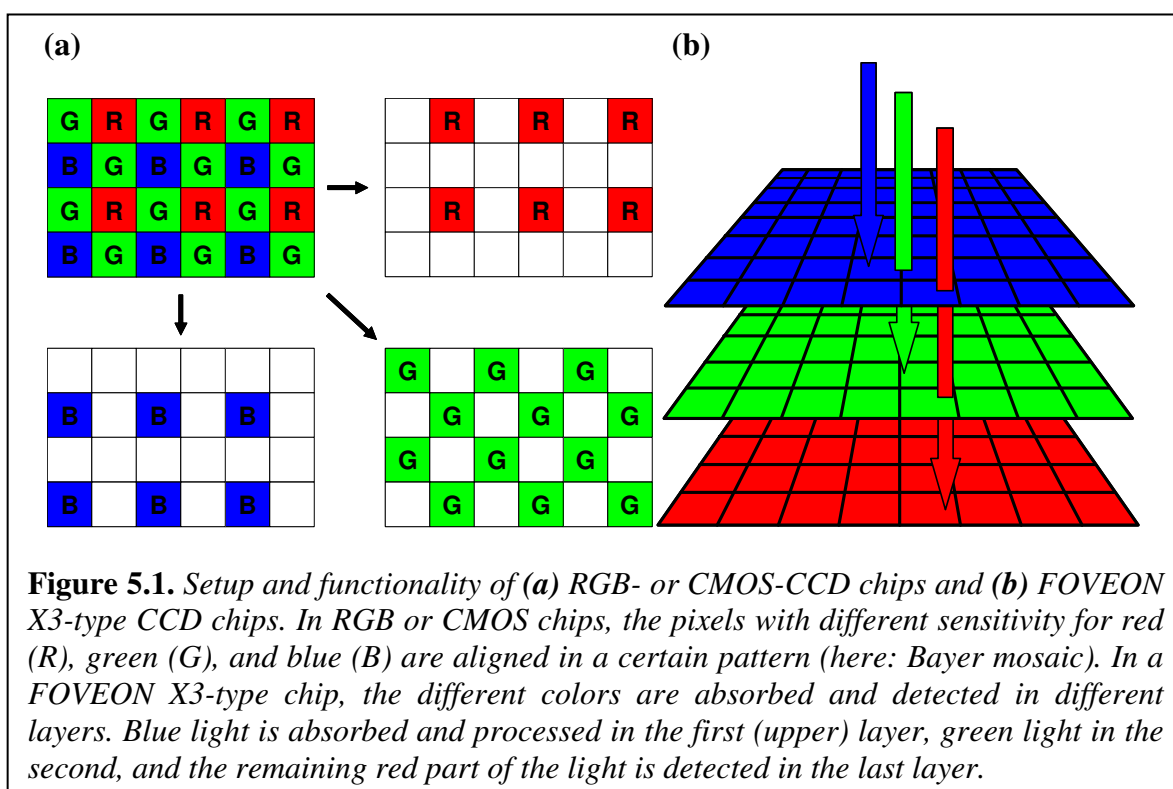
5.1. Introduction

Optical sensors are based on materials that change their optical properties – most notably luminescence intensity – when exposed to the analyte of interest.^[1] The indicator signal has to be referenced with the signal of a second fluorophore in order to obtain unambiguous data.^[2] When dealing with intensity measurements, the reference dye is an inert standard molecule.^[3] In the case of dual optical sensors, the second probe responds to a different analyte in order to compensate for cross-talk.^[4,5] The two signals have to be separated entirely, no matter which method is applied. This is accomplished in the majority of the cases with different

optical emission filters, either mounted in a mechanical filter wheel or in front of two different detection devices (e.g. b/w CCD cameras).^[6] When the emissions of the two probes can not be separated optically, the signals of interest also can be divided due to the different luminescence lifetimes of the indicators by novel time-resolved imaging approaches.^[7]

Here, a novel approach for signal separation is presented, based on the fundamental setup of color cameras. In case of CCD or CMOS camera, the pixels of a normal black-and-white camera are covered with three different optical filters (one kind for blue, red, green, respectively) in a certain pattern. By this means, information about the color distribution is introduced on the chip (see *figure 5.1.*)^[8,9]

FOVEON X3-type chips are based on the application of three different layers, each of them sensitive to another wavelength range. The first layer absorbs and detects the blue fraction of the incoming light, the second layer the green part of



the spectrum, and the remaining red light is registered in the third layer (see *figure 5.1.*)^[10-12] The color information is registered on different areas on the chip, regardless which setup is applied. This information is then transported in three different channels (one for each color) and recombined, resulting in a colored image.

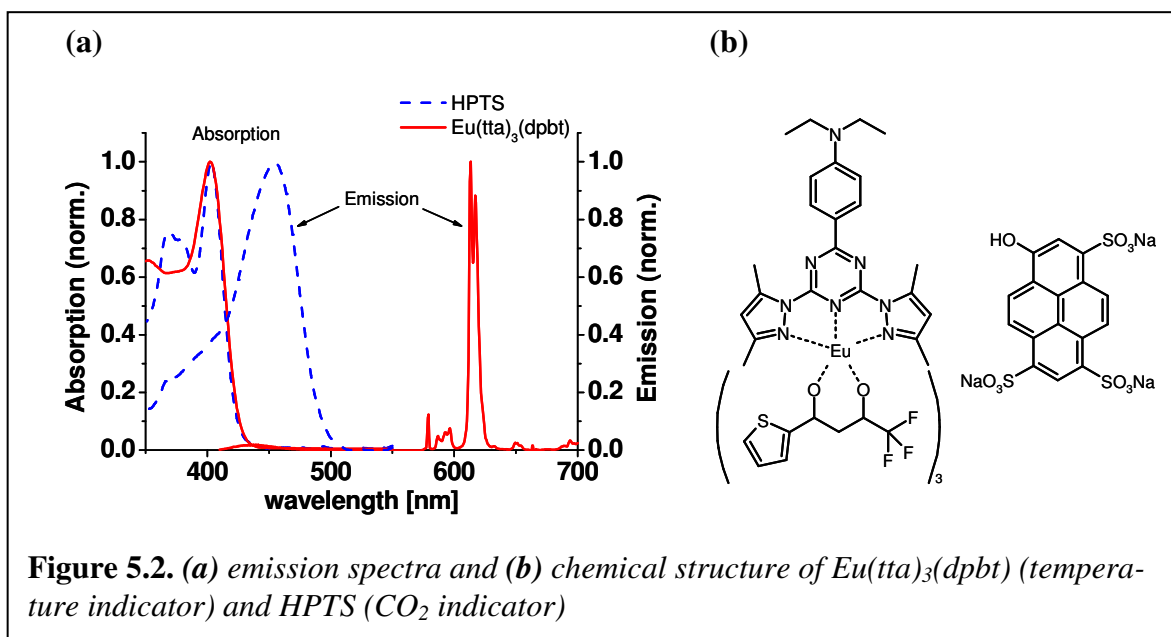


Figure 5.2. (a) emission spectra and (b) chemical structure of $\text{Eu}(\text{tta})_3(\text{dpbt})$ (temperature indicator) and HPTS (CO_2 indicator)

This fundamental setup of digital camera chips can also be utilized for three-channel luminescence imaging. Due to the spatial distribution of the three different types of pixels, it is possible to monitor the intensity (or even lifetime, if a time-gated color camera is used) of three different colors with one single image. For the proof of principle, a dual sensor was designed that exhibits emissions in the blue and in the red area. A carbon dioxide probe based on 8-hydroxypyrene-1,3,6-trisulfonate (HPTS)^[13] with emission in the blue (for the protonated form) and europium(III)-tris(thenoyltrifluoroacetylacetonato)-(2-(4-diethylaminophenyl)-4,6-bis(3,5-dimethylpyrazol-1-yl)-1,3,5-triazine) ($\text{Eu}(\text{tta})_3(\text{dpbt})$)^[14,15] as a temperature indicator^[16] with red emission were combined. The structure and the emission spectra of the two compounds can be seen in *figure 5.2*. Both indicators are excitable at 405 nm and their emissions do not overlap. The two probes, the CO_2 indicator HPTS dissolved in ethyl cellulose (EC, 49% ethoxy content) and the

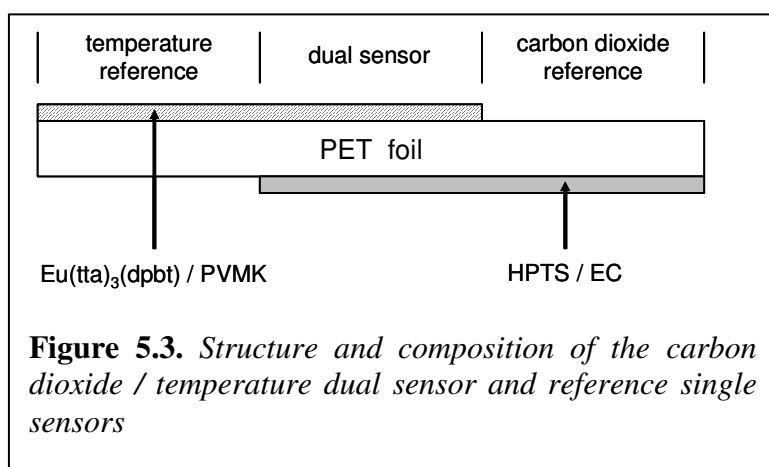


Figure 5.3. Structure and composition of the carbon dioxide / temperature dual sensor and reference single sensors

temperature indicator $\text{Eu}(\text{tta})_3(\text{dpbt})$ dissolved in poly(vinyl methyl ketone) (PVMK) were cast on a transparent poly(ethylene terephthalate) (PET) solid support to give a two-layer dual sensor and two further areas for single

indicator referencing, as described in detail in *section 5.4.2*. A cross-section of the sensor layer is depicted in *figure 5.3*. The area for simultaneous sensing is not a dual sensor in its real sense, because the two layers are separated by the solid support. Hence, it is rather a mixture of two single sensors. However, this setup is appropriate to demonstrate the feasibility of signal separation by means of the novel imaging approach.

5.2. Results and Discussion

The dual sensor was placed in a flow-through cell, which was connected to a thermostat and a gas mixing device. Excitation was performed with a 405 nm LED. The response of the sensor system was studied at seven different temperatures and six different carbon dioxide concentrations. For image acquisition, the sensor foil was illuminated continuously and the emitted light was recorded with a commercially available Canon EOS 350 D digital camera, applying an exposure time of three seconds. For calibration the intensity of the temperature indicator $\text{Eu}(\text{tta})_3(\text{dpbt})$ was evaluated at the temperatures $T = 10\text{ }^{\circ}\text{C}$, $20\text{ }^{\circ}\text{C}$, $30\text{ }^{\circ}\text{C}$, $40\text{ }^{\circ}\text{C}$, $50\text{ }^{\circ}\text{C}$, $60\text{ }^{\circ}\text{C}$, and $70\text{ }^{\circ}\text{C}$ under nitrogen atmosphere to avoid cross-sensitivity to oxygen. The intensity of the CO_2 indicator HPTS was evaluated at different carbon dioxide concentrations in a CO_2/N_2 mixture with $c(\text{CO}_2)=0\%$, 2.5% , 5% , 20% , 50% , and 100% .

5.2.1. Carbon Dioxide Sensor

The intensity of the carbon dioxide indicator HPTS in the sensor layer (see *section 5.4.2*) was monitored in the blue channel (see *figure 5.2*). It increases when increasing the carbon dioxide concentration as it can be seen in *figure 5.4*. The results of the calibration are shown in *figure 5.5*. The sensor response can be described by a usual sigmoidal fit. The sensitivity towards CO_2 is slightly lower compared to the data in literature^[17,18] due to the absence of humidity in the carbon dioxide/nitrogen gas mixture. The sensor seems to be more sensitive at lower temperatures (the slope decreases) than at higher temperatures, which is in

good agreement with the properties of carbon dioxide sensors. The noise of the measurement is very low, showing nearly no intensity in the red channel. The response of the dual sensor is in good agreement with the results of the reference

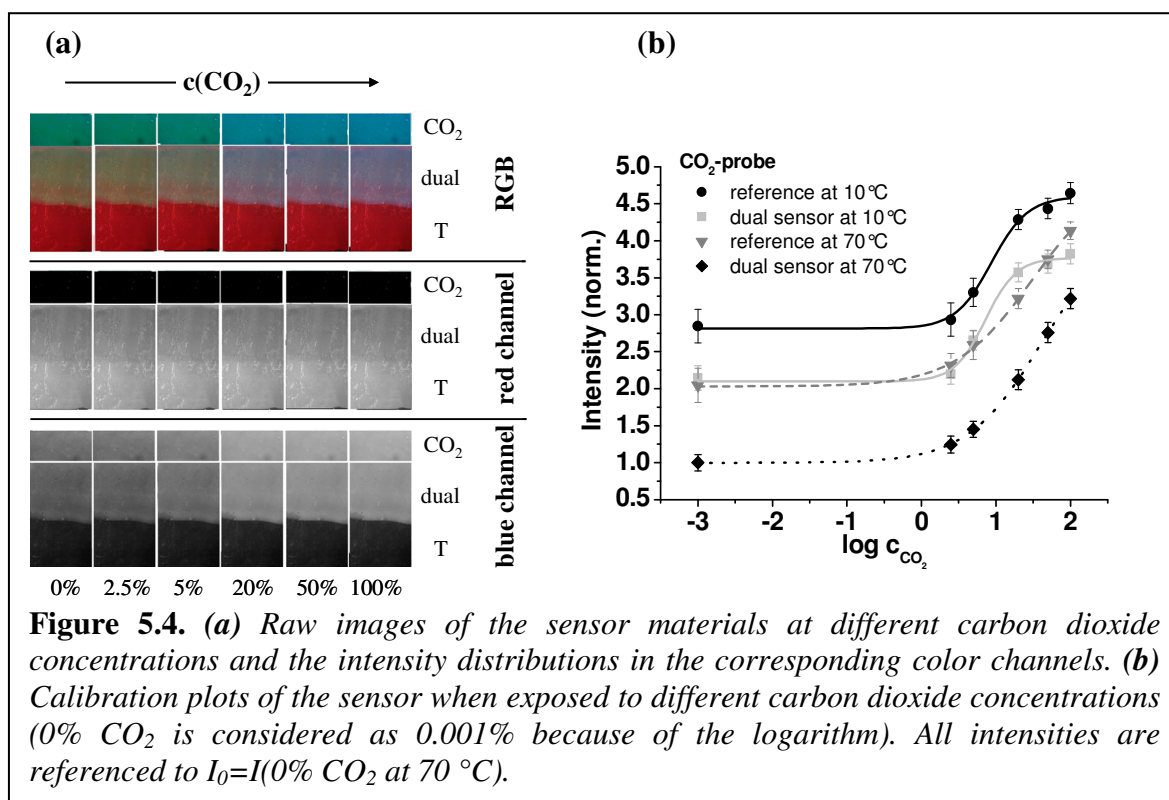


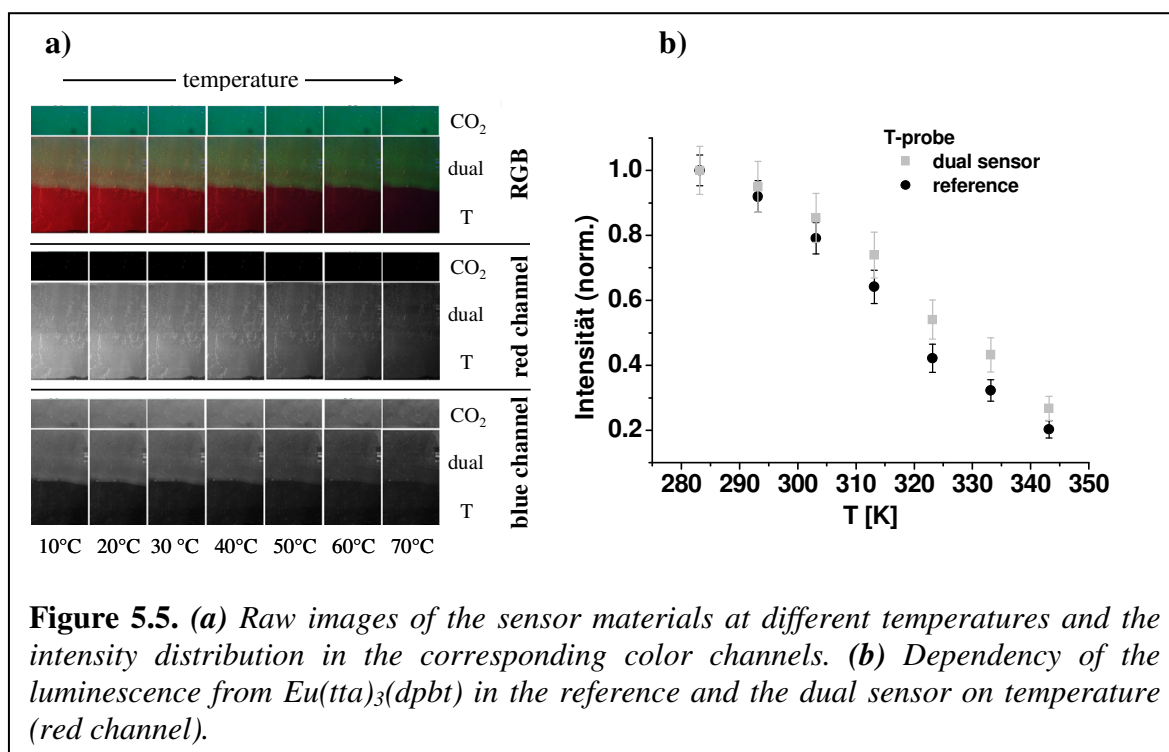
Figure 5.4. (a) Raw images of the sensor materials at different carbon dioxide concentrations and the intensity distributions in the corresponding color channels. (b) Calibration plots of the sensor when exposed to different carbon dioxide concentrations (0% CO₂ is considered as 0.001% because of the logarithm). All intensities are referenced to $I_0 = I(0\% \text{ CO}_2 \text{ at } 70^\circ \text{C})$.

sensor area. The deviations in the overall intensity derive from the assembly of the two-layer sensor system. The signal of the carbon dioxide sensing layer is attenuated by the temperature sensing layer on top of it, whereas the reference area is not affected (see figure 5.3.)

5.2.2. Temperature Sensor

The intensity response of the Eu(tta)₃(dpbt) complex in the sensor layer (see section 5.4.2) to temperature was monitored in the red channel. The emission peak of this metal-ligand complex is very narrow at 618 nm (see figure 5.2) and can thus be easily separated from the other indicator. The colored raw images (see figure 5.5) show clearly a very pronounced change in luminescence intensity when altering temperature, while the CO₂ sensor remains nearly unaffected. In the intensity pictures of the different channels, there is no intensity monitored for the HPTS (CO₂ sensor) in the red channel. The response of the luminescence intensity of the europium complex to temperature is shown in figure 5.5.b. The

trend of the data points can be fitted with an Arrhenius type equation, which describes the temperature quenching effect of metal-ligand complexes very well.^[19-21]



There is some signal in the blue channel which is slightly bigger than in the HPTS measurements, showing an upward trend when increasing temperature. This effect is probably caused by the increase in the fluorescence intensity of the antenna chromophore of the europium complex (see figure 5.2). The response of the temperature probe is not influenced by the carbon dioxide concentration.

5.3. Conclusion

The dual CO₂/temperature sensor was successfully calibrated with a novel digital color camera imaging approach. Signal separation due to the different emission color of the luminescent indicators applied proved to be very effective. The response of the sensor system agrees very well with theory and reference measurements. The deviations in the results of the dual sensor from the reference measurements derive to the bigger part from the assembly of the dual sensor, because the emission from the bottom layer is always attenuated by passing

through the layer above (see *figure 5.3*). This effect diminishes the overall intensity and also the sensor response to a certain extent.

The splitting of the colored raw images into the three RGB channels can be done by every common image editing software (even freeware). The resulting black-and-white intensity images are very definite. Deviations and inaccuracies are caused by well-known sources of error when measuring luminescence intensities.^[2]

The novel imaging method presented here is applicable to many fields of luminescence imaging. The main advantage is the content of information in just one single image. The demands on the experimental setup are reduced significantly, because no optical emission filters have to be applied. The physical values of all sensors are available at the same location and at the same time – unlike in the two camera approach – without the application of sophisticated image manipulation software. Together with the feasibility of low-cost digital cameras (compared to cooled CCD cameras), the overall costs for the imaging setup are cut dramatically. Theoretically, three different indicators can be employed to measure three different analytes (or two analyte-specific probes and one reference), one emitting in the blue, one in the green, and one in the red when excited in the range between 350 nm and ~ 430 nm. Furthermore, referenced intensity imaging can be performed very easily. Regarding for example intensity-based pressure-sensitive paints (PSPs), the oxygen-sensitive probe could be easily and clearly separated from the reference dye. The incorporation of quantum dots into a single or dual sensor can improve the accuracy of intensity-based measurements. They exhibit a rather narrow emission band, are excitable at any wavelength below their emission wavelength and are inert towards the majority of analytes. This enables for ratiometric intensity measurements, thus improving feasibility and precision.

With the new imaging approach presented here, the application of emission filters and additional cameras is not necessary, thus lowering the demands on the experimental setup and the amount of images to be acquired and evaluated. Furthermore, the evaluation of color-shifting sensors can be simplified and maybe specified.^[22] As demonstrated here, even common digital cameras can be used for imaging purposes.^[23] This novel approach is applicable when the indicators of interest show luminescence in different wavelength areas. Even if the dyes do not

emit in the maximum sensitivity areas of the camera for the respective colors (~ 460 nm – 480 nm for blue, ~ 520 nm – 565 nm for green, ~ 625 nm – 700 nm for red), the results are unambiguous and highly reproducible after calibration of the system.

5.4. Experimental

5.4.1. Materials

8-Hydroxypyrene-1,3,6-trisulfonate (HPTS, purity > 97%) trisodium salt and ethyl cellulose (49% ethoxy content) was purchased from Aldrich (Taufkirchen, Germany). Poly(ethylene terephthalate) (Mylar®) foil was obtained from Goodfellow GmbH (Bad Nauheim, Germany). Poly(vinyl methyl ketone) (PVMK, average MW=500 000) was purchased from Acros Organics (Nidderau, Germany). Tetraoctylammonium hydroxide (TOAOH, 25% w/w solution in methanol) was obtained from Fluka. Eu(III)- tris(thenoyltrifluoroacetato) - (2-(4-diethylamino-phenyl) - 4,6 - bis (3,5 -dimethylpyrazol-1-yl)-1,3,5-triazine) (Eu(tta)₃(dpbt)) was synthesized according to Yang's procedure.^[13] The preparation of the ion pair (HPTS(TOA)₃) is reported elsewhere.^[16] All solvents were of analytical grade und were used without further purification. Nitrogen and carbon dioxide gas were obtained from Linde (Munich, Germany).

5.4.2. Preparation of the Dual Sensor

The sensor "cocktail" for CO₂ sensing was prepared by dissolving 200 mg of ethyl cellulose, 2 mg of HPTS(TOA)₃ in 1.8 g of an toluene/ethanol mixture (3:1 w/w). Then 80 µL of TOAOH were added. The "cocktail" for temperature sensing contained 1 mg of Eu(tta)₃(dpbt) and 100 mg of PVMK dissolved in 900 mg of 1,2-dichloroethane. The polymer / indicator blends were cast onto a Mylar support with a thickness of 60 µm using a home-made knife-coating device to give a ~6 µm thick sensor layers after drying (see *figure 5.3*).

5.4.3. Calibration of the Dual Sensor

The dual sensor layer described in *section 5.4.2* was placed in a flow-through cell, which was connected to a thermostat and a gas mixing device. Excitation was performed with a 405 nm LED (405-66-60, Roithner Lasertechnik, Vienna, Austria). Excitation light was filtered through a BG12 filter (Schott AG, Mainz, Germany) and fell on the sensor with an angle of approximately 45°. Color and intensity information was gathered with a commercially available non-scientific Canon EOS 350 D digital camera, placed directly above the sensor foil at a distance of 40-50 cm.

The response of the sensor system was studied at seven different temperatures and six different carbon dioxide concentrations. For image acquisition, the sensor foil was illuminated continuously and the emitted light was recorded with the camera, applying an exposure time of three seconds. The intensity of the temperature indicator $\text{Eu}(\text{tta})_3(\text{dpbt})$ was evaluated at the temperatures $T = 10\text{ }^{\circ}\text{C}$, $20\text{ }^{\circ}\text{C}$, $30\text{ }^{\circ}\text{C}$, $40\text{ }^{\circ}\text{C}$, $50\text{ }^{\circ}\text{C}$, $60\text{ }^{\circ}\text{C}$ and $70\text{ }^{\circ}\text{C}$ under nitrogen atmosphere to avoid cross-sensitivity to oxygen. The intensity of the CO_2 indicator HPTS was evaluated at different carbon dioxide concentrations in a CO_2/N_2 mixture with $c(\text{CO}_2) = 0\%$, 2.5% , 5% , 20% , 50% and 100% .

5.4.4. Data Evaluation

The raw images obtained were transferred from the camera to a PC and were converted into the .tif file format. This format was chosen because it preserves maximum information about an image, while in other file types the images are compressed for smaller file sizes. In this case, some information would be omitted (e.g. areas of low intensities are considered to be black) which is undesirable for imaging applications.

The images were loaded with a standard version of Corel Photo-Paint Version 8.0 and were then divided into their RGB channels. This resulted in additional three black-and-white images, containing the intensity information of the three different color channels, respectively. These intensity distribution images were evaluated with the IDL 5.3 data evaluation software.

5.5. References

- [1] O. S. Wolfbeis, *J. Mater. Chem.* **2005**, 15, 2657
- [2] M. I. J. Stich, O. S. Wolfbeis, in: *Springer Series in Fluorescence, Vol. 5: Standardization in Fluorimetry: State-of-the-Art and Future Challenges*, U. Resch Genger (ed.), Springer, Berlin, **2008**
- [3] C. Klein, R. H. Engler, U. Henne, W. E. Sachs, *Exp. Fluids* **2005**, 39, 475
- [4] S. M. Borisov, A. S. Vasilevska, C. Krause, O. S. Wolfbeis, *Adv. Funct. Mater.* **2006**, 16, 1536
- [5] B. Zelelow, G. E. Khalil, G. Phelan, B. Carlson, M. Gouterman, J. B. Callis, L. R. Dalton, *Sens. Actuators B* **2003**, 96, 304
- [6] G. E. Khalil, C. Kostin, J. Crafton, G. Jones, S. Grenoble, M. Gouterman, J. B. Callis, L. R. Dalton, *Sens. Actuators B* **2004**, 97, 13
- [7] M. I. J. Stich, S. Nagl, O. S. Wolfbeis, U. Henne, M. Schäferling, *Adv. Funct. Mater.* **2008**, 18, 1399
- [8] J. Janesick, G. Putnam, *Annu. Rev. Nucl. Part. Sci.* **2003**, 53, 263
- [9] B. E. Bayer, *US Patent 3971065*, **1976**
- [10] H. Nozaki, T. Adachi, *US Patent 4677289*, **1987**
- [11] C. F. Gay, R. D. Wieting, *US Patent 4581625*, **1986**
- [12] M. B. Chouikha, G. N. Lu, M. Sejl, G. Sou, *US Patent 5883421*, **1999**
- [13] X. Ge, Y. Kustov, G. Rao, *Biotechnol. Bioeng.* **2005**, 89, 329
- [14] C. Yang, L. – M. Fu, Y. Wang, J. – P. Zhang, W. – T. Wong, X. – C. Ai, Y. – F. Qiao, B. – S. Zou, L. – L. Gui, *Angew. Chem. Int. Ed.* **2004**, 43, 5009
- [15] L. – M. Fu, X. – F. Wen, X. – C. Ai, Y. Sun, Y. – S. Wu, J. – P. Zhang, Y. Wang, *Angew. Chem. Int. Ed.* **2005**, 44, 747
- [16] S. M. Borisov, O. S. Wolfbeis, *Anal. Chem.* **2006**, 78, 5094
- [17] O. S. Wolfbeis, E. Führlinger, H. Kroneis, H. Marsoner, *Fresenius Z. Anal. Chem.* **1983**, 314, 119
- [18] D. A. Nivens, M. V. Schiza, S. M. Angel, *Talanta* **2002**, 58, 543
- [19] J. N. Demas, B. A. DeGraff, *Anal. Chem.* 63 (**1991**) 829A
- [20] L. M. Coyle, M. Gouterman, *Sens. Actuators B* 61 (**1999**) 92
- [21] G. Liebsch, I. Klimant, O. S. Wolfbeis, *Adv. Mater.* 11 (**1999**) 1296
- [22] R. C. Evans, P. Douglas, J. A. G. Williams, D. L. Rochester, *J. Fluores.* 16 (**2006**) 201
- [23] U. Henne, R. Engler, M. I. J. Stich, S. M. Borisov, S. Nagl, M. Schäferling, O. S. Wolfbeis, German patent DE 102007 054602.7_52 (**2007**)

CHAPTER 6

Multicolor Fluorescent and Permeation-Selective Microbeads Enable Simultaneous Sensing of pH, Oxygen, and Temperature

We have envisioned the design of a sensor material that would simultaneously respond to pH, temperature (T), and oxygen (O₂) by exploiting the capability of optical sensor materials to give a multitude of optical signals in parallel. Such a sensor does not yet exist and cannot be designed on the basis of non-optical sensing schemes where signals of the three parameters cannot be separated.

6.1. Introduction

Optical chemical sensors – with few exceptions – rely on the use of smart probes and materials that respond to the species of interest by change in their optical properties, often in luminescence.^[1-10] They have the specific option of optical multiplexing. In other words, sensors can be designed such that they give a multitude of spectral and time-dependent information which – in turn – enables sensing of several parameters simultaneously if the signals can be separated and attributed in an unambiguous way. We and others^[11-16] previously have designed dual sensors, e.g. for oxygen and temperature or oxygen and pH, and related multiplex approaches (with one probe responding to more than one parameter) have been reported recently.^[17-19]

Our interest in sensors for pH, T, and O₂ (in gaseous or dissolved form) results from the fact that these are the parameters probably determined most often in chemistry, biology, environmental sciences, and numerous industrial areas, not to talk about more specific areas such as clinical chemistry or marine sciences. Electrochemical devices for these parameters do exist, are widely distributed and perform fairly well. Optical single sensors for these species also do exist for many years,^[1] are less common and have specific merits because information is gathered via photons rather than by electrons, often in combination with fiber optic light guides. This can substantially reduce the risk of explosions in chemical

plants, enables sensing at patients with heart pacemakers and in strong electromagnetic fields, and – in case of fiber optics – paves the way to sensing over large distances.

On a first glance it would appear that triple sensing can be achieved by simply using the three best working indicator probes (one each for pH, T, and O₂) with highly different optical spectra and to incorporate them into an appropriate polymer matrix which then is exposed to the sample to be analyzed. A closer look into the situation reveals that the solution is not as simple for several reasons. Notably, the spectral overlap of practically all indicator probes results in substantial spectral cross-talk. In fact, most probes have bands that extend over more than 150 nm in width so that the spectral range that can be exploited in practice (400 – 750 nm) is almost fully covered by two indicator dyes, not considering the fact that pH probes exist in two forms depending on pH. A second and quite serious limitation results from the effect of fluorescence resonance energy transfer (FRET) whenever indicator probes with overlapping bands are applied in high concentrations so that the critical distance for FRET to occur (typically 5 – 7 nm) is reached; this can result in a heavy cross-talk of signals. Thirdly, pH-dependent color changes are likely to lead to inner filter effects which are disadvantageous if luminescence intensity (rather than lifetime) is measured. Finally, each of the three probes demands for an optimized polymer matrix which not only acts as a mechanical support, but also needs to be permeable to the analyte of interest, ideally is impermeable to any conceivable interferents, and – in the case of all sensors except for oxygen – also prevents quenching of fluorescence by molecular oxygen.^[20,21]

6.2. Sensor Composition

The use of micro- or nanoparticles, each type consisting of an optimized combination of indicator probe and polymer matrix, contained in a bulk polymer matrix (the “binder”) appears to be the solution of choice. We therefore have developed several types of sensing microspheres, each consisting of a different polymer and a specific indicator probe whose spectral property was chosen such that it can be clearly identified by either spectral or temporal resolution. One

additional prerequisite set by us when designing a triple sensor system was that all the luminescent probes used can be photoexcited at the same wavelength (405 nm in our case), since anything else would be of limited practicability mainly for technical reasons. As will be shown below, the three kinds of sensor beads can be incorporated into a sensor matrix (in our case a hydrogel) in varying ratios, thus allowing the intensity of the single signals easily to be adjusted by proper variation of the ratio of beads.

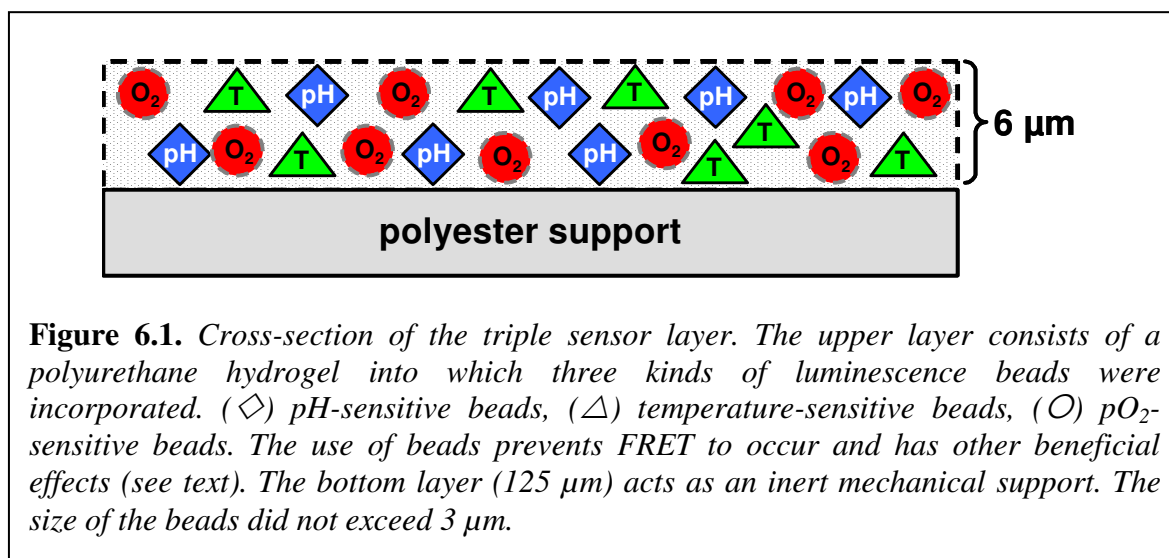
6.2.1. First Triple Sensor System

Two kinds of triple sensors are being presented here. In the first (referred to as TS-1, see *section 6.5.5*), the optical signals of the three kinds of beads are being distinguished by using different emission filters along with time-resolved spectroscopy (see later). In view of the prerequisite of a single wavelength to be used, HPTS (8-hydroxypyrene-1,3,6-trisulfonate) was used as a probe for pH,^[22] the indicator PtTFPL [Pt(II)-5,10,15,20-tetrakis (2,3,4,5,6-pentafluorophenyl) porpholactone] as a luminescent probe for oxygen,^[11] and the europium complex Eu(tta)₃(dpbt) [Eu(III) - tris(thenoyltrifluoroacetylacetonato) - (2 - (4 - diethyl-amino-phenyl) - 4,6- bis(3,5 – dimethylpyrazol – 1 - yl) -1,3,5-triazine)] as the luminescent probe for temperature.^[23,24] The pH probe HPTS covers the physiological pH range and was covalently immobilized to amino-modified poly-HEMA particles^[25] in order to avoid leaching by flowing samples. The luminescence of the temperature probe Eu(tta)₃(dpbt) is measurably quenched by oxygen but this effect can be prevented by incorporating the probe into high molecular weight poly(vinyl chloride) which possesses a very low oxygen permeability coefficient ($P = 3.4 \cdot 10^{-15} \text{ cm}^2 \cdot \text{Pa} \cdot \text{s}^{-1}$).^[20] PtTFPL, in turn, was incorporated into microparticles of the moderately oxygen permeable^[20] copolymer poly(styrene-co-acrylonitrile) (PSAN; $P = 3.5 \cdot 10^{-14} \text{ cm}^2 \cdot \text{Pa} \cdot \text{s}^{-1}$) in order not to cause full quenching at even low $p\text{O}_2$ but rather to cover the range up to air saturation. As a result, three types of polymer particles were obtained possessing distinguishable optical signals, optimized permeation selectivity, and whose cross-sensitivity via FRET interaction is minimized. For details, see *section 6.5*.

6.2.2. Second Triple Sensor System

We also have designed a second type of triple sensor (referred to as TS-2, see section 6.5.6) that exploits the fact that the decay times of the probes used for O_2 and T, respectively, strongly differ. Typical lifetimes are 4 ns for HPTS, 600 μ s for $Eu(tta)_3(dpbt)$, and 50 μ s for PtTFPP. Hence, the intensity of even overlapping spectral signals (see Fig. 2, right panel) can be separated by temporal resolution, a technique known as time-resolved ("gated") spectroscopy. This is to be differentiated from measurement of luminescence decay time, a parameter independent of the respective luminescence intensity. Chemical sensing based on gated spectroscopy or time-resolved spectroscopy can have distinct advantages.^[26] The signal of the temperature probe and the O_2 probe can be separated exploiting their different luminescence decay times. The oxygen probe PtTFPL of TS-1 was replaced by the probe Pt(II)-5,10,15,20-tetrakis(2,3,4,5,6-pentafluorophenyl) porphyrin (PtTFPP)^[27] whose emission overlaps the emission of the temperature probe $Eu(tta)_3(dpbt)$. Its comparably short decay time of approximately 50 μ s enables signal separation from the much longer lived europium(III) temperature probe ($\sim 600 \mu$ s) by applying the dual lifetime determination (DLD) method.^[16]

The three kinds of beads were finally dispersed, in varying ratio, into an ethanol/water solution of a polyurethane hydrogel which acts as the binder polymer (see Fig. 6.1) and represents a most suitable material for such sensors as

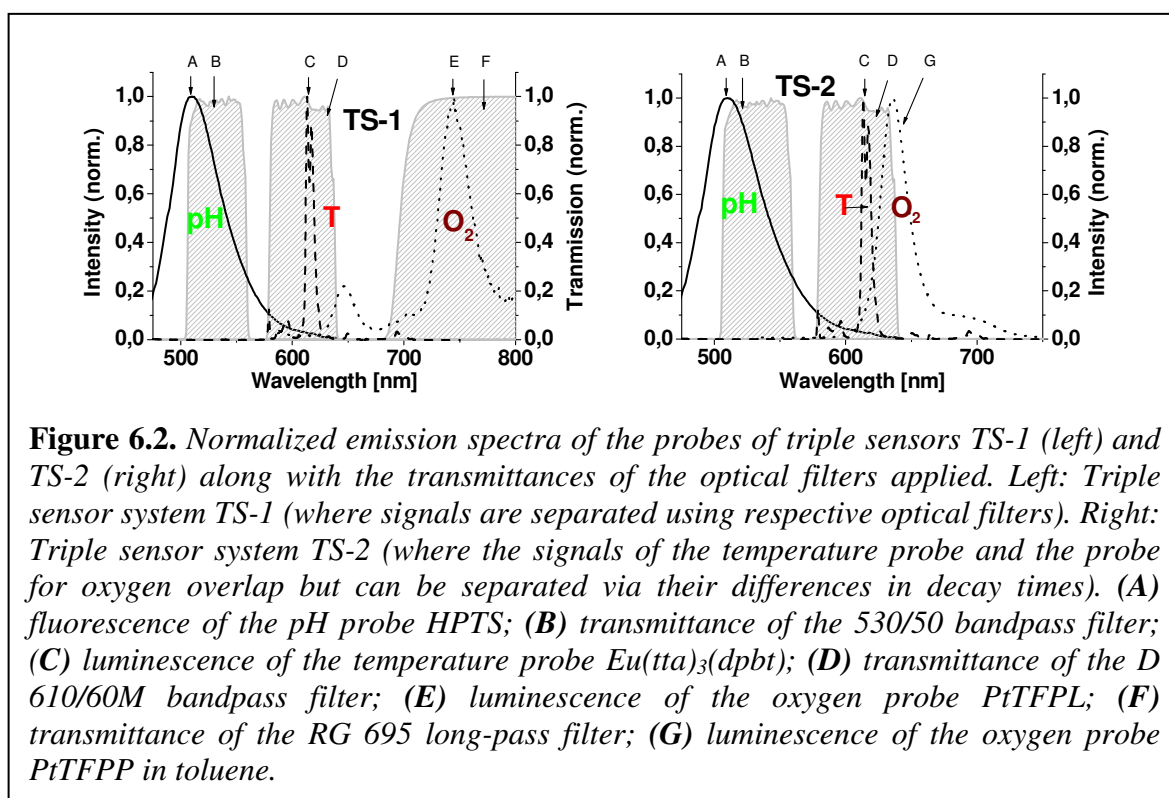


it exhibits excellent permeability for oxygen and protons. It is one of the materials used in contact lenses, biocompatible, and soluble in non-hazardous solvent

mixtures such as ethanol/water (9/1; v/v). The resulting solution/suspension was cast on an optically transparent and inert solid support consisting of poly(ethylene terephthalate) (PET) to give a planar sensing layer whose thickness is 6 μm after solvent evaporation. Such a sensor membrane (in contrast to plain molecular probes) is expected to enable measurements in strongly colored samples such as whole blood or other strongly colored or scattering samples as they are encountered in chemical industry or biotechnology.

6.3. Results and Discussion

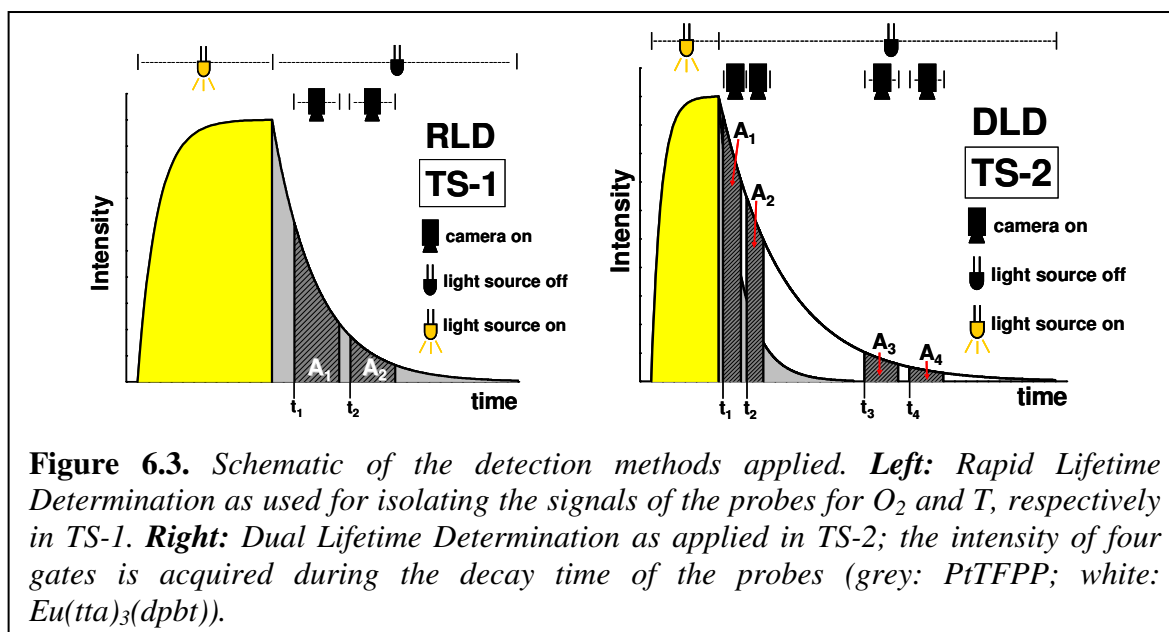
The signal of the pH indicator HPTS in sensor TS-1 was separated from the others using an optical bandpass filter and intensity was measured. The luminescence spectra of all probes are depicted in *figure 6.2*. The signals of the oxygen probe (PtTFPL in PSAN) and of the temperature probe [Eu(tta)₃(dpbt) in PVC] were



separated from each other via different optical filters (see experimental part). To do so, the so-called “Rapid Lifetime Determination” (RLD) time-resolved imaging method^[28] was applied in order to separate the signal of the Eu-complex for temperature from residual short-lived fluorescence of HPTS. In the RLD method, two images are taken in the luminescence decay period of the indicator (see *figure*

6.3). The intensity information in these two gates is then used to calculate the lifetime of the probe (see Experimental Part).

The sensor response of the triple sensors TS-1 and TS-2 was studied by exposing the respective films to, respectively, various pO_2 (using a gas pressure cell), temperatures, and aqueous solutions of varying pH values. The



sensor layers were placed in a thermostatted pressure chamber in which air pressure and temperature were varied from 50 to 2000 mbar, and from 274 K to 309 K, respectively. The pH dependence of the sensors obtained by placing sensor layers in a flow-through cell through which buffers of varying pH were passed. Calibration plots for TS-1 are given in figure 6.4. The data agree very well with the results from reference sensor systems, where only a single kind of bead was incorporated in the hydrogel (data not shown).

In the second sensor system (TS-2), the luminescences of the temperature-sensing particles $[Eu(tta)_3(dpbt)/PVC]$ and of the oxygen probe $[PtTFPP/PSAN]$ overlap and jointly pass the same optical interference filter. However, the different luminescence decay times ($\sim 50 \mu s$ for the Pt complex, but $\sim 600 \mu s$ for the Eu-complex) enable separation of the signals via gated measurements of luminescence.^[29-31]

The DLD method^[16] is particularly useful in such a situation. In this approach, four gates are taken during the decay of the luminescence of the two probes (see figure 6.3). The first pair of gates yields the combined intensity of the two indicators (here the Eu(III) probe and the Pt(II) probe). The second pair of gates is opened only once the luminescence of the shorter lived indicator (here: PtTFPP)

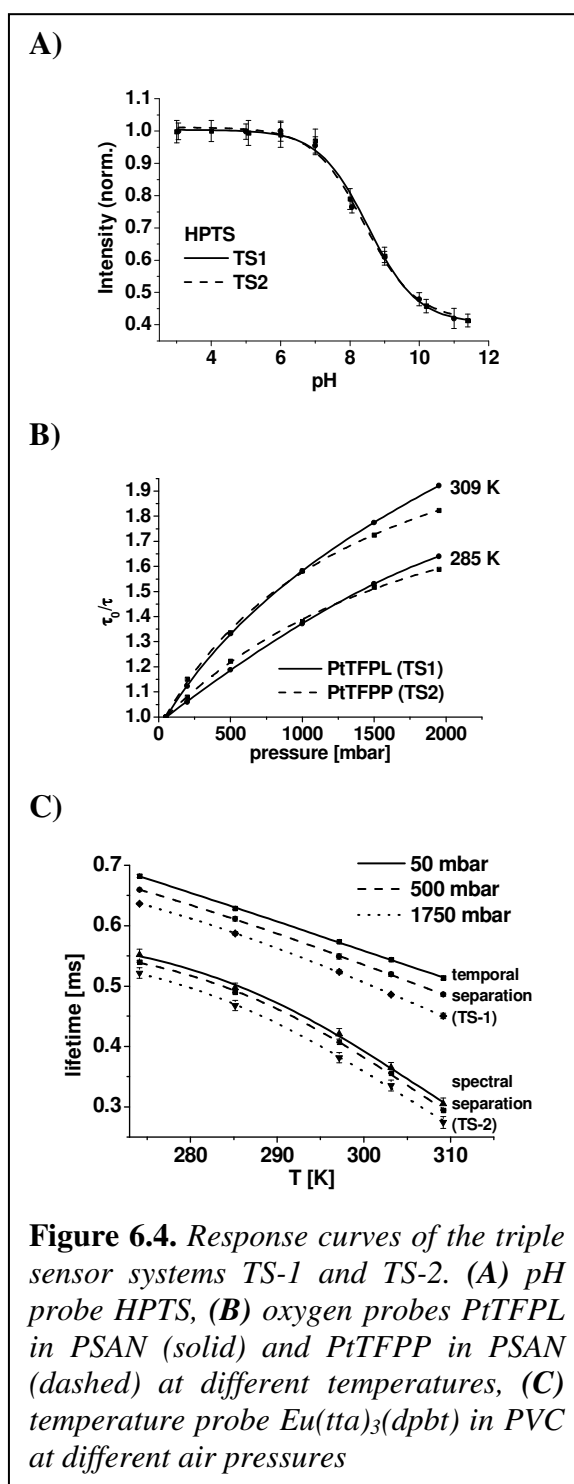


Figure 6.4. Response curves of the triple sensor systems TS-1 and TS-2. (A) pH probe HPTS, (B) oxygen probes PtTFPL in PSAN (solid) and PtTFPP in PSAN (dashed) at different temperatures, (C) temperature probe $\text{Eu}(\text{tta})_3(\text{dpbt})$ in PVC at different air pressures

has decayed, thus detecting exclusively the intensity of the long-lived probe (in this case the Eu(III) temperature probe) (see experimental part). This information can then be used to compensate for the temperature cross-sensitivity of the oxygen data obtained in the first two gates. The results (for algorithms see ref.^[16]) were used to construct the response functions shown in figure 6.4.

The deviations in the response of the temperature probe (see figure 6.4c) derive from the different parameters applied for time resolved imaging of TS-1 and TS-2 (see the Experimental Part). Unfortunately, the luminescence decay profile of the Eu(III) complex is multi-exponential, so that the lifetimes depend on the particular time settings.

The data show that both triple sensor materials respond to pH, T, and O_2 in the respective ranges. This makes the sensors well suited for continuous sensing of these parameters in blood or other bioliquids. Notably, the data of the triple sensors agree very well with the data obtained with the respective single

sensor materials, this indicating the absence of any cross-talk. The situation is quite different (in that responses are highly interdependent and virtually irreproducible) if the three probes are not incorporated into microbeads but rather used as homogeneous solution in the hydrogel binder polymer.

6.4. Conclusion

The composition of the sensor cocktail renders the system very versatile. The triple sensor layer, if deposited in the form of a small spot, can be optically interrogated e.g. by conventional spectroscopy or by imaging.^[29-31] If small enough, it may be read out via optical microfibers^[32,33] and thus enable sensing of three parameters with high spatial resolution at a single spot. The sensing layer may as well be spread, or sprayed, on supports such as skin, tissue, or industrial products.^[34]

It comes with some surprise when noting that optical sensors for pH (unlike practically all pH electrodes) have not been designed so far that would automatically be compensated for effects of temperature. By omitting the O₂ probe in these triple sensor systems, the first optical pH sensor is obtained whose response is corrected for effects of temperature. Moreover, pH sensors can be converted into sensors for acidic or basic gases by covering the sensing layer with gas-permeable but proton-impermeable polymers.^[1,32,33] As a result, proper modification of the triple sensor with adequate materials will enable sensing of carbon dioxide^[35] or ammonia^[36,37] and will lead to multiple sensors for either CO₂/O₂/T or NH₃/O₂/T. By incorporating the enzyme glucose oxidase as shown several times previously in case of single sensors,^[38,39] the triple sensor may be converted into a triple sensor for glucose, pH, and temperature because the oxygen sensor will now report the consumption of oxygen as a result of enzymatic activity, whilst the pH sensor may report any (albeit undesired) changes in pH, and the temperature sensor will simultaneously enable for a correction of effects of temperature.

6.5. Experimental

6.5.1. Materials

Poly(styrene-co-acrylonitrile) (PSAN; 30 wt% of acrylonitrile, MW 185,000 D), high molecular poly(vinyl chloride) (PVC), and trisodium 8-hydroxypyrene-1,3,6-trisulfonate (= HPTS) were obtained from Aldrich (www.sigmaaldrich.com). Platinum(II)-5,10,15,20-tetrakis(2,3,4,5,6-penta-fluorophenyl)porphyrin (PtTFPP), was purchased from Porphyrin Systems (www.porphyrin-systems.de), platinum(II)-5,10,15,20-tetrakis(2,3,4,5,6-penta-fluorophenyl)porpholactone (PtTFPL) from frontier-scientific (www.frontiersci.com), PET foil (Mylar[®]) from Goodfellow (www.goodfellow.com; product no. ES301425), and the polyurethane hydrogel (Hydromed[®], type D4) from Cardiotech (www.cardiotech-inc.com). All solvents (ethanol, tetrahydrofurane, hexane, heptane, and dimethylformamide) were of analytical purity and used as obtained from Fluka (www.sigmaaldrich.com). Europium(III)-tris(thenoyltrifluoroacetylacetonato)-(2-(4-diethylaminophenyl)-4,6-bis(3,5-dimethylpyrazol-1-yl)-1,3,5-triazine) [= Eu(tta)₃(dpbt)] was synthesized according to the procedure of Yang et al.^[24] To establish the response curve of the pH component of the triple sensor, a 15 mM Britton-Robinson wide-range buffer was used that was adjusted to the desired pH values with hydrochloric acid.

6.5.2. Preparation of Oxygen-Sensitive Beads

PtTFPP/PSAN particles were prepared by dissolving 10 mg of PtTFPP in a solution of 220 mg poly(styrene-co-acrylonitrile) in 45 mL of dimethylformamide (DMF). Particles were precipitated by dropwise addition of 120 mL of doubly distilled water while ultrasonication of the polymer/dye solution. The suspension was centrifuged and the remaining particles were washed with ethanol and water. Subsequent freeze drying yielded in a red colored powder. The diameter of the beads was determined by fluorescence microscopy to be ~1 μm .

PtTFPL/PSAN particles were prepared by analogy to the above protocol in that 10 mg of PtTFPL were dissolved in a solution of 220 mg of poly(styrene-co-acrylonitrile) in 120 mL of DMF. The particles were precipitated by dropwise

addition of 120 mL of doubly distilled water to the cocktail while ultrasonically it. The resulting suspension was centrifuged and the remaining particles were washed with ethanol and water. Freeze drying yielded in a red colored powder with a particle size of $\sim 1 \mu\text{m}$ as determined by fluorescence microscopy.

6.5.3. Preparation of pH-Sensitive Beads

The pH indicator HPTS was covalently immobilized on amino-modified poly(hydroxyethyl methacrylate) microparticles of typically $3 \mu\text{m}$ in diameter as described in the literature.^[25]

6.5.4. Preparation of Temperature-Sensitive Beads

$\text{Eu}(\text{tta})_3(\text{dpbt})/\text{PVC}$ particles were prepared by dissolving 3 mg of $\text{Eu}(\text{tta})_3(\text{dpbt})$ in a solution of 75 mg high molecular weight poly(vinyl chloride) in 15 mL of tetrahydrofuran (THF). After addition of 80 mL of heptane, the THF was removed slowly on the rotary evaporator. The resulting particles were centrifuged, washed with ethanol and water, and freeze dried to give a slightly yellow powder with a particle size of $\sim 2 - 3 \mu\text{m}$ as determined by fluorescence microscopy.

6.5.5. Preparation of Triple Sensor TS-1

A suspension was prepared from 20.0 mg of the $[\text{Eu}(\text{tta})_3(\text{dpbt})/\text{PVC}]$ particles, 21.5 mg of the $[\text{HPTS}/\text{poly-HEMA}]$ particles, and 23.5 mg of the $[\text{PtTFPL}/\text{PSAN}]$ particles in a 5% (wt.) solution of the polyurethane hydrogel in a 9:1 mixture of ethanol and water. The pink cocktail was then spread onto the PET foil (that acts as a solid support) using a knife-coating device. The sensing layer was $6 \mu\text{m}$ thick after solvent evaporation.

6.5.6. Preparation of Triple Sensor TS-2

A suspension was prepared from 30.0 mg of the $[\text{Eu}(\text{tta})_3(\text{dpbt})/\text{PVC}]$ particles, 15.5 mg of the $[\text{HPTS}/\text{poly-HEMA}]$ particles, and 20.0 mg of the $[\text{PtTFPP}/\text{PSAN}]$ particles in a 5% (wt.) solution of the polyurethane hydrogel in a 9:1 mixture of ethanol and water. The pink cocktail was then spread onto the PET foil (that acts as a solid support) using a knife-coating device. The sensing layer was 6 μm thick after solvent evaporation.

6.5.7. Acquisition of Spectra and Experimental Setup

Absorption and emission spectra were recorded on a Lambda 14 p Perkin-Elmer UV-VIS spectrophotometer (www.perkinelmer.com) and an Aminco AB 2 luminescence spectrometer (Thermo Scientific Inc., Waltham, USA; www.thermo.com), respectively. All time-resolved measurements were performed with a PCO SensiCam 12 bit b/w CCD camera (PCO, Kelheim, Germany; www.pco.de) equipped with a xenon 0.95/17 lens (Schneider Optische Werke, Bad Kreuznach, Germany; www.schneiderkreuznach.com) and a 405-66-60 LED with a peak emission at 405 nm (from Roithner Lasertechnik, Vienna; www.roithner-laser.com). The excitation light was focused by a PCX 18 x 18 MgF₂ TS lens (from Edmund Optics; www.edmundoptics.com) and hit the sensor layer at an angle of approximately 20° (relative to the CCD) after having passed a 2 mm thick BG12 filter (Schott, Mainz, Germany; www.schott.com). Further details are given in ref.^[16].

6.5.8. Response Functions of Triple Sensor TS-1

The signals of the three types of sensor beads were separated by applying the following optical filters: A BP 530/50 bandpass filter for HPTS (the pH probe), a D610/60M bandpass filter for $\text{Eu}(\text{tta})_3(\text{dpbt})$ (the temperature probe), and a RG695 long-pass filter for PtTFPL (the oxygen probe). From the information gathered by applying the Rapid Lifetime Determination method, the luminescence lifetime can

be calculated according to *equation 2.13* presuming, for the sake of simplicity, mainly mono-exponential decay of luminescence. If the decay profile is multi-exponential, the results depend – to a certain extent – on the widths and the positions of the gates. The parameter settings applied in our case are summarized in *table 6.1*.

Table 6.1. *Parameter settings for the triple sensor material TS-1 where reading was performed by applying the rapid lifetime determination method. In essence, two gated images are taken in the (isolated) emission phase of the indicators.*

probe	excitation pulse [μ s]	gate width [μ s]	t_1 [μ s] ^{a)}	t_2 [μ s]
PtTFPL (oxygen)	160	60	1	21
Eu(tta) ₃ (dpbt) (temperature)	2000	400	1	101

a) the delay was applied to separate the signal of Eu(tta)₃(dpbt) from residual short-lived fluorescence of HPTS

6.5.9. Response Functions of Triple Sensor TS-2

The signal of the pH indicator HPTS was separated from the other luminescences via a BP 530/50 optical bandpass filter, after which its intensity is measured that is related to pH as shown in *figure 6.4a*. The luminescences of the Eu(III)-based temperature probe and of the oxygen probe (PtTFPP) were detected after having passed a D610/60M bandpass filter. They were separated via the Dual Lifetime Determination method.^[16] The lifetime of the faster decaying pressure-sensitive probe (PtTFPP/PSAN) can be deduced from these data by iteration as demonstrated in ref.^[16]. The parameter settings applied are listed in *table 6.2*. Lifetimes were calculated with *equation 2.13* (see *section 2.4.2.3*) using the different gate pairs and their associated starting times (t_1 , t_2 with A_1/A_2 ; and t_3 , t_4 with A_3/A_4 , respectively).

Table 6.2. Parameter settings for the triple sensor material TS-2 where reading was performed using the dual lifetime determination method. Four gated images are taken in the emission phase of both indicators.

probe	excitation pulse [μs]	gate width [μs]	t ₁ [μs] ^{a)}	t ₂ [μs]	t ₃ [μs]	t ₄ [μs]
PtTFPP (oxygen)	150	50	1	21	---	---
Eu(tta) ₃ (dpbt) (temperature)	1000	400	---	---	400	500

a) the delay was applied to separate the signal of PtTFPP from residual short-lived fluorescence of HPTS

6.6. References

- [1] C. McDonagh, C. S. Burke, B. D. MacCraith, *Chem. Rev.* **2008**, *108*, 400
- [2] M. W. Blades, H. G. Schulze, S. O. Konorov, C. J. Addison, A. I. Jirasek, R. F. B. Turner, *ACS Symposium Series* **2007**, *963*, 1, American Chemical Society, Washington, DC
- [3] G. J. Mohr, in *Springer Series on Chemical Sensors and Biosensors*, Vol. 1: *Optical Sensors* (ed. R. Narayanaswamy), Springer, Berlin, **2004**, 51
- [4] O. S. Wolfbeis, in *Fluorescence Methods and Applications: Spectroscopy, Imaging, and Probes*, (ed. O. S. Wolfbeis), *Ann. New York Acad. Sci.* **2008**, *1430*, 1
- [5] Q. Zheng, G. Xu, P. N. Prasad, *Chem. Eur. J.* **2008**, *14*, 5812
- [6] E. Ergen, M. Weber, J. Jacob, A. Herrmann, K. Muellen, *Chem. Eur. J.* **2006**, *12*, 3707
- [7] Y.-E. L. Koo, Y. Cao, R. Kopelman, S. M. Koo, M. Brasuel, M. A. Philbert, *Anal. Chem.* **2004**, *76*, 2498
- [8] M. Bedoya, M. T. Diez, M. C. Moreno-Bondi, G. Orellana, *Sens. Actuators B* **2006**, *113*, 573
- [9] R. A. Potyrailo, *Angew. Chem. Int. Ed.* **2006**, *45*, 702
- [10] P. Chojnacki, G. Mistlberger, I. Klimant, *Angew. Chem. Int. Ed.* **2007**, *46*, 8850
- [11] B. Zelelow, G. E. Khalil, G. Phelan, B. Carlson, M. Gouterman, J. B. Callis, L. R. Dalton, *Sens. Actuators B* **2003**, *96*, 304
- [12] M. E. Koese, A. Omar, C. A. Virgin, B. F. Carrol, K. S. Schanze, *Langmuir* **2005**, *21*, 9110
- [13] I. Klimant, M. Kuehl, R. N. Glud, G. Holst, *Sens. Actuators B* **1997**, *38*, 29
- [14] C. R. Schroeder, G. Neurauder, I. Klimant, *Microchim. Acta* **2007**, *158*, 205
- [15] S. Nagl, O. S. Wolfbeis, *Analyst* **2007**, *132*, 507
- [16] M. I. J. Stich, S. Nagl, O. S. Wolfbeis, U. Henne, M. Schaeferling, *Adv. Funct. Mater.* **2008**, *18*, 1399
- [17] S. Uchiyama, K. Iwai, A. P. deSilva, *Angew. Chem.* **2008**, *120*, 4745
- [18] S. Nagl, C. Beleizão, S. M. Borisov, M. Schaeferling, M. – N. Berberan-Santos, O. S. Wolfbeis, *Angew. Chem. Int. Ed.* **2007**, *46*, 2317

- [19] H. Komatsu, T. Miki, D. Citterio, T. Kubota, Y. Shindo, Y. Kitamura, K. Oka, K. Suzuki, *J. Am. Chem. Soc.* **2005**, *127*, 10798
- [20] *Polymer Handbook* (eds: J. Brandrup, E. H. Immergut, E. A. Grulke), Wiley, New York, 1999
- [21] Y. Amao, *Microchim. Acta* **2003**, *143*, 1
- [22] B. S. Gan, E. Krump, L. D. Shrode, S. Grinstein, *Am. J. Physiol.* **1998**, *275*, C1158
- [23] S. M. Borisov, O. S. Wolfbeis, *Anal. Chem.* **2006**, *78*, 5094
- [24] C. Yang, L. M. Fu, Y. Wang, J. P. Zhang, W. T. Wong, X. C. Ai, Y. F. Qiao, B. S. Zou, L. L. Gui, *Angew. Chem. Int. Ed.* **2004**, *43*, 4009
- [25] G. S. Vasylevska, S. M. Borisov, C. Krause, O. S. Wolfbeis, *Chem. Mat.* **2006**, *18*, 4609
- [26] C. Moore, S. P. Chan, J. N. Demas, B. A. DeGraff, *Appl. Spec.* **2004**, *58*, 603
- [27] B. Valeur, *Molecular Fluorescence, Principles and Applications*, 1st edition, Wiley-VCH, Weinheim, **2002**
- [28] E. Puklin, B. Carlson, S. Gouin, C. Costin, E. Green, S. Ponomarev, H. Tanji, M. Gouterman, *J. Appl. Polym. Sci.* **1999**, *17*, 2795
- [29] J. Hradil, C. Davis, K. Mongey, C. McDonagh, B. D. MacCraith, *Meas. Sci. Technol.* **2002**, *13*, 1552
- [30] S. P. Chan, Z. J. Fuller, J. N. Demas, B. A. DeGraff, *Anal. Chem.* **2001**, *13*, 4486
- [31] B. A. Flusberg, E. D. Cocker, W. Piyawattanametha, J. C. Jung, E. L. M. Cheung, M. J. Schnitzer, *Nat. Meth.* **2005**, *2*, 941
- [32] I. Klimant, F. Ruckruh, G. Liebsch, A. Stangelmayer, O. S. Wolfbeis, *Microchim. Acta* **1999**, *131*, 35
- [33] A. S. Kocincova, S. M. Borisov, C. Krause, O. S. Wolfbeis, *Anal. Chem.* **2007**, *79*, 8486
- [34] O. S. Wolfbeis, *Adv. Mat.* **2008**, *20*, 3759
- [35] C. von Bueltzingsloewen, A. K. McEnvoy, C. McDonagh, B. D. MacCraith, I. Klimant, C. Krause, O. S. Wolfbeis, *Analyst* **2000**, *127*, 1478
- [36] G. J. Mohr, *Anal. Bioanal. Chem.* **2006**, *386*, 1201
- [37] K. Waich, T. Mayr, I. Klimant, *Meas. Sci. Technol.* **2007**, *18*, 3195
- [38] H. Xu, J. W. Aylott, R. Kopelman, *Analyst* **2002**, *127*, 1471
- [39] D. B. Papkovsky, J. Olah, I. N. Kurochkin, *Sens. Actuators B* **1993**, *11*, 525

CHAPTER 7

Summary

This thesis describes various methods for time-resolved luminescence lifetime determination, and their applications to imaging barometric pressure and temperature. These approaches are superior to luminescence intensity imaging in that they are less influenced by sources of errors like light scattering, inhomogeneous indicator distribution, photobleaching, or background fluorescence because they are intrinsically referenced. The data obtained are precise and unambiguous. Novel sensor materials and methods for time-resolved imaging are described, characterized, and applied.

Chapter 1 gives a brief historical overview of the development of pressure-sensitive and temperature-sensitive sensor systems. Their importance not only for aerodynamic research but also for life science applications is highlighted. The motivation and the aim of this thesis are introduced.

In chapter 2, the physical and chemical mechanisms of pressure-sensitive and temperature-sensitive luminescent probes are explained in detail. The materials required for preparation of PSPs and/or TSPs are introduced. Furthermore, the requirements on the different components of an experimental setup for time-resolved or gated luminescence imaging are discussed. The state-of-the-art of pressure-sensitive and temperature-sensitive paints applied in aerodynamic research and the respective methods of interrogation are presented.

A novel dual PSP/TSP system, consisting of a platinum porpholactone and a ruthenium-diimine complex, for time resolved luminescence imaging is introduced in chapter 3. The choice of the materials is explained and discussed. Different wind tunnel systems and their specifications, along with the areas of application are presented. The dual paint was applied to a delta wing model for wind tunnel testing. Despite of drawbacks due to unexpected effects and problems, the dual paint has proven to be applicable for aerodynamic research. Temperature can be determined with an accuracy of 0.5 K and the surface pressure topology coincides with theory and with the data from conventional pressure measurements.

A novel kind of an optical dual sensor, allowing for signal separation due to different luminescence lifetimes without the need of additional spectral separation is introduced in chapter 4. This technique expands the possible spectrum of combination of probes applicable to optical dual sensing. The new sensor system consists of a platinum porphyrin and a europium chelate complex, capable of determining oxygen and temperature simultaneously, without the need for different optical filters. The preparation of the sensor material is described, and its performance and accuracy validated.

In chapter 5, a novel general approach for imaging is presented. It makes use of the fundamental setup of digital cameras and enables to monitor the spectrally resolved luminescence of up to three signals with one single image. Data evaluation can be performed with even freeware image editing software. For the proof-of-principle, a dual sensor containing HPTS as pH probe and a europium chelate complex as temperature probe in a hydrogel as binder was calibrated applying a commercially available digital camera. The results were compared with the sensor response of the reference single sensors and exhibit good consistence.

The new materials and methods developed during this dissertation led to the fabrication of the first optical triple sensor systems. Two kinds of sensors are reported. They are capable of simultaneously determining the three important analytes pH, T, and O₂. The first system consisted of HPTS as the pH-indicator, a Eu-chelate complex as the temperature probe, and a Pt-porpholactone as the probe for oxygen, all encapsulated in appropriate polymer particles. The three signals are separated using optical filters. In the second triple sensor system (TS-2), the O₂ probe of the first system was replaced by a Pt-porphyrin, enabling for time-resolved separation of the temperature signal from the O₂ signal. Both systems are calibrated, compared with reference single sensors, and validated. With these new kind of sensors, it is possible to monitor the three clinically relevant parameters pH, T, and O₂ non-invasively, online, and in surpassing spatial resolution. By omitting the oxygen probe, the first temperature compensated optical pH sensor ever described in literature is obtained.

CHAPTER 8

Abbreviations, Acronyms, and Symbols

4-CTFT	4-Chloro- α,α,α -trifluorotoluene
α	Angle of attack
AA	Anodised aluminum
BAE	Britisch Aerospace
BOS	Background oriented Schlieren technique
Bs	Brightness (product of molar absorbance and quantum yield)
c	Concentration
CCD	Charge-coupled device
CMOS	Complementary metal oxide semiconductor
$\Delta\Phi$	Phase shift
DLR	German Aerospace Center (Deutsches Zentrum für Luft- und Raumfahrt)
DLR	Dual Lifetime Referencing
DO	Dissolved oxygen
ϵ	Molar absorption coefficient
E_a	Arrhenius activation energy
EC	Ethyl cellulose
E_p	Activation energy of permeation
ET	Energy transfer
Eu(tta) ₃ (dpbt)	Europium(III)-tris(thenoyltrifluoroacetylacetonato)-(2-(4-diethylaminophenyl)-4,6-bis(3,5-dimethylpyrazol-1-yl)1,3,5-triazine)

Φ	Quantum yield
FIB	Poly(hexafluoroisopropyl methacrylate-co-heptafluoro-n-butyl methacrylate)
FLIM	Fluorescence Lifetime Imaging
I	Intensity
ICCD	Intensified charge-coupled device
IPCT	Image pattern correlation technique
I_{ref}	intensity at reference conditions
JAXA	Japan Aerospace Exploration Agency
K_{SV}	Stern-Volmer constant
LED	Light emitting diode
LOD	Limit of detection
LT	Lifetime
MLC	Metal-ligand complex
MOSAIC	Molecular sensors for aerodynamic research
ONERA	Office National d'Études et de Recherches Aérospatiales, (French Aerospace Center)
P	Permeability coefficient
p	Pressure
PAH	Polycyclic aromatic hydrocarbons
PAN	Poly(acrylonitrile)
PDMS	Poly(dimethyl siloxane)
PdOEP	Pd(II)-2,3,7,8,12,13,17,18-octaethylporphyrin
PdOEPK	Pd(II)-2,3,7,8,12,13,17,18-octaethylporphyrinketone
PDR	Phase Delay Rationing
PdTFPP	Pd(II)-5,10,15,20-tetrakis(2,3,4,5,6-penta-fluorophenyl)porphyrin

PdTPTBP	Pd(II)-meso-tetraphenyltetrabenzoporphyrin
PIV	Particle image velocimetry
PMMA	Poly(methyl methacrylate)
pO ₂	Oxygen partial pressure
Poly(IBM-co-TFEM)	Poly(isobutyl methacrylate-co-trifluoroethyl methacrylate)
PolyTMSP	Poly(trimethyl silyl-propyne)
PS	Polystyrene
PSAN	Poly(styrene-co-acrylonitrile)
PSP	Pressure-sensitive paint (for barometric pressure)
PtOEP	Pt(II)-2,3,7,8,12,13,17,18-octaethylporphyrin
PtOEPK	Pt(II)-2,3,7,8,12,13,17,18-octaethylporphyrinketone
PtTFPL	Pt(II)-5,10,15,20-tetrakis(2,3,4,5,6-penta-fluorophenyl)porpholactone
PtTFPP	Pt(II)-5,10,15,20-tetrakis(2,3,4,5,6-penta-fluorophenyl)porphyrin
PVP	Poly(vinyl pyrrolidone)
QY	Quantum yield
R	General gas constant
Re	Reynolds number
RLD	Rapid Lifetime Determination
ROI	Region of interest
Ru(bpy) ₃ ²⁺	Ru(II)-tris(2,2'-bipyridine)
Ru(dpp) ₃ ²⁺	Ru(II)-tris(4,7-diphenyl-1,10-phenanthroline)
Ru(phen) ₃ ²⁺	Ru(II)-tris(1,10-phenanthroline)
Ru(trpy) ₂ ²⁺	Ru(II)-bis(2,2':6',2''-terpyridine)
SNR	Signal-to-noise ratio
τ	Lifetime of luminescence
T	Temperature
t	Time
TPT	Thermographic phosphor thermography

t_{ref}	Lifetime at reference conditions
TsAGI	Central Aerohydrodynamic Institute, Russian Aerospace Center
TSP	Temperature-sensitive paints

CHAPTER 9

Curriculum Vitae

Name: Stich
First Name: Matthias Ignaz Johann
Date of Birth: 26.08.1977
Place of Birth: Regensburg
Nationality: German
Address: Deutschhernnweg 2, 93053 Regensburg

Education:

09/1984 - 07/1988	Grundschule Sinzing
09/1988 - 06/1998	Von - Müller Gymnasium Regensburg
06/1998	Graduation: Allgemeine Hochschulreife (Abitur)

Military Service:

07/1998 - 08/1999

Studies:

11/1999 - 12/2004	Chemistry (Diploma) at the University of Regensburg, Regensburg
01/2005 - 10/2005	Diploma Thesis at the University of Regensburg, Institute of Analytical Chemistry, Chemo- and Biosensors, Prof. Dr. Otto S. Wolfbeis, Topic: <i>"Preparation and Calibration of Pressure- Sensitive and Temperature-Sensitive Paints"</i>
11/2005	Graduation: Diplom Chemiker

01/2006 - 12/2008

PhD student at the University of Regensburg,
Institute of Analytical Chemistry, Chemo- and
Biosensors, Prof. Dr. Otto S. Wolfbeis, Topic:
*“Preparation and Calibration of Pressure-
Sensitive and Temperature – Sensitive Paints
for Fluorescence Lifetime Imaging
Applications”* (this thesis)

CHAPTER 10

Patents, Publications, and Presentations

Diploma Thesis

“Preparation and Calibration of Pressure-Sensitive and Temperature-Sensitive Paints”,
Institute of Analytical Chemistry, Chemo- and Biosensors, University of Regensburg, **2005**

Patents

M. I. J. Stich, S. M. Borisov, S. Nagl, M. Schäferling, O. S. Wolfbeis, U. Henne, R. Engler, „*Verfahren und Messaufbau zum Erfassen der Verteilung mindestens einer Zustandsgröße in einem Messfeld mit verschiedenen Sonden*“ German patent DE 102007 054602.7_52 (**2007**)

Book Chapters

- [1] S. M. Borisov, T. Mayr, A. A. Karasyov, I. Klimant, P. Chojnacki, C. Moser, S. Nagl, M. Schäferling, M. I. J. Stich, A.S. Vasylevska, O. S. Wolfbeis, “*New Plastic Microparticles and Nanoparticles for Fluorescent Sensing and Encoding*”, In: *Springer Series on Fluorescence Vol. 4*, M. N. Berberan-Santos (ed.), Springer, Berlin Heidelberg (**2007**)

- [2] M. I. J. Stich, O. S. Wolfbeis, “*Fluorescence Sensing and Imaging Using Pressure-Sensitive Paints and Temperature-Sensitive Paints*”, In: *Springer Series on Fluorescence, Vol. 5, Part 1*, U. Resch-Genger (ed.), Springer, Berlin Heidelberg (**2008**)

Papers

- [1] M. I. J. Stich, S. Nagl, O. S. Wolfbeis, U. Henne, M. Schäferling, “*A Dual Luminescent Sensor Material for Simultaneous Imaging of Pressure and Temperature on Surfaces*”, *Adv. Funct. Mater.* **2008**, 18, 1399

- [2] S. Nagl, M. I. J. Stich, M. Schäferling, O. S. Wolfbeis, **“Method for Simultaneous Luminescence Sensing of Two Species Using Optical Probes of Different Decay Time, and its Application to an Enzymatic Assay at Varying Temperature”**, *Anal. Bioanal. Chem.* **2008**, available online
- [3] M. I. J. Stich, S. M. Borisov, U. Henne, M. Schäferling, **“Read-Out of Multiple Optical Chemical Sensors by Means of Digital Color Cameras”**, *Sens. Actuators B* **2009**, accepted
- [4] M. I. J. Stich, M. Schäferling, O. S. Wolfbeis, **“Multicolor Fluorescent and Permeation-Selective Microbeads Enable Simultaneous Sensing of pH, Oxygen, and Temperature”**, *Adv. Mater.* **2009**, accepted
- [5] L. H. Fischer, M. I. J. Stich, N. Tian, E. Holder, M. Schäferling, **„Red and green iridium(III) triplet emitters in dual barometric and temperature sensor application”**, in preparation

Oral Presentations

- [1] M. I. J. Stich, **„Die optische Sensorik des Kohlendioxids”**. Invited Lecture at the Cluster Meeting **“Nanotechnologie & Sensorik”**, Fa. VIASYS, Würzburg, 3rd November, **2007**
- [2] M. I. J. Stich, **„Technologien in der optischen Sensorik”**. Invited lecture at the symposium **„Optische Technologien in der Photodynamik – Technologie und Potential”**, Bayern Photonics & Cluster Sensorik Regensburg, Regensburg, 11th March **2009**

Poster Presentations

- [1] M. I. J. Stich, S. Nagl, O. S. Wolfbeis, M. Schäferling, U. Henne, R. H. Engler, C. Klein, **“Calibration of Dual Pressure- and Temperature-Sensitive Paints by Luminescence Lifetime Imaging”**. 9th Conference on Methods and Applications of Fluorescence: Spectroscopy, Imaging and Probes (MAF), September 4-7, **2005**, Lisbon, Portugal

- [2] M. I. J. Stich, S. Nagl, M. Schäferling, O. S. Wolfbeis, ***“Luminescence Lifetime-Based Simultaneous Imaging of Pressure and Temperature”***. Europt(r)ode VIII, April 2-5, **2006**, Tübingen, Germany

- [3] M. I. J. Stich, M. Schäferling, O. S. Wolfbeis, “Lifetime-Based Simultaneous Imaging of Pressure and Temperature Using a Single Camera”. ANAKON, March 27-30 **2007**, Jena, Germany,
This poster was awarded the **“Best Poster Award”**

- [4] M. I. J. Stich, S. M. Borisov, M. Schäferling, O. S. Wolfbeis, ***“Read-Out of Dual Sensors by Means of a Digital Color Camera”***. 10th Conference on Methods and Applications of Fluorescence: Spectroscopy, Imaging and Probes (MAF), September 9-12, **2007**, Salzburg, Austria

- [5] M. I. J. Stich, S. M. Borisov, M. Schäferling, O. S. Wolfbeis, ***“Calibration of Dual Optical Sensors Based on Digital Color Cameras”***. Europt(r)ode IX, March 30th – April 2nd, **2008**, Dublin, Ireland

- [6] M. I. J. Stich, U. Henne, M. Schäferling, O. S. Wolfbeis, ***“Read-Out of Multiple Luminescent Sensors Based on Color Imaging”***. 1st German Japanese Seminar on PSP/TSP, September 1-5, **2008**, Sendai, Japan,

Erklärung

Hiermit erkläre ich, dass ich die vorliegende Arbeit selbst verfasst, und keine anderen als die angegebenen Hilfsmitteln und Quellen verwendet habe.

Regensburg, den 04.02.2009

Stich Matthias